

Dissertation for the attainment of
the academic title
doctor rerum naturalium

**Pathogenicity of UCH-L1 autoantibodies in
membranous nephropathy**

Presented by

Sarah Frömbling

Department of Biology
Faculty of Mathematics, Informatics and Natural Sciences
University of Hamburg

Hamburg, 2025

Defense: 27.06.2025

Reviewer:

1. Prof. Dr. Catherine Meyer-Schwesinger

Institut für Zelluläre und Integrative Physiologie, Universitätsklinikum Hamburg-Eppendorf

2. Prof. Dr. Julia Kehr

Institut für Pflanzenwissenschaften und Mikrobiologie, Universität Hamburg

The presented work was conducted from April 2020 until March 2025 externally in the Department of Physiology in the Institute of Cellular and Integrative Physiology at the University Medical Center Hamburg-Eppendorf under the supervision of Prof. Dr. Catherine Meyer-Schwesinger. Prof. Dr. Julia Kehr supervised this work in the Department of Biology at the University of Hamburg.

Table of Contents

List of figures	1
List of tables	2
Abbreviations	3
Zusammenfassung	6
Abstract	8
1 Introduction	10
1.1 The kidney and renal filtration	10
1.1.1 The podocyte	11
1.1.2 The glomerular basement membrane	12
1.2 Membranous nephropathy	13
1.3 Rodent models of membranous nephropathy.....	16
1.4 Protein degradation and the deubiquitinase Ubiquitin C-terminal Hydrolase L1 (UCH-L1).....	18
1.4.1 The ubiquitin proteasome system	18
1.4.2 Ubiquitin C-terminal Hydrolase L1	20
1.5 The role of UCH-L1 in diseases	20
1.6 Extracellular vesicles	21
1.7 Objectives.....	22
2 Material and Methods.....	24
2.1 Material	24
2.1.1 Chemicals, kits and antibodies.....	24
2.1.2 Materials, devices and software	30
2.1.3 Plasmids	36
2.2 Methods.....	36
2.2.1 Cell culture	36
2.2.2 Animal work.....	39
2.2.3 Enrichment of extracellular vesicles	41
2.2.4 Protein-biochemical methods	43
2.2.5 Molecular biological methods	51
2.2.6 Histology and Immunofluorescence	56
2.2.7 Statistical analysis	58
3 Results	59
3.1 UCH-L1 antigen expression in membranous nephropathy	59

3.2	Anti-UCH-L1 antibody second hit aggravates membranous nephropathy	60
3.2.1	Characterization of anti-UCH-L1 antibodies	61
3.2.2	Verification of UCH-L1 antibody localization in the kidney of the THSD7A-MN+2 nd hit mouse model	62
3.2.3	Membranous nephropathy is aggravated in THSD7A-MN with anti-UCH-L1 second hit in mice	66
3.2.4	Antibody burden is increased in THSD7A-MN+2 nd hit	69
3.3.5	Collagen IV production is increased in THSD7A-MN+2 nd hit.....	72
3.2.6	Anti-UCH-L1 second hit leads to an altered pattern and increased <i>de novo</i> expression of UCH-L1	75
3.3	Extracellular vesicles as an exit route for MN antigens	79
3.3.1	EV release is increased in MN	80
3.3.2	UCH-L1 is released in EVs as a non-functional form	83
3.3.3	THSD7A is released as a proteolytically cleaved protein within cell culture podocyte derived EVs	87
4	Discussion.....	89
4.1	UCH-L1 expression in membranous nephropathy.....	89
4.2	MN is worsened in the THSD7A-MN+2 nd hit mouse model	90
4.3	A higher antibody burden and altered GBM synthesis contribute to the worsening of MN in the anti-UCH-L1-abs 2 nd hit	92
4.4	UCH-L1 <i>de novo</i> expression is altered by anti-UCH-L1-abs 2 nd hit while activity (ubiquitin binding) is not impaired.....	94
4.5	Extracellular vesicles as a potential exit route for MN antigens.....	96
4.6	Conclusion.....	97
5	Literature	99
6	Publications.....	108
7	Acknowledgements	109
8	Eidesstattliche Versicherung	110

List of figures

Scheme 1: Structure of the kidney and nephron.	11
Scheme 2: The podocyte and the glomerular basement membrane in the glomerulus.	13
Scheme 3: Hallmarks of membranous nephropathy (MN).	16
Figure 1: UCH-L1 localizes to the podocyte membrane and FP in MN patients.	59
Figure 2: UCH-L1 in the passive mouse model of THSD7A-associated MN.	60
Figure 3: Characterization of the U104 anti-UCH-L1 antibody.	62
Figure 4: Second hit anti-UCH-L1 antibodies are found in the kidney.	65
Figure 5: Anti-UCH-L1-abs 2nd hit worsened disease development in THSD7A-MN mice.	68
Figure 6: Antibody burden of mouse/rat-IgG is increased in THSD7A-MN+2nd hit mice.	71
Figure 7: Collagen IV synthesis is altered in THSD7A-MN+2nd hit mice.	74
Figure 8: UCH-L1 expression pattern is altered in human cell culture podocytes.	77
Figure 9: UCH-L1 antigen levels are elevated in THSD7A-MN+2nd hit.	79
Figure 10: Characterization of human cell culture podocyte-derived extracellular vesicles.	81
Figure 11: EV release is increased in MN conditions.	82
Figure 12: Non-functional UCH-L1 is found in urinary EVs in MN patients.	84
Figure 13: UCH-L1 antigen is altered in EVs.	86
Figure 14: THSD7A is predominantly present as a cleaved fragment in EVs in MN conditions.	88

List of tables

Table 1: Chemicals.....	24
Table 2: Isolation systems and reaction kits	27
Table 3: DNA and Protein ladder.....	27
Table 4: Antibodies and dyes	28
Table 5: Consumable materials.....	30
Table 6: Devices.....	34
Table 7: Software	35
Table 8: Plasmids.....	36
Table 9: qPCR Primer	54
Table 10: Real-time qPCR program	55
Table 11: Dehydration and paraffin embedding protocol	56

Abbreviations

ABP *activity-based probe*

ABPP *activity-based protein profiling*

abs *antibodies*

ACR *albumin to creatinine ratio*

AD *Alzheimer's disease*

ADAM10 *A Disintegrin And Metalloproteinase 10*

ALP *autophagosome-lysosome pathway*

AR *aldose reductase*

ATP *adenosine 5' triphosphate*

BSA *bovine serum albumin*

cDNA *complementary DNA*

chol *cholesterol*

CP *core particle*

ctrl *control*

DMSO *dimethylsulfoxide*

DNA *deoxyribonucleic acid*

DTT *dithiothreitol*

DUB *deubiquitinating enzyme*

ECD *extracellular domain*

ELISA *enzyme-linked immunosorbent assay*

ESRD *end-stage renal disease*

EV *extracellular vesicle*

EXT 1/2 *exostosin 1/2*

FBS *fetal bovine serum*

FcRn *neonatal Fc receptor*

FP *foot processes*

FSD *filtration slit density*

FSGS *focal segmental glomerulosclerosis*

GBM *glomerular basement membrane*

GFB *glomerular filtration barrier*

HN *Heymann nephritis*

ICD *intracellular domain*

Abbreviations

IgG *immunoglobulin*

ITS *insulin, transferrin selenium*

KO *knockout*

lys *lysine*

MAE *Mouse-Albumin-ELISA*

MCD *minimal change disease, minimal change disease*

MN *membranous nephropathy*

MW *molecular weight*

n.t. *non-transfected*

NC *negative control*

NCAM1 *neural cell adhesion molecule 1*

Nell-1 *neural epidermal growth factor-like 1 protein*

NEP *neutral endopeptidase*

NTA *nanoparticle tracking analyses*

PAGE *polyacrylamide gel electrophoresis*

PC *positive control*

PCR *polymerase chain reaction*

PD *Parkinson's disease*

PEMP *podocyte exact morphology measurement*

PGP9.5 *protein gene product 9.5*

PLA₂R1 *phospholipase A₂ receptor 1*

PTSA *para-toluenesulfonic acid*

qPCR *quantitative PCR, quantitative PCR*

rb *rabbit*

RNA *ribonucleic acid*

ROS *reactive oxygen species*

RP *regulatory particle*

SD *slit diaphragm*

SDS *sodium dodecyl sulfate*

SLE *systemic lupus erythematosus*

SOD2 *superoxide dismutase 2*

THSD7A *thrombospondin type-1 domain containing 7A*

trig *triglycerides*

ub *ubiquitin*

Abbreviations

UCH *Ubiquitin C-terminal Hydrolases*

UCH-L1 *Ubiquitin C-terminal Hydrolase L1*

UPS *ubiquitin proteasome system*

UT *untreated*

WT *wildtype*

α ENO *α -enolase*

Zusammenfassung

Die Membranöse Nephropathie (MN) ist eine Autoimmunerkrankung der Niere, welche Podozyten, spezialisierte Zellen der Niere, betrifft. Diese sind an der Filtration des Blutes und der Synthese der glomerulären Basalmembran beteiligt. Die MN wird durch primäre Autoantikörper gegen Podozytenantigene wie THSD7A, welche an den Fußfortsätzen exprimiert werden, ausgelöst. Die entstehenden Immunkomplexe werden entlang der glomerulären Filtrationsbarriere abgelagert und führen zu einer Zerstörung der glomerulären Filtrationsbarriere. In den letzten Jahren wurden neben den primären Autoantikörpern weitere MN-assoziierte Autoantikörper identifiziert, die unter anderem gegen intrazelluläre Proteine gerichtet sind und vermutlich als sekundäre Immunreaktion auftreten. Es ist unklar, ob diese zur Pathogenität der MN beitragen, allerdings zeigen MN-Patienten, die solche sekundären Autoantikörper aufweisen, eine Verschlechterung des Krankheitsverlaufs. Einige MN-Patienten weisen spezifisch Autoantikörper gegen das in geschädigten Podozyten *de novo* exprimierte, intrazelluläre deubiquitinierende Enzym Ubiquitin C-terminale Hydrolase L1 (UCH-L1) auf. Hypothese dieser Arbeit ist, dass diese sekundären anti-UCH-L1 Antikörper durch ihre Präsenz an der glomerulären Filtrationsbarriere oder durch die Beeinflussung der UCH-L1 Protein Aktivität, zu einer Verschlechterung der MN führen. Um die Pathogenität sekundärer anti-UCH-L1 Antikörper im Zusammenhang mit der MN zu untersuchen, wurden Versuche in etablierten humanen Zellkulturpodozyten und Maus Modellen der THSD7A-MN durchgeführt. Nach MN-Entwicklung wurden anti-UCH-L1 Antikörper als sekundäre Behandlung appliziert (THSD7A-MN+2nd hit). Um einen pathogenen Einfluss zu haben, müssen Antikörper Zugang zu dem entsprechenden Antigen haben. Dies konnte in MN-Patienten und dem THSD7A-MN Maus Modell durch die Lokalisierung an der Podozytenfußfortsatzmembran gezeigt werden. Die Applizierung des sekundären anti-UCH-L1 Antikörpers führte zu einem verschlechterten Krankheitsverlauf mit verstärkter Proteinurie und Fußfortsatzverschmelzung. Morphologisch-funktionell zeigten THSD7A-MN+2nd hit Mäuse zudem eine erhöhte Antikörper Last an der glomerulären Filtrationsbarriere und eine Veränderung in der Kollagen IV Produktion hin zu einer Form, welche nur im sich entwickelnden Glomerulus vorkommt. Weiterhin wurde beobachtet, dass der podozytäre UCH-L1 Gehalt anstieg und das Protein in Podozyten aggregierte. Mittels Zellkultur- und Urinuntersuchungen konnte eine vermehrte Abgabe von

Zusammenfassung

Extrazellularvesikeln gezeigt werden, welche mit anti-THSD7A Antikörpern beladen sind. Zusätzlich enthielten die Extrazellularvesikel nicht-funktionales UCH-L1 ebenso wie ein proteolytisch gespaltenes THSD7A, wodurch Extrazellularvesikel eine mögliche Austrittspforte für geschädigte Antigene darstellen. Zusammenfassend gibt die zugrundeliegende Arbeit gibt einen ersten Hinweis auf einen krankheitsverschlechternden Einfluss der sekundären anti-UCH-L1 Antikörper und trägt zu einem besseren Verständnis der Faktoren bei, welche zu einer Verschlechterung der MN führen. Sie zeigt somit auch die Notwendigkeit weitere mögliche (sekundäre) Antigene und ihren Einfluss zu untersuchen.

Abstract

The autoimmune disease membranous nephropathy (MN), affects podocytes, specialized cells of the kidney, which contribute to the filtration of the blood and the secretion of glomerular basement membrane (GBM) components. MN is caused by primary autoantibodies directed against foot process (FP) proteins such as THSD7A, binding their target antigen and accumulating as immune complexes along the glomerular filtration barrier (GFB). In the past years next to the primary autoantibodies a multitude of putative MN-associated autoantibodies were discovered, which among others are directed to intracellular proteins and might occur as a secondary immune response. Although their relation to MN pathogenesis is unclear, MN patients with secondary autoantibodies against intracellular proteins are linked to a poor clinical outcome. A subset of MN patients presents with secondary autoantibodies directed against the intracellular deubiquitinating enzyme Ubiquitin C-terminal Hydrolase L1 (UCH-L1), which is *de novo* expressed in injured podocytes. Hypothesis of the current work is that secondary anti-UCH-L1 antibodies lead to a worsening of MN either through their presence at the GFB or by interference with UCH-L1 functionality. To investigate the pathogenicity of those secondary antibodies in MN, experiments were performed in established human podocyte cell culture and THSD7A-MN mouse models. After MN induction, secondary anti-UCH-L1 antibodies were applied to achieve a second hit (THSD7A-MN+2nd hit). For pathogenicity, antibodies need to have access to the antigen, which could be verified through a foot process/plasma membrane localization of UCH-L1 in the THSD7A-MN setting. The THSD7A-MN+2nd hit led to an aggravation of the disease, demonstrated by increased proteinuria and a worsening of FP effacement. Mechanistically 2nd hit anti-UCH-L1-abs exhibited pathogenicity through a higher antibody load at the GFB, especially within the glomerular immune complex containing protein fraction. Additionally, GBM synthesis was dysregulated with a shift in collagen IV α -chain synthesis towards a form expressed by podocytes during GBM development. Furthermore, protein amounts of UCH-L1 were elevated in THSD7A-MN+2nd hit and showed aggregates in podocytes. Investigations in podocyte cell culture medium as well as human and mouse urine were significant for an increased release of THSD7A antibody loaded extracellular vesicles (EVs). Those EVs furthermore contained non-functional UCH-L1, next to proteolytically processed THSD7A, demonstrating that EVs represent a potential exit route for MN antigens. This could potentially represent a first step towards antigen-spreading in MN.

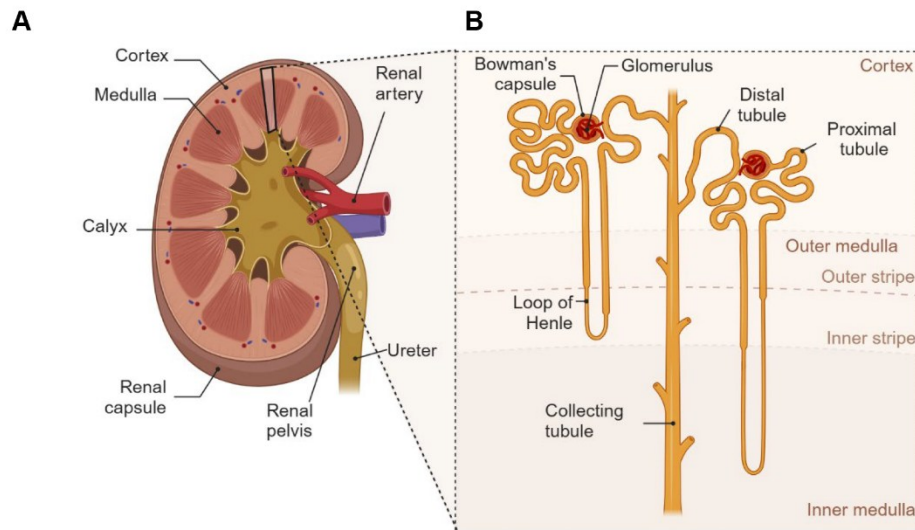
Abstract

In conclusion anti-UCH-L1 antibodies aggravate clinical and morphologic podocyte injury by contributing to GFB damage and binding membrane-bound UCH-L1. This work contributes to a more detailed understanding of factors leading to a poor clinical outcome of MN and demonstrate the necessity for investigations on other putative secondary antigens.

1 Introduction

1.1 The kidney and renal filtration

Membranous nephropathy (MN) as the most common cause of nephrotic syndrome [1] affects the kidney, a major excretory organ. The kidney comprises several functions including the removal of metabolic waste, volume and electrolyte control of body fluids, acid-base balance, and reabsorption of nutrients such as glucose and amino acids [2]. Kidney function starts with the filtration of blood wherein about 20% of the cardiac output or approximately 1-1.2 L blood per minute are filtered. This requires a relatively high amount of metabolic energy (approximately 10% of basal O₂ consumption) [3]. The kidneys are supplied with blood through a single renal artery arising from the abdominal aorta, which branches into two or three segmental arteries and further into several interlobar arteries. Structurally the kidney is divided into two distinct regions, the outer region (cortex) and the inner region (medulla) (Scheme 1 A). The smallest functional unit of the kidney is the nephron. It consists of the glomerulus, a capillary tuft encapsulated by the Bowman's capsule followed by the proximal tubule, the loop of Henle, the distal tubule and the collecting duct (Scheme 1 B). Within the nephron actual filtration and urine production take place in the glomerulus, which produces a primary filtrate that is further modified by selective reabsorption and secretion of specific substances along the tubular segments of the nephron [4]. Glomerular filtration of the blood occurs through the glomerular filtration barrier (GFB), a three-layered structure which comprise of fenestrated glomerular endothelial cells, the glomerular basement membrane (GBM) and visceral epithelia cells, the podocytes [5]. This structure serves a selective permeability with water and small molecules (glucose, salt and amino acids) are free to pass, while it is partial impermeable towards albumin. Of the GFB, podocytes are thought to be the most affected cells in the pathogenesis of MN [6].



Scheme 1: Structure of the kidney and nephron. (A) Longitudinal section of the kidney with the most important anatomic structures labeled, modified from [4, 7]. **(B)** Scheme of two nephrons, the smallest functional unit of the kidney, modified from [4, 7]. Created with BioRender.

1.1.1 The podocyte

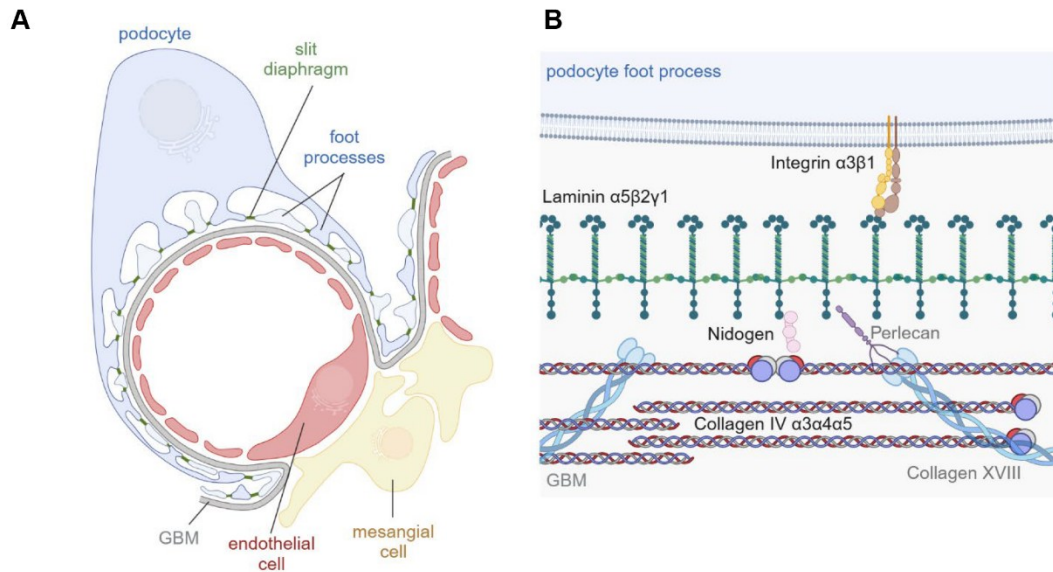
Podocytes are highly differentiated cells, which derive from the mesenchyme during nephrogenesis [8]. Their main biologic functions are to synthesize GBM components, maintain and stabilize the GFB and regulate glomerular filtration through the slit diaphragm additional to the clearance of the GFB [6]. Morphologically podocytes comprise a cell body with long branching cellular processes, the so called major processes which further branch into foot processes (FP) [5] (Scheme 2 A). Furthermore, podocytes exhibit an apical-basal polarity, perpendicular to the GBM to orient the podocyte between the GBM and the urinary space. This polarity is separated by cell-cell junctions connecting the interdigitating FPs, also called the slit diaphragm (SD) [9]. The SD serves as a molecular sieve, limiting the passage of albumin and other macromolecules [5]. Furthermore, it appears as a continuous band between adjacent FP [10], with the type 1 transmembrane protein nephrin spanning the gap and probably overlapping in *trans* configuration in the middle of the gap. Besides nephrin, neph1 and podocin are essential for the development and maintenance of the SD [11]. Nephrin and neph1 together provide an adjustable morphology of the barrier, in which the shorter neph1 molecules are located to the more basal parts of the SD close to the GBM and the longer nephrin molecules more apically [12]. Podocin, a cytoplasmic anchor protein, however, is thought to act as a linker between the plasma membrane and the cytoskeleton [13]. Next to the filter function, protein components of the SD

serve as a signaling complex to regulate FP plasticity, connect the SD to the actin cytoskeleton and anchor the FP to the GBM [11]. The cytoskeleton is important for contractility, cell shape and polarity of podocytes [5]. Major processes and the cell body contain microtubules as well as intermediate filaments [14]. In podocyte FPs the cytoskeleton is composed of actin filaments, which run longitudinally in the FP as a central actin bundle and a cortical actin network at the cell periphery [15]. Together with α -actinin and myosin, actin forms the contractile apparatus of the FP [14]. Actin bundles of the FP connect to the intermediate filaments and microtubules of the major processes [16]. Furthermore, FP are attached to the GBM through adhesion complexes via integrins and dystroglycans [17], to be able to withstand filtration forces [18]. Next to the podocytes, the GBM is another key component of the GFB and through the regulation of its components by podocytes affected by MN as well.

1.1.2 The glomerular basement membrane

The glomerular basement membrane (GBM) is responsible for the size selectivity of the GFB [19]. It is formed during nephron development by the fusion of two separate basement membranes which are produced by endothelial cells and podocytes [19, 20]. The GBM is comprised of laminin, collagen IV, nidogen and the proteoglycans agrin, perlecan and collagen XVIII [21], with laminin and collagen forming the two major networks [22] (Scheme 2 B). Laminins are heterotrimeric glycoproteins comprising α -, β - and γ -chains, which are essential for the formation of a functional GBM [19]. During glomerular development and maturation laminin and collagen IV isoforms change [20]. While in the developing GBM laminin $\alpha1\beta1\gamma1$ and $\alpha5\beta1\gamma1$ and collagen IV $\alpha1\alpha1\alpha2$ isoforms are expressed, the mature GBM contains laminin $\alpha5\beta2\gamma1$ and collagen IV $\alpha3\alpha4\alpha5$ isoforms. Proper GBM assembly involves the α -chain of laminin $\alpha5\beta2\gamma1$ binding to the α -subunit of integrin $\alpha3\beta1$ or α -dystroglycan, to mediate adhesion of podocyte FP to the GBM. Laminin $\alpha5\beta2\gamma1$ molecules polymerize through binding of their N-terminal arms and further connect to the collagen IV network through nidogen [19]. Collagen IV comprises the three α -chains $\alpha3\alpha4\alpha5$ which assemble in the extracellular space and form a network through cross linking of four 7S domains at the N-terminus or two neighboring C-terminal NC domains of collagen IV [19, 22].

Introduction



Scheme 2: The podocyte and the glomerular basement membrane in the glomerulus. (A) Schematic view of a glomerular capillary with endothelial cells (red), the glomerular basement membrane (GBM, grey) and the podocyte (blue). The interdigitating foot processes of two podocytes (blue and light blue) are connected by the slit diaphragm (green), as a specialized cell-cell junction. Modified from [23]. **(B)** Detailed scheme of the glomerular basement membrane (GBM) with its most prominent components. Modified from [19]. Created with BioRender.

1.2 Membranous nephropathy

Membranous nephropathy (MN) is next to focal segmental glomerulosclerosis (FSGS), minimal change disease (MCD) and diabetes, the most common cause of nephrotic syndrome, the clinical hallmark of podocyte injury. Nephrotic syndrome is characterized by proteinuria of 3.5 g/24h (normal protein excretion <150 mg/24h [24]), hypoalbuminemia, edema and hyperlipidemia [1]. MN is classically divided into primary and secondary MN, where about 70-80% of MN cases are of primary origin [25]. Primary MN, also referred to as idiopathic MN is an autoimmune disease caused by autoantibodies towards an intrinsic antigen [26]. Those autoantibodies are directed against podocyte FP antigens, which initiate disease by binding their targets. The hallmarks of MN are electron-dense immune deposits which comprise IgG (IgG4 predominantly) and to date only partially identified corresponding antigens, a thickened GBM [27] and podocyte FP effacement [28] (Scheme 3). Immune deposits are described to activate the complement system and further co-localize with the membrane attack complex of the complement, which inserts into the podocyte membrane and cause cell injury [29, 30]. Further, oxidative stress occurs through production of reactive oxygen species (ROS) [31], and alterations in protein

Introduction

degradation systems are found in MN [32]. The disease outcome of MN is very heterogenous, with about 40% of patients undergoing spontaneous remission, while another 30% face end-stage renal disease (ESRD) with the need of dialysis or a kidney transplant. About 40% of patients which received a kidney transplant are likely to face recurrence of MN or even lose their graft [27], caused by high serum levels of anti-PLA₂R1 autoantibodies [33, 34]. Secondary MN occurs within systemic autoimmune diseases such as systemic lupus erythematosus (SLE), infections with for example hepatitis B or C, or is drug- or malignancy-related [26], and is not further described and investigated in this study.

The first identified human antigen in idiopathic MN was the neutral endopeptidase (NEP) by Debiec *et al.* in 2002. This antigen was identified in an alloimmune antenatal MN, in which neonates develop renal complications due to NEP antibodies produced by the NEP-deficient mother [35, 36]. In 2009 the predominant MN antigen phospholipase A₂ receptor 1 (PLA₂R1) was discovered [37], followed by thrombospondin type-1 domain containing 7A (THSD7A) in 2014 [38]. Both are podocyte foot process-located transmembrane glycoproteins [29]. Depending on the investigated cohort, 50-80% of MN patients exhibit autoantibodies against PLA₂R1 and only 1-3% against THSD7A [39]. Approximately 70% of MN cases are either positive for PLA₂R1 or THSD7A. About 30% of patients remain of unknown target. However, in recent years, new potential target antigens have been discovered. Those include the intracellular proteins aldose reductase (AR), superoxide dismutase 2 (SOD2) [40], α -enolase (α ENO) [41] and Ubiquitin C-terminal Hydrolase L1 (UCH-L1) [32, 42]. Even though patients exhibit antibodies (of IgG4 subtype) directed against AR, SOD2 and α ENO, it is not clear whether those antibodies are causative of disease induction [40, 41]. Similar observations were made for the deubiquitinating enzyme UCH-L1, which is *de novo* expressed in podocytes in MN [32, 42]. Likewise, autoantibodies directed against UCH-L1 could be found in MN patients [40, 43]. By using mass spectrometry analyses of micro-dissected glomeruli, further antigens have been described [44]. Among those were exostosin 1/2 (EXT 1/2), which were present along the GBM. Nevertheless, antibodies against EXT1 or EXT2 could not be detected in patients [45]. Exostosins are glycosyltransferases that are involved in synthesis of the heparan sulfate backbone which in turn is essential for heparan sulfate proteoglycans, a major component of the GBM [45]. The neural epidermal growth factor-like 1 protein (Nell-1) was found to be another dominant antigen with approximately 10% of MN patients

Introduction

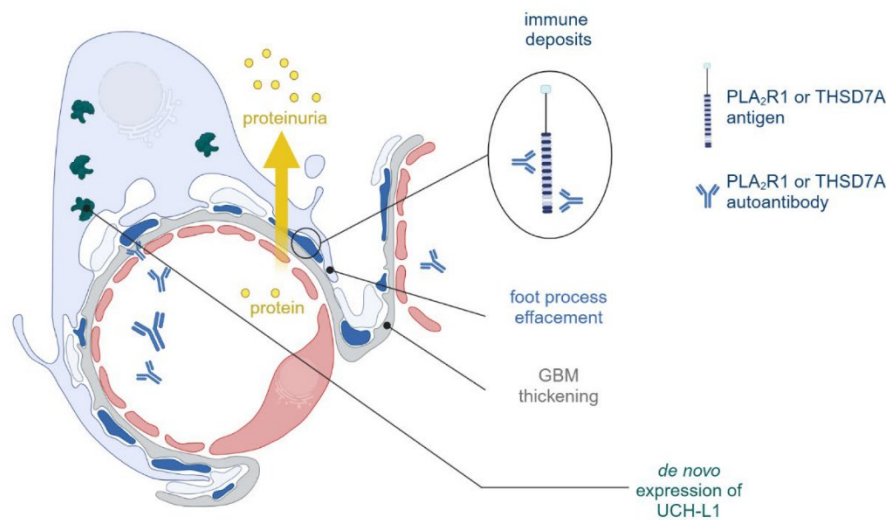
exhibiting antibodies against Nell-1 [39, 46]. Nell-1 is a secreted protein, which is strongly expressed in neurons and in MN patients was found to deposit along the GBM [46]. Further semaphorin 3B could be identified as an antigen, specifically present in pediatric MN patients with circulating antibodies. Semaphorins are secreted or transmembrane bound proteins which were first identified as axon guidance proteins in neurons [47]. Apart from that the neural cell adhesion molecule 1 (NCAM1) was identified by Caza *et al.* in 2021, especially in patients with systemic lupus erythematosus. In addition to mass spectrometry analysis of micro-dissected glomeruli, a protein G immunoprecipitation was performed from frozen kidney tissue to confirm NCAM1 as a putative antigen. Next to the typical co-localization with IgG, anti-NCAM1 antibodies were found in the sera of MN patients [48]. Additionally, seven other putative MN antigens have been identified in 2023, namely FCN3, CD206, EEA1, SE6L2, NPR3, MST1 and VASN, which accumulate within the patient glomeruli. However, no circulating antibodies against those proteins have been found yet [49]. Together these findings demonstrate a high degree of heterogeneity in terms of antigens involved in MN pathogenesis.

Autoantibodies, especially for PLA₂R1, Nell-1 and THSD7A are found circulating in patient sera and further lead to *in situ* formation of immune complexes [27]. Those antibodies were found to be causative of MN as reoccurrence of THSD7A-associated MN could be observed in a patient after kidney transplantation [50]. A similar observation was made in a PLA₂R1-associated MN patient [33]. Apart from that, studies demonstrated a correlation of autoantibody levels as well as intramolecular epitope spreading and remission risk in PLA₂R1-associated MN patients [51]. The concept of epitope spreading encompasses that new epitopes within the same antigen are additionally recognized by autoantibodies over time. PLA₂R1-associated MN patients which exhibit autoantibodies against the predominant PLA₂R1 epitope (CysR) as well as “secondary” PLA₂R1 epitopes (CTLD1 and CTLD7) show a poor clinical outcome [52]. In addition to patients with intramolecular epitope spreading, a subset of patients was found to exhibit intermolecular epitope spreading. Those patients exhibit additional autoantibodies directed against the intracellular antigens SOD2 and α ENO next to the “primary” PLA₂R1 antigen and are found to have worse clinical outcomes. The authors proposed that autoantibodies targeting the intracellular proteins appear during pathogenesis of MN as a “second wave”, possible due to intermolecular epitope

Introduction

spreading [53]. How antigens reach the immune system for this to occur, is not known, as podocytes reside within an immunologically protected niche [54].

Together these findings indicate that MN is a heterogeneous disease [44]. Therefore, it is critical to further characterize MN antigens and different autoantibodies in respect of their propensity to initiate disease, and influence disease progression.



Scheme 3: Hallmarks of membranous nephropathy (MN). Schematic view of the glomerular capillary during MN conditions with *in situ* formation of immune deposits, which consist of autoantibodies that bind their respective antigen (PLA₂R1 or THSD7A) at the base of the foot processes. Morphologic hallmarks of MN are, foot process effacement and GBM thickening. UCH-L1 is *de novo* expressed in injured podocytes, especially in MN. Modified from [55]. Generated with BioRender.

1.3 Rodent models of membranous nephropathy

To investigate pathomechanisms of MN in depth, animal models are beneficial. They have the advantage of a whole organism in comparison to rather basic single cell investigations and further circumvent ethical policies in regard of human material. Especially rodent models have been developed in the past to allow mechanistic studies. The first model to study MN was the so called Heymann nephritis (HN), a model in which MN is induced either passively or actively in rats. To induce passive HN, rats are immunized with sheep or rabbit tubular brush border antibodies while in active HN immunization takes place with a rat kidney antigen extract. Those models show histopathological and clinical aspects of MN, making them a suitable model to study pathophysiology of MN [25]. In HN, the podocyte foot processes protein megalin (gp330) is the main antigen, which is found in immune deposits together with

Introduction

corresponding antibodies. Further in this model the involvement of the complement, especially of the membrane attack complex could be identified [56]. Megalin, however, is not found in humans, making this model not sufficient to study detailed mechanisms underlying MN in humans. With the identification of the first human MN antigens, antigen specific mouse models could be developed, which additionally provide the advantage of a broad variety of genetically modified mouse strains [25]. Since PLA₂R1, unlike THSD7A, is not endogenously expressed in rodents, most current MN mouse models are based on THSD7A [57, 58]. The rodent THSD7A protein shows 90% sequence homology with the human protein [28]. A well-defined model is the heterologous model of THSD7A-associated MN (passive THSD7A-MN model). For this model, anti-THSD7A antibodies are produced by immunization of rabbits with full-length THSD7A plasmids (human and mouse). Immunized rabbits then produce antibodies against THSD7A [59]. Purified rabbit anti-THSD7A antibodies and as a control purified pre-immune (before immunization took place) serum of the rabbits are injected into BALB/c mice to induce THSD7A-associated MN. Mice develop typical clinical aspects of MN such as proteinuria and hyperlipidemia over a time course of 14 days. Further, injected rabbit anti-THSD7A antibodies can be detected in a granular pattern and in co-localization with THSD7A antigen along the GBM in immunofluorescence staining. In addition, GBM thickening as well as electron-dense immune deposits can be shown by ultrastructural analysis. However, the induction of THSD7A-associated MN is mouse strain-dependent as C57BL/6 and DBA/J1 mice do not develop nephrotic range proteinuria [59]. Additionally, this model lacks the possibility to investigate autoantibody formation. Recently Seifert *et al.* introduced an antigen-specific autoimmune model of MN (active MN model), in which BALB/c mice are immunized with THSD7A domain proteins, representing the predominant recognized THSD7A epitopes. To induce disease, mice are immunized for a total of four times with either immunogenic THSD7A domains or PBS as a control each in combination with Freud's adjuvant. THSD7A antibodies are present after 4 weeks, and further proteinuria starts to occur after 5 weeks of initial disease induction. Mice show significant signs of MN such as hypoalbuminemia, hyperlipidemia and weight gain, when observed over a total period of 20 weeks. Furthermore, mouse autoantibodies co-localize with THSD7A along the GBM [60]. Although these two mouse models give detailed insights into MN pathogenesis, specific mechanisms for PLA₂R1-associated MN development, the most common form of MN in humans, remain to be further

investigated in detail. As described above, mice do not express PLA₂R1 endogenously, making the analysis more difficult than for THSD7A. By genetically generating mouse (m)PLA₂R1-positive mice which are immunized with rabbit anti-PLA₂R1 antibodies a novel PLA₂R1-associated MN model was developed. Rabbit anti-PLA₂R1 antibodies were generated by cDNA immunization of rabbits [61]. Those antibodies are sufficient to cause MN in mPLA₂R1-positive mice, demonstrated by the development of proteinuria, hypercholesterolemia and further by the accumulation of rabbit-IgG along the GBM as well as the presence of electron-dense immune deposits [60].

The heterologous (passive) THSD7A-associated MN model [59] is of great importance for this work, as it is the model used for the *in vivo* studies.

1.4 Protein degradation and the deubiquitinase Ubiquitin C-terminal Hydrolase L1 (UCH-L1)

As described earlier an upregulation of protein degradation systems occurs in MN [32]. Two major pathways, the autophagosome-lysosome pathway (ALP) and the ubiquitin proteasome system (UPS) ensure degradation of misfolded proteins [62]. [62]. The ALP mainly degrades large protein aggregates or damaged organelles [63, 64]. It can degrade extracellular proteins, delivered via endocytosis as well as cytosolic proteins and organelles, delivered by autophagy [65]. Micro-autophagy, chaperone mediated autophagy and macro-autophagy are the three types of autophagy, with macro-autophagy as the best characterized form that is further believed to be the predominant type of autophagy [62-64]. Macro-autophagy is characterized by the engulfment of the substrate by a double-membrane structure (phagophore), which then forms the autophagosome [63]. Subsequently autophagosomes fuse with lysosomes for degradation of their engulfed content by lysosomal hydrolases [63, 64]. While the ALP can degrade large extracellular as well as intracellular proteins and aggregates, the UPS is responsible for degradation of mostly short-lived, regulatory, damaged and misfolded cytosolic proteins [55]. However, recent studies could show that especially podocytes of the renal filtration barrier depend on an intact proteasome system [66].

1.4.1 The ubiquitin proteasome system

Degradation by the proteasome is dependent on the ubiquitination of proteins. Ubiquitin, a 76-amino acid protein, is conjugated to proteins by an adenosine triphosphate-consuming enzymatic process [55, 62]. This process involves E1, E2 and

Introduction

E3 ubiquitin ligases, which attach ubiquitin to the substrate either as ubiquitin monomers or as chains (polyubiquitination). In humans over 1000 different E3 enzymes are identified, which ensure substrate specificity of the ubiquitination process [55]. Proteins are tagged with either one single ubiquitin molecule (monoubiquitination) or with linear or branched ubiquitin chains (polyubiquitination) [62, 67]. Polyubiquitination occurs predominantly at lysine (lys) residues of ubiquitin, and especially lys48-linked polyubiquitination leads to degradation by the proteasome [55, 62]. The proteasome is a complex protease, which exists in different structural forms. The 20S core particle (CP) consists of 28 subunits, which are arranged as a cylindrical stack with 2 outer α -rings and 2 inner β -rings. The β 1, β 2 and β 5 subunits serve as three distinct proteolytic enzymes. Together with one 19S regulatory particle (RP) the 20S CP forms the 26S, or with two 19S RPs the 30S proteasome [55]. Proteasomal degradation of ubiquitinated proteins involves a cascade of substrate binding, deubiquitination at the 19S RP, which is dependent on ATPase function of 19S RP subunits and protein unfolding [68]. Subsequently, proteins translocate to the 20S CP and are cleaved into short peptides by the β -subunits [68].

Ubiquitination of proteins is a reversible process and is tightly regulated by deubiquitinating enzymes (DUBs). To prevent proteasome congestion, they control protein turnover and recycle ubiquitin molecules [55]. To date about 100 DUBs are identified in human [69], divided into two major classes, metalloproteases and cysteine proteases, latter being further divided into six families. Ubiquitin C-terminal Hydrolases (UCH) are one of the six families of cysteine proteases. This family contains four members in mammals, UCH-L1, UCH-L3, UCH-L5 and BAP1 [70].

The central part of cysteine proteases is a reactive cysteine residue, which appears in two different states, an inactive state containing an inactive thiol (-SH) or an active state with a reactive thiolate ($-S^-$) group. Transition between active and inactive states is caused by conformational changes through substrate binding [70]. Deubiquitination occurs through hydrolyzation of the isopeptide bond [69, 70]. Cysteine proteases are highly susceptible to oxidative stress modification, due to cysteine oxidation and thus inhibition of the active site enzymatic activity [70]. Of the cysteine protease UCH family the DUB Ubiquitin C-terminal Hydrolase L1 (UCH-L1) is of great interest, as the work centers around its role in MN.

1.4.2 Ubiquitin C-terminal Hydrolase L1

UCH-L1 also known as protein gene product 9.5 (PGP9.5) is a small protein with a size of approximately 25 kDa [71]. It is mainly expressed in neurons where it can make up to 5% of total brain protein content [67]. In neurons UCH-L1 contributes to neuronal differentiation, regulation of synaptic structure and function as well as cell process formation [72]. Besides the abundant expression in neuronal tissue, UCH-L1 is found in the testis as well as pancreatic, colorectal and invasive breast cancer cells [67]. UCH-L1 is a mainly cytosolic protein, which can associate with plasma membranes [73] and is also hypothesized to be expressed on the cell surface of podocytes, thus targetable by autoantibodies [74].

Structurally UCH-L1 forms a “gordian” knot, one of the most complicated protein structures discovered so far. The loop spanning the active site of the enzyme, restricts access of larger proteins to the active site, leading to a substrate specificity. Structural changes of UCH-L1, associated with protein unfolding, lead to the exposure of the hydrophobic core and a toxic gain-of-function, probably through aberrant protein interactions [67]. UCH-L1 function appears to be diverse. As a deubiquitinase it is described to have only relatively weak hydrolase activity compared to UCH-L3 but is also found to possess a ubiquitin ligase activity [75]. Furthermore, it is well described to associate with and thereby stabilize mono-ubiquitin [76, 77].

1.5 The role of UCH-L1 in diseases

Alterations and loss of the complex UCH-L1 protein are associated with diseases. In mice a total loss of UCH-L1 through an in-frame deletion in the *Uchl1* gene, cause a gracile axonal dystrophy phenotype which leads to sensory ataxia, followed by hind limb paralysis and early death [67]. In humans a genetic point mutation of UCH-L1 leading to an exchange of isoleucine at position 93 to a methionine, the so called I93M mutation, is associated with Parkinson’s disease (PD) [78]. This mutation causes partial loss of catalytic activity [78] and is associated with decreased solubility of the protein [79]. In addition, oxidative modification of UCH-L1 is linked to PD and Alzheimer’s disease (AD) [80]. The oxidative-modified form of UCH-L1 as well as the I93M mutated form of UCH-L1 are described to share structural similarities. Both exhibit altered interaction properties with other proteins, such as tubulin [79] and the lysosome-associated membrane protein type 2A [81].

Introduction

In the kidney UCH-L1 is found to be *de novo* expressed in podocytes of MN patients [32, 42], which further correlates with elevated amounts of cytoplasmic ubiquitin abundance [42]. Similar observations were made in Heyman Nephritis, the rat model of MN [82]. As UCH-L1, especially the non-functional form of UCH-L1 (I93M or oxidative-modified) have been shown to abnormally interact with other proteins in neurodegenerative diseases, it is very likely that UCH-L1 exhibits abnormal functions in the kidney as well. In MN UCH-L1, especially non-functional UCH-L1, is associated with podocyte injury. As such UCH-L1 binds to the proteasome and thereby inhibits its proper function [43]. UCH-L1 is also involved in podocyte hypertrophy by stabilization of the cell cycle regulator p27Kip1 [83] and mediates tumor necrosis factor-induced podocyte necroptosis [84]. Lastly, UCH-L1 expression correlates with disrupted homeostasis of FP proteins such as α -actinin-4 [42].

As described previous a subset of MN patients exhibit anti-UCH-L1 autoantibodies [40, 43], additionally to the established MN-associated primary autoantibodies against PLA₂R1 or THSD7A. These anti-UCH-L1 autoantibodies were found to predominantly recognize the non-functional form of UCH-L1 and are linked to non-remitting MN [43].

1.6 Extracellular vesicles

Extracellular vesicles (EVs) might play a role in MN as a potential exit route for MN antigens to either contribute to the clearing of autoantibody bound antigen or to autoantibody formation by presenting the antigen to the immune system. EVs are defined as lipid bilayer membrane enclosed particles, which are released by cells [85]. Initially EVs were described to function as “waste carriers” for excretion of unneeded cellular compounds [86]. However, emerging research on EVs in the past years revealed more complex biological functions of EVs, including mediation of cell-cell interactions and signaling in homeostasis and pathology [86, 87]. Structurally, EVs comprise a rather heterogenous group on account of their size, origin and cargo. Regarding their size EVs are divided into small EVs (< 200 nm) medium (200-800 nm) and large sized EVs ($\geq 1 \mu\text{m}$) [85, 88]. Based on their origin EVs are either classified as exosomes, originating from internal cell compartments, which are released via multivesicular bodies, a part of the lysosomal degradation system [85, 89], or ectosomes, which are shed through plasma membrane budding [86]. In view of their heterogeneity, EV composition differs in the various EV populations and is thought to be related to function and origin of the respective EVs [86, 87]. Therefore, definitions

Introduction

of EVs beyond their size and origin is difficult since no universal markers for ectosomes, exosomes or other EV subtypes are defined yet [85]. However, some proteins are found to be general present on EVs, including Annexin A1, tetraspanins (CD9, CD63 and CD81), TSG101, ALIX, Flotillin-1 as well as adhesion molecules such as integrins [86, 87]. After secretion, EVs can travel even for relatively long distances and reach potential recipient cells, where they either activate cell surface receptors, induce signaling or fuse with the target cell [86, 90].

The role of EVs in diseases is complex and yet not fully understood. They have been reported to play a role in immune response via different, sometimes opposing mechanisms. In innate immunity, EVs are found to have pro-inflammatory as well as anti-inflammatory effects and further play a role in lymphocyte development and antigen presentation. Moreover, through their ability to carry self or donor antigens and by activating inflammatory pathways, EVs are involved in autoimmunity and transplant rejection [88].

In the kidney, EVs are secreted by all cells facing the urinary space, namely podocytes, as well as cells of the proximal and distal tubule, and the collecting duct [91]. Urinary EVs are thought to be able to reflect the status of the kidney, and on account of that are associated with podocyte injury and proteinuria [90, 92].

Therefore, EVs might play an important but not yet fully understood role in renal disease development through clearing mechanisms and/or by contributing to autoimmunity.

1.7 Objectives

Previous data show anti-UCH-L1 autoantibodies of MN patients predominantly recognize UCH-L1^{I93M}, suggesting a secondary formation scenario towards oxidative-modified UCH-L1 [43]. We therefore hypothesize that UCH-L1 autoantibodies contribute to aggravate MN. Two possible mechanisms are conceivable: 1) Antigen-unspecific mechanisms, in which an enhanced antibody burden of glomerular deposition leads to enhanced podocyte injury, GBM alterations and an increased need for subepithelial space clearance. 2) Antigen-specific mechanisms as a result of anti-UCH-L1 autoantibodies affecting the biological function of the deubiquitinating enzyme. Further it is unknown through which route these autoantibodies are formed.

Introduction

A possible mechanism is the podocyte release of oxidative-modified UCH-L1 through extracellular vesicles (EVs).

In this study the pathogenicity of secondary anti-UCH-L1 antibodies was investigated in *in vitro* as well as *in vivo* models in order to further the understandings in the basal mechanisms, leading to anti-UCH-L1 antibody formation in MN. Further, extracellular vesicles were examined as an antigen exit route in patient material, as well as *in vitro* and *in vivo* models. Together these data will provide knowledge about the pathophysiological significance and origin of secondary autoantibody formation.

2 Material and Methods

2.1 Material

2.1.1 Chemicals, kits and antibodies

Table 1: Chemicals

Chemical	Supplier	Order number
Acrylamid 40%, 3.3% C, 29:1	Serva	10680.01
Adenosine 5' triphosphate disodium salt (ATP)	Sigma-Aldrich	A3377
Agarose	Sigma	A-5030
Albumin Standard	Thermo Scientific	23210
Aqua ad iniectabilia	Braun	2351744
Bioethanol 99%, denatured	Chemsolute	2211.5000
Bovine Serum Albumin (BSA)	Sigma-Aldrich	A7030-50G
Bromphenol Blue-Xylene Cyanole dye solution	Sigma-Aldrich	B-3269
BupH Phosphate Buffered Saline	Thermo Scientific	28372
Carbonate-Bicarbonate Buffer	Sigma Aldrich	C3041-50CAP
Chloroform	J.T. Baker	7386
Collagen type IV from human cell culture	Sigma-Aldrich	C6745-1ML
Collagenase from Clostridium h. Typ IA	Merk	C9891-1G
Creatinine	Sigma-Aldrich	C4255-10g
Cy5-Ub-VME	UbiQ	UbiQ-071
Dimethylsulfoxide (DMSO)	Roth	4720.2
Dithiothreitol (DTT)	Fluorochem	M02712
DMEM	Gibco	41965-039
DNase I	Roche	101041590011
dNTP Mix	Thermo Scientific	R0242
DPBS	Gibco	14190-094

Material and Methods

Dodecylsulfate-Na-salt (SDS)	Serva	20765.03
DreamTaq™ Green DNA Polymerase	Thermo Scientific	EP0713
EGTA	Roth	3054.2
Epoxomicin	Enzo	BML-PI127-0100
Ethanol, absolute	Supelco	1.00983.1000
EZ-Link™ Sulfo-NHS-LC-Biotin, Sulfosuccinimidyl-6-(biotinamido) Hexanoate	Thermo Scientific	21335
Fetal Bovine Serum (FBS), hi	Gibco	10500-640
FBS, exosome depleted	Gibco	A27208-01
Fluoromount-G	SoutherBiotech	0100-01
Glycine	Roth	3908.2
Glycerol	Sigma-Aldrich	G9012
Hank's Balanced Salt Solution (HBSS)	Gibco	14170-088
IgG Elution Buffer	Thermo Scientific	21004
ISF-1 medium	PAN Biotech	P04-995968
Isoflurane Sedaconda® 100% V/V	sedanamedical	
ITS solution II	PAN Biotech	P07-03200
Magnesium chloride (MgCl ₂)	Panreac Applichem	141396.1211
Medunasal®-Heparin 500 I.U.	Sintetica	0373
2-Mercaptoethanol	Gibco	31350-010
NaCl 0.9 %	B.Braun	
N,N,N',N'-Tetramethylethylenediamine (TEMED)	Sigma-Aldrich	T9281-50ml
Normal horse serum	Vector Laboratories	VEC-S-2000
Penicillin Streptomycin	Gibco	15140-122
Phenylmethanesulfonylfluoride (PMSF)	Sigma-Aldrich	P7626-25G
Phosphoric acid (H ₃ PO ₄) 85%	Roth	6366.1

Material and Methods

Ponceau S solution	Serva	33427.01
Powdered milk	Roth	T145.2
PowerUp™ SYBR™ Green Master Mix	Applied Biosystems	A25742
ProLongGold	Thermo Scientific	P10144
Proteinase, bacterial – Type XXIV	Sigma-Aldrich	P8038
2-Propanol	Roth	CP41.3
Puromycin	Sigma-Aldrich	P7255-25MG
Rnase ZAP	Sigma-Aldrich	R2020
RNA-Solv Reagent	Omega	R6830-02
ROTI®Quant universal	Roth	0120.2
RPMI 1604 medium, GlutaMAX™-I supplement	Gibco	61870-010
SIGMAFAST™ Protease Inhibitor Cocktail Tablets, EDTA-Free	Sigma-Aldrich	S8830-20TAB
Sodium azide (NaN ₃)	Sigma-Aldrich	S2002-100G
Sodium chloride	ChemSolute	6307.1000
Sodium Pyruvate	Gibco	11360-039
SuperBlock™ Blocking Buffer in TBS	Thermo Scientific	37535
SuperSignal™ West Pico PLUS Chemiluminescence Substrate	Thermo Scientific	34578
SuperSignal™ West Femto Maximum Sensitivity Substrate	Thermo Scientific	34095
Target Retrieval Solution, Citrate pH 6	Dako	S236984-2
Tissue-Tek®	Sakura	4583
TMB ELISA Peroxidase Substrate	Aviva	OORA01684

Material and Methods

p-Toluenesulfonic acid monohydrate (PTSA)	Sigma-Aldrich	402885
T-PER™ Tissue Protein Extraction Reagent	Thermo Scientific	78510
Tris	T.H. Geyer	8085.1000
Tris Buffered Saline, with BSA, pH 8.0	Sigma-Aldrich	T6789-10PAK
Trypsin-EDTA 0.05 %	Gibco	25300-054
Tween 20	Roth	9127.1
10 % Tween 20	Bethyl	E108
T-x-100 (Triton)	Sigma-Aldrich	T8787
Urea	Sigma Aldrich	U0631-500g

Table 2: Isolation systems and reaction kits

Kit	Supplier	Order number
Creatinin-Kit Jaffe	Hengler Analytik	114444
jetPEI®	Polyplus-transfection	101000053
Nab™ Protein A/G Spin Column	Thermo Scientific	89962
rDNase Set	Macherey-Nagel	740963

Table 3: DNA and Protein ladder

Marker	Supplier	Order number
1 Kb Plus DNA Ladder	Invitrogen	10787026
BlueElf Prestained Protein Marker	Jena Bioscience	PS-105
CozyXL™ Prestained Protein Ladder	highQu	<prl0302c1

Table 4: Antibodies and dyes

Antibody	Supplier	Host	Dilution
Antibodies for disease induction			
Anti-THSD7A	self-made	Rabbit	-
Unspecific rabbit-IgG	Sigma, I5006	rabbit	-
Rabbit serum	Bio & Sell, RAB.SE.0100	rabbit	-
Anti-UCH-L1 (U104)	Own production (hybridoma monoclonal ab)	rat	-
Unspecific rat-IgG	Sigma, I4131	rat	-
Primary antibodies			
(Pan-)14-3-3 (H-8)	Santa Cruz, Sc1657	mouse	WB 1:1000
(Pan-)14-3-3 (H-8) AF546	Santa Cruz, Sc1657 AF546	mouse	ImageStream 1:100
β -actin	Sigma, A5441	mouse	WB 1:10000
Annexin A1	Abcam, ab214486	rabbit	WB 1:1000
Biotin	Thermo Fisher, #PA126792	goat	WB 1:1000
Collagen IV	Southern BioTech, 1340-01	goat	WB 1:500 IF 1:400
Flotillin-1	BD Biosciences, 61082	mouse	WB 1:1000
Mouse Albumin	Bethyl, A90-134A	goat	ELISA 1:100
c-Myc	Santa Cruz, Sc-40	mouse	WB 1:400
Nephrin	ProGene, GP-N2	guinea pig	WB 1:1000 IF 1:200
PGP9.5 (UCH-L1)	Abcam, ab27053	rabbit	WB 1:1000
THSD7A	Merk (Atlas), HPA000923	rabbit	WB 1:1000

Material and Methods

THSD7A c-terminal	Paul Saftig, Kiel	rabbit	WB 1:1000
TSG-101	Abcam, ab125011	rabbit	WB 1:1000
UCH-L1 (PGP 9.5)	Abcam, ab27053	rabbit	WB 1:1000
UCH-L1 clone 13C4	Abcam, AB8189	mouse	WB 1:500
UCH-L1 (U104)	Own production (hybridoma monoclonal ab)	rat	WB 1:200 (milk)
Western blot secondary antibodies			
anti-goat HRP	Jackson ImmunoResearch, 705-035-147	donkey	1:10000
anti-guinea pig HRP	Jackson ImmunoResearch, 706-175-148	donkey	1:10000
anti-mouse HRP	Jackson ImmunoResearch, 715-035-150	donkey	1:10000
anti-rabbit HRP	Jackson ImmunoResearch, 711-035-152	donkey	1:10000
Mouse TrueBlot® ULTRA: Anti-Mouse Ig HRP	Rockland, 18-8817-33	rat	1:10000
Rabbit TrueBlot®: Anti-Rabbit IgG HRP	Rockland, 18-8816-33	mouse	1:10000
ELISA secondary antibodies			
anti-mouse albumin HRP	Bethyl, #A90-13P	goat	1:40000
Immunofluorescence secondary antibodies			

Material and Methods

anti-guinea pig AF488	Jackson ImmunoResearch, 706-225-148	donkey	1:100
anti-rabbit AF488	Jackson ImmunoResearch, 711-545-152	donkey	1:100
anti-rabbit AF546	Jackson ImmunoResearch, 711-165-152	donkey	1:100
anti-rabbit AF647	Jackson ImmunoResearch, 711-175-152	donkey	1:100
anti-goat AF546	Jackson ImmunoResearch, 705-165-147	donkey	1:100
anti-goat AF647	Jackson ImmunoResearch, 305-606-045	rabbit	1:100
Dyes			
Hoechst 33342	Invitrogen, H3570	-	IF 1:1000
MemBrite Fix 594/615	Biotium, 30096-T	-	ImageStream 1:200
Streptavidin AF 488	Vector Laboratories, SA- 5001	-	IF 1:100
Streptavidin HRP	Pierce, 21130	-	WB 1:10000

2.1.2 Materials, devices and software

Table 5: Consumable materials

Material	Supplier	Order number
BD Micro-Fine™ U-100 Insulin	Becton Dickinson	324826

Material and Methods

Cell Scraper, Small, 2-POS Blade	Sarstedt	83.3950
Cell strainer, 100 µm	Sarstedt	83.3945.100
Cover slips, High Precision	Marienfeld	0107222
Criterion Empty Cassettes, 18 well	BIO RAD	#3459902
Criterion Empty Cassettes, 26 well	BIO RAD	#3459903
Criterion™ TGX Stain-Free™ Precast Gels, 4-15%, 18 Well Comb	BIO RAD	#5678084
Criterion™ TGX Stain-Free™ Precast Gels, 4-15%, 26 Well Comb	BIO RAD	#5678085
CultureSlides, 8 chamber polystyrene vessel	Falcon	354108
Dynabeads™ M-450 Tosylactivated	Invitrogen	2801713
ELISA plate, High Binding, F	Sarstedt	82.1581.200
Extra thick blot paper	BIO RAD	1703958
Filter 100 µm	Sarstedt	83.3945.100
Filter tip, 1000 µl	Sarstedt	70.3060.255
Filter tip, 100 µl	Sarstedt	70.3030.255
Filter tip, 10 µl	Sarstedt	70.3010.255
Filter tip, 2.5 µl	Sarstedt	70.3010.265
Immobilon®-P Transfer Membrane (PVDF, 0.45 µm pore size)	Merk Millipore Ltd.	#IPVH00100
Micro tube 1.5 ml, Safe Seal	Sarstedt	72.706.400
Micro tube 2.0 ml	Sarstedt	72.691

Material and Methods

MicroAmp® Optical 96-Well Reaction Plate	Applied Biosystems	N8010560
MicroAmp® Optical Adhesive Film	Applied Biosystems	4311971
Microfuge Tube Polypropylene	Beckman Coulter Inc.	357448
Microtest Plate 96 Well, F	Sarstedt	82.1581
Mini-PROTEAN TGX Stain-Free Gels, 4-15%, 10 well comb	BIO RAD	#4568083
Mini-PROTEAN TGX Stain-Free Gels, 4-15%, 12 well comb	BIO RAD	#4568085
Mini-PROTEAN TGX Stain-Free Gels, 4-15%, 15 well comb	BIO RAD	#4568086
Ministart® Filter Unit	Sartorius	16541-K 0.22
Nanosep with 300K Omega	Pall Corporation	OD300C34
Nitrile Examination Gloves	WRP	D1100-24
Pasteur pipette, long form	Duran Wheaton Kimble	263302303
Pipette tip, 5 ml	Sarstedt	70.1183.002
Pipette tip, 1000 µl	Sarstedt	70.3050.200
Pipette tip, 200 µl	Sarstedt	70.3030.200
Pipette tip, 10 µl	Sarstedt	70.3010.255
SafeSeal tube 0.5 ml	Sarstedt	72.704
SafeSeal tube 1.5 ml, brown	Sarstedt	72.708.001
Scalpels	Dahlhausen	11.00000.522
Serological pipette 2 ml	Sarstedt	86.1252.001
Serological pipette 5 ml	Sarstedt	86.1253.001
Serological pipette 10 ml	Sarstedt	86.1254.001
Serological pipette 25 ml	Sarstedt	86.1685.001

Material and Methods

SPHERO™ Polystyrene Magnetic Particles, 2.5 % w/v, 4.17 µm	Spherotech	PM-40-10
Sterican® cannula 30G	B. Braun	4656300
Super PAP PEN	Science Services	N71310-N
Syringe 0.01 – 1 ml, Omnifix®-F Luer Solo	B. Braun	9161406V
Syringe 2 ml, BD Discardit™ II	Becton Dickinson	300928
Syringe 10 ml Inject® Luer Solo	B. Braun	4606108V
Syringe 50 ml Original Perfusor®, Luer Lock	B. Braun	8728852F-06
TC Dish 100, Standard	Sarstedt	83.3902
TC Flask T75, Standard, Vent. Cap,	Sarstedt	83.3911.002
TC Flask, T75, Suspension, Vent. Cap	Sarstedt	83.3911.502
TC Flask, T175, Suspension, Vent. Cap	Sarstedt	83.3912.502
TC-Plate, 6 Well, Standard, F	Sarstedt	83.3920
Tube 15 ml	Sarstedt	62.554.502
Tube 50 ml	Sarstedt	62.547.254
Tungsten Carbide Beads, 3mm	Qiagen	69997
Vivaspin 20, 50 000 MWCO	Sartorius	VS2032
Zeba™ Spin Desalting Columns, 7 K MWCO	Thermo Scientific	89882

Table 6: Devices

Device		Supplier
Analytic scale	Mettler AC 100	Mettler Waagen GmbH (DE)
Biological safety cabinets	Maxisafe 2030i	Thermo Fisher Scientific (US)
	HERAsafe	Heraeus (DE)
Blotter	Trans-Blot® Turbo™ Transfer System	BIO RAD (US)
Centrifuges	Centrifuge 5427 R	Eppendorf (DE)
	Centrifuge 5804 R	Eppendorf (DE)
CO ₂ incubator	BB15	Thermo Fisher Scientific (US)
Confocal microscopes	LSM800	Zeiss (DE)
	LSM980	Zeiss (DE)
Fluorescence microscope	Axio Observer A.1	Zeiss (DE)
Fridges and freezers	4°C	Liebherr (DE)
	-20°C	Liebherr (DE)
	-80°C	Tritec (DE)
Hemocytometer	Neubauer grid hemocytometer	Brand (DE)
ImageStream	ImageStreamX MkII	Cytek Biosciences (US)
Imager	Vilber Fusion FX7	Vilber Lourmat (DE)
Light microscope	Axiovert 25	Zeiss (DE)
Magnetic hotplate stirrer	HR Hei-Standard	Heidolph (DE)
Magnetic Particle Concentrator	DynaMag2™	Invitrogen/Thermo Fisher Scientific (US)
Microplate Photometer	Multiskan FC	Thermo Fisher Scientific (US)
NanoPhotometer®		Implen (DE)
Pipettes	0.5 – 5 ml	Eppendorf (DE)
	100 – 1000 µl	Eppendorf (DE)

Material and Methods

	20 – 200 µl	Eppendorf (DE)
	2 – 20 µl	Eppendorf (DE)
	1 – 10 µl	Eppendorf (DE)
	0.1 – 2.5 µl	Eppendorf (DE)
Pipetus®		Hirschman
qPCR Thermocycler	QuantStudio 5	Applied Biosystems by Thermo Fisher Scientific (US)
Shaker	Varioshake VS 8 B	Lauda (DE)
Speed Vac	Concentrator plus	Eppendorf (DE)
Spectrophotometer	EL808 Ultra Microplate Reader	BioTek Instruments (US)
Spinning disk microscope	Visitron SD-TIRF	Visitron Systems (DE)
Spin tissue processor	STP120	Thermo Fisher Scientific (US)
Steam cooker	FS10	Braun GmbH (DE)
Table centrifuge	Galaxy Mini	VWR (DE)
Thermocycler	T-1 Thermoblock	Biometra (DE)
Thermoblock	ThermoMixer® F1.5	Eppendorf (DE)
Ultracentrifuge	Optima™ MAX-TL Ultracentrifuge	Beckman Coulter (US)
Ultramicrotome	UC6	Leica (DE)
Vortexer	BR-2000	BIO RAD (US)
Water bath	Water bath	GFL, Gesellschaft für Labortechnik (DE)

Table 7: Software

Software	Version	Supplier
Adobe Illustrator	29	Adobe Inc. (US)
Adobe Photoshop	25.12.0	Adobe Inc. (US)
BioRender		Science Suite Inc. (CA)
GraphPad PRISM	10	GraphPad Software, Inc. (US)

Material and Methods

ImageJ	1.52V	Wayne Rasband, National Institutes of Health, (US)
KC Junior		BioTek Instruments (US)
Microsoft 365		Microsoft (US)
QuantStudio™ Design and Analysis Software	V1.51	Applied Biosystems by Thermo Fisher Scientific (US)
SkantIt for Multiscan		Thermo Fisher Scientific (US)
Vilber Fusion FX7 Edge	18.03	Vilber Lourmat (DE)
VisiView	V4	Visitron Systems (DE)
ZEN Blue	3.8	Zeiss (DE)

2.1.3 Plasmids

Table 8: Plasmids

Vector	Insert	Restriction sites	Comment
pCMV6-Entry	huUCH-L1 ^{WT}	<i>Sgfl/Mlul</i>	c-term. myc-flag-tag
pCMV6-Entry	huUCH-L1 ^{I93M}	<i>Sgfl/Mlul</i>	c-term. myc-flag-tag
pCMV6-Entry	mUCH-L1 ^{WT}	<i>Sgfl/Mlul</i>	c-term. myc-flag-tag
pCMV6-Entry	mUCH-L1 ^{I93M}	<i>Sgfl/Mlul</i>	c-term. myc-flag-tag

2.2 Methods

2.2.1 Cell culture

2.2.1.1 Hybridoma cells

To produce monoclonal anti-UCH-L1 antibodies established hybridoma cells were utilized. The used U104 hybridoma clone was generated in 2013 [84] by immunizing

Material and Methods

Wistar rats with purified human UCH-L1 protein. Spleen cells of the immunized rat were subsequently isolated and fused with the mouse myeloma cell line Ag8.653.

For expansion, hybridoma cells were cultivated in RPMI 1640 medium, supplemented with 10% fetal bovine serum (FBS), 1% penicillin-streptomycin, 1 mM sodium-pyruvate and 50 μ M beta-mercaptoethanol, at 37°C and 5% CO₂ in T75 flasks for suspension cells. Cells were split 1:10 every 3-4 days. For antibody production cells were transferred to ISF-1 medium in multiple steps. First, cells growing in RPMI medium, were split 1:5 to ISF-1 medium (day 1). On day 3 again 1:5 to ISF-1 and on day 5 1:10 to ISF-1. On day 8, 60% of total volume ISF-1 medium were added to the cell suspension and the cells were cultivated for an additional 5 days to produce antibodies. For antibody harvesting, the cell suspension was centrifuged at 1000 x g for 5 minutes at 4°C. The supernatant was filtered through a 0.22 μ m filter to remove cell debris and was stored at -20°C until further use, the pellet was discarded.

Rat anti-UCH-L1 U104 antibodies were used for western blot detections as well as treatment for 2nd hit experiments (described in 2.2.2.2). For the application as primary antibody in western blot detections (described in 2.2.4.11), pure supernatant was used. Antibodies were purified (described in 2.2.4.1) prior to the use for treatment of cells or mice.

2.2.1.2 Human podocytes

Human immortalized podocytes (a kind gift from Moin Saleem, University of Bristol), which are stably transduced with C-terminally myc.flag-tagged human full length THSD7A [93] were used for *in vitro* experiments. Usually, the cultivation of podocytes is challenging because podocytes dedifferentiate during *in vitro* cultivation. Dedifferentiation is characterized by the loss of podocyte foot processes and loss of podocyte-specific protein expression such as i.e., nephrin, THSD7A, PLA₂R1. Furthermore, it is characterized by the absence of PCNA, a marker for cell proliferation alongside strong expression of cyclin kinase inhibitors p27 and p57, regulators of the cell cycle process, which results in an irreversible growth arrest of the mature podocyte [94]. The immortalized human podocytes generated by Saleem *et al.* were obtained from the kidney of a 3-year-old child after nephrectomy and transfected with retroviral constructs containing the temperature-sensitive SV40 large T antigen gene [94]. This SV40 large T antigen is known to force cells to re-enter the synthesis phase of the cell

Material and Methods

cycle and thus escape apoptosis [95]. By using this technique, cells grow under permissive conditions at 32°C and a shift of the cells to non-permissive conditions at 37°C leads to inactivation of the SV40 large T antigen which results in differentiation of cells [94].

Podocytes were cultivated in vented cell culture flasks under permissive conditions at 32°C and 5% CO₂ in RPMI 1640, supplemented with 10% FBS, 1X insulin, transferrin selenium (ITS) and 1 µg/µl puromycin as the selection agent. For differentiation, cells were transferred to non-permissive conditions with RPMI 1640 medium, supplemented with 10% FBS and 1X ITS for 10 days at 37°C, 5% CO₂. Experiments were conducted in either uncoated six-well plates, with 80000 cells per well, for protein-biochemical and molecular analyses or in collagen IV coated eight-well chamber slides, with 5000 cells per well, for immunofluorescent staining. For the possibility to analyze released extracellular vesicles, medium containing normal FBS was replaced by medium containing exosome-depleted FBS. This change was made after nine days of differentiation, one day before treatment to avoid cultivation in exosome-depleted FBS, and to circumvent alterations in dynamics of extracellular vesicle (EV) release, due to the external factor of EV depletion.

Antibody treatment of cells was carried out at different time points. For the assessment of anti-THSD7A-antibody-associated effects, a time course experiment with treatments for 1, 6, 24, and 48 hours was performed with rabbit anti-THSD7A antibodies or unspecific control rabbit antibodies at a final concentration of 20 ng/µl respectively. For second hit (2nd hit) experiments with anti-UCH-L1 antibodies, cells were incubated with rabbit anti-THSD7A (20 ng/µl) or unspecific control rabbit antibodies (20 ng/µl) for 3 hours prior to the addition of purified specific U104 rat anti-UCH-L1 antibodies or unspecific control rat antibodies for another 3 hours, at a final concentration of 20 ng/µl respectively.

For analysis, cells and corresponding EVs released to the medium were harvested. Medium was collected into tubes and EVs were enriched (described in 2.2.3). Cells were harvested following two washes with ice cold PBS by scraping in 750 µl ice cold PBS. This step was repeated, and both fractions were collected. The cell suspension was centrifuged at 1000 x g, 4°C for 10 minutes and supernatant was discarded. Cell pellets were stored at -80°C until further processing.

2.2.1.3 Transient transfection of HEK cells

HEK293-T (human embryonic kidney) cells were used for the expression of target proteins as controls for western blot analyses. Therefore, the cells were transiently transfected with the respective vectors.

Cells were cultivated in DMEM medium supplemented with 10% FBS and 1% penicillin-streptomycin at 37°C and 5% CO₂. Cells with a confluency of 70-80% in a 10 cm dish were cultivated overnight in DMEM medium supplemented with 10% FBS and 1% penicillin-streptomycin at 37°C and 5% CO₂. Prior to transfection the medium was changed to DMEM medium supplemented with 10% FBS. Transfection was carried out by slowly adding transfection solution, prepared according to manufacturers' protocol (Polyplus-transfection), containing 10 µg of DNA. Cells were harvested 24 h after transfection.

2.2.2 Animal work

All experiments were performed in 10-15 weeks old male BALB/c mice, obtained from Charles River. After arrival, mice were acclimated for two weeks in the facility before experiments were conducted. Mice were housed with a 12 h light/12 h dark cycle at 20-24°C and 45-65% humidity. The mice had free access to water and standard food (Altromin 1328 P). Starting with the experiment mice were scored daily. Experiments were performed according to institutional and national guidelines and were approved prior to experimentation by the Behörde für Justiz und Verbraucherschutz der Freie und Hansestadt Hamburg.

2.2.2.1 THSD7A-MN induction

To investigate membranous nephropathy (MN) in BALB/c mice, the heterologous (passive) THSD7A-associated MN model [59] was used. To induce THSD7A-MN, mice were exposed to 100 µl (0.75 mg) specific rabbit anti-THSD7A antibody or unspecific rabbit serum as a control by retrobulbar injection under 3.5% isoflurane anesthesia.

2.2.2.2 UCH-L1-abs second hit

Since it is currently thought that anti-UCH-L1 antibodies appear during MN progression, anti-UCH-L1 antibodies were administered six days after initial disease induction with anti-THSD7A, or unspecific rabbit antibodies, to mimic this occurrence.

Therefore, 100 µl (0.8 mg) of antibody, either U104 rat anti-UCH-L1 antibodies or unspecific rat-IgG as a control were injected retrobulbar under 3.5% isoflurane anesthesia.

2.2.2.3 Disease score

To evaluate disease severity a disease score was developed. On that account, points were allocated for different clinical parameters as follows, 1 point for proteinuria >10 g/g, 1 point for proteinuria >100 g/g and 1 point for serum albumin levels <20%, serum lipids (cholesterol or/and triglycerides) >50%, weight gain >10% or FSD <15% of control mice. A maximum of 6 points could be reached, indicating severe disease progression, while a score of 0-1 indicates healthy mice. The control group comprises BALB/c mice injected with control antibodies (unspecific rabbit-IgG and rat-IgG).

2.2.2.4 Urine collection

Urine was collected one day before disease induction and at different timepoints during the experiment, to analyze proteinuria and the amount and content of extracellular vesicles that were released to the urine. For urine collection, mice were injected subcutaneously with 1 ml 0.9% NaCl and subsequently placed in metabolic cages. Urine was collected for a period of 3-4 hours. 50 µl of urine were frozen directly at -20°C for albumin and creatinine measurements. The remaining urine was prepared for EV enrichment (described in 2.2.3) and frozen at -80°C.

2.2.2.5 Organ extraction

On day 11 or day 14 after disease induction, mice were sacrificed by cervical dislocation under 3.5% anesthesia. Kidneys and blood were collected. To remove the red blood cells the blood was centrifuged at 1500 x g for 10 minutes at 4°C and the upper phase, containing the plasma, was transferred to a fresh tube and stored at -20°C.

2.2.2.5 Glomeruli isolation

Collagenase solution

1.2 mg/ml Collagenase IA
100 U/ μ l DNase I
ad HBSS

Magnetic bead solution

50 ml HBSS
150 μ l SPHERO™ beads
50 μ l Dynabeads™

Kidneys were perfused with 5 ml HBSS containing magnetic beads (Dynabeads™ and SPERO™ beads each). After perfusion, the kidney capsule was removed. Prior to glomeruli isolation a kidney piece was removed for histology or cryo preservation. The remaining kidney pieces were chopped with a scalpel and divided into two 2 ml tubes. Per tube 1.5 ml collagenase solution was added and digested for 15 minutes at 37°C and 1300 rpm. The reaction was stopped on ice and the kidney suspensions of both tubes were each filtered through a 100 μ m cell strainer with a syringe plunger. After filtration the cell strainer was rinsed with 10 ml HBSS. The filtered kidney solution was filtered again through a 100 μ m cell strainer and afterwards rinsed with 10 ml HBSS. The filtered kidney solution was centrifuged for five minutes, 4°C, 600 x g. The supernatant was discarded, and the pellet was solved in 6 ml HBSS and divided onto four 2 ml tubes. The tubes were placed on a DynaMag2™ magnetic Particle Concentrator and washed for a total of three times, five minutes each with 1.5 ml HBSS + 0.05% bovine serum albumin (BSA). The isolated glomeruli of the four 2 ml tubes per animal were collected in 1 ml HBSS. The number of glomeruli and contamination with tubuli was counted in 10 μ l glomeruli suspension under a light microscope. Glomeruli were centrifuged for five minutes, 4°C at 1500 x g. Pellets were frozen on dry ice and stored at -80°C.

2.2.3 Enrichment of extracellular vesicles

For the enrichment of extracellular vesicles from either human podocyte cell culture media, mouse urine, or patient urine, stabilization solutions (200 mM EGTA + 660 mM NaN₃ in dest. H₂O and 100 mM PMSF in ethanol) were added in a 1:100 dilution to the samples prior to further preparations.

Material and Methods

Cell culture medium was centrifuged two times at 2000 x g for 10 minutes at 4°C to remove cell debris. The supernatant was transferred to a fresh tube after each centrifugation step and the pellet was discarded.

For mouse urine two different centrifugation steps were performed. First, the urines were centrifuged at 1500 x g for 10 minutes at 4°C, then at 5000 x g for 10 minutes at 4°C. The supernatant was transferred to a fresh tube after each centrifugation step and the pellet was discarded.

Patient urine was first centrifuged at 2500 x g for 10 minutes at 4°C and then filtered through 5 µm syringe filters. Afterwards, the filtered urine was centrifuged through 100 kDa cut-off filter tubes, to reduce proteins present in the highly proteinuric urine.

All samples were stored at -80°C until further analysis.

For EV enrichment the pre-processed samples were ultra-centrifuged at 100000 x g for 1.5 hours at 4°C in the Optima MAX-TL ultracentrifuge. Supernatant was removed and pellets were resolved in PBS.

2.2.3.1 Podocyte-specific EV purification

Blocking buffer

2% fish gelatine
1:1 dilution SuperBlock™
in PBS

Wash buffer

0.1 M sodium phosphate
ad dest. H₂O, adjust to pH 8

Binding buffer

2 mM EDTA
ad PBS, adjust to pH 7.4

Collected patient urine contains EVs derived from all kidney cells. To investigate podocyte-specific EVs, immunoprecipitation with antibodies against the podocyte specific proteins Glepp1 and CD35 was performed. Therefore, magnetic Dynabeads™ were coupled with Glepp1 and CD35 antibodies according to the manufacturers' instructions (Invitrogen). The coupled beads were incubated with blocking buffer for 1 hour at room temperature on a rolling shaker. After washing twice with wash buffer, enriched EVs (described in 2.2.3) were added to the antibody coupled beads and binding buffer was added to a total volume of 250 µl. The EV-bead solution was incubated overnight at 4°C on a rolling shaker. Podocyte-specific EVs, bound to

Material and Methods

magnetic beads were isolated with the DynaMag2™ magnetic Particle Concentrator and eluted in PBS by vortexing over 2 minutes. For SDS-PAGE a total of 1×10^{10} EV particles (determined via ImageStream measurement, described in 2.2.3.2) were loaded.

2.2.3.2 ImageStream measurement

Staining solution

8% exosome-depleted FBS in PBS

MemBrite Fix 594/615

anti-rabbit AF488

Total EV amounts as well as specific antibody containing EVs were determined using ImageStream measurements. For this, 500 μ l cell culture medium, obtained from 80000 cells, or 100 μ l of mouse urine were ultracentrifuged (described in 2.2.3). The obtained EV pellet was resolved in staining solution and incubated for 45 minutes at room temperature in darkness. After incubation unbound dye and potential antibody aggregates were removed, using NanoSep centrifugation columns. Subsequently, 500 μ l 2% exosome depleted FBS in PBS were placed to the column and the EVs in staining solution were added to the 2% FBS solution. The columns were centrifuged for 10 minutes at 7000 x g at 4°C and EVs were removed from the column by resuspension in 50 μ l 2% exosome depleted FBS in PBS. This solution was analyzed at the ImageStream.

2.2.3.3 Nanoparticle tracking analyses (NTA)

The size distribution of EVs derived from human cell culture podocytes was determined by nanoparticle tracking analyses (NTA). Per sample 30 μ l of cell culture supernatant were added to 1.5 ml PBS. A total amount of 500 μ l of this EV/PBS solution was loaded to the LM10 unit (Nanosight) sample chamber. Measurement was performed with a screen gain of 2 and camera level of 15. Five videos per sample with a duration of 1 minute at 25°C temperature was recorded. Data was analyzed with NTA 3.0 software with software settings of a detection threshold of 6 and a screen gain of 10.

2.2.4 Protein-biochemical methods

2.2.4.1 Antibody purification

Binding buffer

BupH Phosphate Buffered Saline Packs (Thermo Scientific)

Material and Methods

Neutralization buffer

1 M Tris

ad dest. H₂O, adjust to pH 8

Elution buffer

IgG Elution Buffer (Thermo Scientific)

Monoclonal antibodies from hybridoma cells were purified using NabTM Protein A/G Spin Columns. Prior to purification, supernatant was concentrated using 50 kDa cut-off filter tubes, in the way that 50 ml of supernatant were concentrated to 5 ml. Subsequently, 5 ml of concentrated supernatant were diluted in 5 ml binding buffer before loading onto the column. The samples were run by gravity flow through the column. Afterwards, the column was washed three times with 10 ml binding buffer each, to remove unspecific proteins. Antibodies were eluted for a total of three elution steps, each adding 5 ml of elution buffer. Elution fractions were collected in tubes containing neutralization buffer. Antibody concentrations of the elution fractions were quantified photometrically at the NanoPhotometer® (described in 2.2.5.6). The elution fractions that contained measurable concentrations were pooled and concentrated. Therefore, samples were centrifuged in 50 kDa cut-off filter tubes at 3000 x g and 4°C. During concentration three wash steps were included, in which 35 ml of PBS were added to the column and centrifuged at 3000 x g and 4°C until the volume was concentrated to approximately 2-4 ml. During the last wash step, the antibody was concentrated to a final concentration of 8 µg/µl.

2.2.4.2 Biotinylation of antibodies

Purified U104 rat anti-UCH-L1, or unspecific rat antibodies (rat-IgG, Sigma) were used for application in mice. A central aspect of UCH-L1 antibody treatment is the specific detection of the applied antibodies in the glomerulus. Unfortunately, due to cross-species reactivity of mouse and rat antibodies, a specific differentiation cannot be made using secondary antibodies. Therefore, anti-UCH-L1 and unspecific rat-control antibodies were biotinylated using EZ-Link Sulfo-NHS-LC-Biotin. For biotinylation, a 10 mM solution of the biotin reagent in dest. H₂O was added to the desired amount of antibody to be biotinylated. The antibody-biotin solution was incubated for 2 hours on ice. Afterwards, unbound biotin was removed via ZebaTM Spin Desalting Columns by applying antibody-biotin solution to the columns, and subsequently were centrifuged for 2 minutes at 1500 x g and 4°C. The flowthrough contained the purified biotin-

labeled antibody, which was afterwards tested in western blot analysis for proper biotinylation.

2.2.4.3 Lysis of cells

Lysis buffer

T-PER™

1 x SIGMAFAST™ Protease Inhibitor Cocktail, EDTA free

Cell pellets were lysed in lysis buffer for 30 minutes on ice, by vortexing every 5 minutes. After lysis, the lysates were centrifuged at 16000 x g for 10 minutes at 4°C. Supernatant was transferred to a fresh tube and stored at -80°C until further analysis.

2.2.4.4 Lysis of glomeruli

Lysis buffer I (“T-PER™” protein fraction)

T-PER™

1 x SIGMAFAST™ Protease Inhibitor Cocktail, EDTA free

Lysis buffer II (“urea” protein fraction)

8 M Urea

10 mM DTT

ad 50 mM Tris pH 8.0

Protein analysis of isolated mouse glomeruli was performed in two distinct lysates. To obtain soluble proteins, glomeruli were lysed in 150 µl lysis buffer I per 5000 glomeruli. First, 50 µl lysis buffer were added, and glomeruli were mechanically shredded with a pestle. Afterwards the remaining volume of the lysis buffer I was added to the glomeruli suspension and incubated 30 minutes on ice with vortexing every five minutes. The glomeruli lysate was centrifuged at 16000 x g, 4°C, 30 minutes. Supernatant, containing soluble proteins, was transferred into a fresh tube and the remaining pellet was lysed in lysis buffer II to lyse the insoluble proteins. After adding 50 µl lysis buffer II to the pellet obtained from lysis I, the pellet was mechanically shredded with a pestle and incubated 30 minutes on ice with vortexing every five minutes. The lysate was centrifuged at 16000 x g, 4°C, 30 minutes and the supernatant was transferred to a fresh tube. The samples were stored at -80°C until further analysis.

2.2.4.5 Antibody elution from cryosections

Antibodies from mice with MN induction and 2nd hit treatment should be checked for their presence in the kidney by elution from kidney cryosections. Therefore,

Material and Methods

200 x 10 µm cryosections per kidney were collected into 2 ml tubes, resuspended in 1 ml sterile PBS and centrifuged on quick spin with a table centrifuge. The pellet was washed three times with 1 ml PBS each, with quick spin centrifugation in between. For the first antibody elution step, the pellet was resuspended in 150 µl of 25 mM citrate, pH 3.2 and incubated for 20 minutes on ice with vortexing every 5 minutes. The eluate was centrifuged on quick spin with a table centrifuge and the supernatant was transferred to a fresh tube containing 150 µl of 1 M Tris, pH 8 for neutralization. A second antibody elution was performed with 150 µl of 25 mM citrate, pH 2.5 added to the pellet remaining from the first elution. After incubation for 20 minutes on ice with vortexing every 5 minutes, the second eluate was centrifuged on quick spin with a table centrifuge and the supernatant was transferred to a fresh tube containing 150 µl of 1 M Tris, pH 8 for neutralization. Both elutions were pooled and subsequently used as primary antibody on western blot analyses (described in 2.2.4.11) to detect whether reactivity to either UCH-L1 or THSD7A was present as a readout for the specific deposition/binding of anti-UCH-L1/THSD7A antibodies within the kidney.

2.2.4.6 Mouse-Albumin-ELISA (MAE)

MAE wash buffer

50 mM Tris
138 mM NaCl
2,7 mM KCl
ad dest. H₂O, adjust to pH 8

Postcoat solution

1% BSA
in washing buffer

Coating buffer

1 capsule carbonate-bicarbonate buffer
in 100 ml dest. H₂O

Conjugate diluent

0.5 ml 10% Tween20
in 100 ml postcoat solution

Stop solution

5,7% H₃PO₄
ad dest. H₂O

Material and Methods

The amount of albumin in either mouse urine or serum was determined by a sandwich enzyme-linked immunosorbent assay (ELISA) using a commercially available kit (Bethyl). For this, high binding 96-well plates, were coated with anti-mouse albumin antibody, diluted 1:100 in coating buffer and incubated overnight, shaking at 4°C. The primary antibody was removed, and the plates were washed for a total of three times with MAE washing buffer. 200 µl of postcoat solution was added per well and the plate was incubated for 30 minutes at room temperature on a shaker. After washing for a total of three times with MAE washing buffer, 100 µl of in conjugate diluent diluted urine or serum were added per well in addition to a standard. Samples were incubated for 1 hour at room temperature on the shaker. Then the plate was washed for a total of five times with MAE wash buffer, and afterwards 100 µl of secondary antibody (diluted 1:40000 in conjugate diluent) was added to the plate and incubated for 1 hour at room temperature. The secondary antibody was removed, and the plate was washed for a total of five times with MAE washing buffer. The TMB substrate was added to the samples and incubated for approximately 2-5 minutes, until a color switch of the substrate towards a blue color could be observed. The reaction was stopped with the stop solution, and absorption was measured at the EL808 Ultra Microplate Reader at 450 nm.

2.2.4.7 Creatinine measurement from urine

Creatinine amount in the urine was determined using Jaffe's reaction. This method is based on the reaction of creatinine with picric acid in alkaline solution, which leads to the formation of a red-colored complex that can be measured at an absorbance of 520 nm [96]. Therefore, 10 µl of standard or urine per well were added to a 96-well microwell plate. 50 µl reaction buffer (containing reagent 1 [alkaline buffer] and reagent 2 [picric acid] from the kit in a 4:1 ratio) were added and incubated for one minute. The absorption was measured in a kinetic program at the EL808 Ultra Microplate Reader at 492 nm directly and after five minutes.

2.2.4.8 Albumin to creatinine ratio (ACR)

Measurements of protein loss to the urine were performed by measuring albuminuria, the loss of albumin through the urine. This was performed through albumin to creatinine ratio (ACR) by calculating the albumin amount (mg/ml) to the creatinine (mg/ml) to obtain the ACR in mg/mg.

2.2.4.9 Serum measurement

Mouse serum was analyzed for cholesterol and triglycerides. For this, 150 μ l serum were used for determination of serum parameters by automated measurement using a COBAS (Roche) system.

2.2.4.10 Activity-based protein profiling

ABP buffer

50 mM	Tris pH 7.4
250 mM	Sucrose
5 mM	MgCl ₂
ad dest. H ₂ O	

5 x assay buffer

250 mM	Tris pH 7.4
25 mM	MgCl ₂
5 mM	DTT
10 mM	ATP
ad dest. H ₂ O	

To determine the ability of deubiquitinating enzymes to bind ubiquitin, the commercially available activity-based probe (ABP) *Cy5-Ub-VME* was used. The lyophilized powder was dissolved in DMSO and slowly added to the ABP buffer while vortexing, to receive a stock concentration of 55.95 μ M. The dissolved ABP was stored in aliquots at -80°C, each aliquot was only thawed once.

The ABP was added to a protein reaction solution in a final concentration of 2.24 μ M. The reaction solution contained 5 μ g protein with 5 x assay buffer, diluted to a 1-fold concentration in dest. H₂O, and was incubated for one hour at 37°C. Afterwards the solution was prepared for SDS-PAGE analyses with 5 x solubilizer (diluted to a 1-fold concentration) and denatured for 10 minutes at 70°C. The prepared samples were analyzed via SDS-PAGE and western blot (described in 2.2.4.11).

2.2.4.11 SDS-PAGE and western blot

Migration buffer

25 mM	Tris
192 mM	Glycine
0.1%	SDS
ad dest. H ₂ O	

Material and Methods

5 x solubilizer, reducing

1.25 M	Tris pH 6.8
50%	(w/v) glycerol
10%	(w/v) SDS
2.5 M	DTT
0.25% (w/v)	Bromphenol Blue

5 x solubilizer, non-reducing

1.25 M	Tris pH 6.8
50%	(w/v) glycerol
10%	(w/v) SDS
0.25% (w/v)	Bromphenol Blue

12.5 % Tris-glycine gel

Separating gel

3.75 ml	aqua dest
2.5 ml	4 x separating gel buffer (1.5 M Tris pH 8.8)
3.2 ml	40% acrylamide (3.3% C)
500 µl	glycerol
100 µl	10% SDS
50 µl	10% APS
8 µl	TEMED

Stacking gel

2.84 ml	aqua dest.
1.125 ml	4 x stacking gel buffer (0.5 M Tris pH 6.8)
450 µl	40% acrylamide (3.3% C)
45 µl	10% SDS
45 µl	10% APS
5.55 µl	TEMED

TBS-T

1 M	NaCl
100 mM	Tris pH7.4
0.05%	Tween 20
ad dest. H ₂ O	

Transfer buffer

25 M	Tris
192 mM	Glycine
20% (v/v)	Ethanol
ad dest. H ₂ O	

Material and Methods

Stripping buffer

0.2 M Glycine
0.1% (w/v) SDS
1% (v/v) Tween 20
ad dest. H₂O, adjust to pH 2.2

PTSA

0.01 M para-toluenesulfonic acid
ad dest. H₂O

Protein analyses were performed in sodium dodecyl sulfate-polyacrylamide gel electrophoresis (SDS-PAGE) using Criterion™ TGX Stain-Free™ Precast 4-15% gradient gels with corresponding Bio-Rad electrophoresis systems. The Bio-Rad Stain-Free™ system uses a trihalo compound which is incorporated into the precast gels. Tryptophan residues of proteins covalently bind to the trihalo compound and can be visualized through their fluorescence, when exposed to UV light (Bio-Rad).

For SDS-PAGE and western blot analyses 5 µg protein obtained from cells or tissue, or 200 glomeruli were used. The samples were denatured with 5 x solubilizer (reducing or non-reducing), diluted to a 1-fold final concentration in dest. H₂O, for 10 minutes at 95°C. The samples and 5 µl CozyXL™ marker for molecular weight distribution, were loaded onto gels and the SDS-PAGE was run at 100 V for approximately 10 minutes then at 120-150 V for approximately 1.5-2 hours in migration buffer. Total protein amounts were visualized via Stain-Free™ using UV light at the Vilber Fusion FX7 imager, as an equal loading control, additional to housekeeping proteins. For activity-based protein profiling self-made 12.5% Tris-glycine gels were used to separate especially lower molecular weight proteins. For this, samples were prepared as described in 2.2.4.10 and loaded to the gel. For visualization of molecular weight distribution, BlueElf marker was used. SDS-PAGE was run at 100 V for 10 minutes followed by 120-150 V for approximately 3 hours in migration buffer. *Cy5-Ub-VME* fluorescence was captured at the Vilber Fusion FX7 imager, with the 640 nm filter. Since those gels do not contain the Stain-Free™ system, equal loading of total proteins was visualized after western blotting using ponceau S.

To specifically quantify proteins within gels, they were transferred with the semi-dry western blot technique using the BioRad Trans-Blot Turbo system. Proteins were transferred to a PVDF membrane, which was activated with 99% bioethanol, to reduce the hydrophobic property of the membrane. The negative charged proteins migrate in

Material and Methods

current flow direction and transfer from the gel to the membrane. Blotting was performed at 2.5 A and 25 V for 30 minutes. Membranes of Stain-Free™ gels were directly washed in TBS-T, while membranes of self-made 12.5% Tris-glycine gels were stained with ponceau S to visualize total protein load. After three wash steps with TBS-T, the membrane was blocked with 3% milk in TBS-T for one hour at room temperature, to avoid unspecific antibody binding and strong background signals. After blocking, membranes were washed four times 5 minutes each with TBS-T prior to the application of primary antibody solution. Membranes were incubated overnight at 4°C with primary antibody solution. The primary antibody solution was removed, and the membranes were washed again four times 5 minutes each, before adding HRP conjugated secondary antibody solution for one hour at room temperature. Membranes were subsequently washed four times 5 minutes each. Protein signals were visualized using SuperSignal™ West Pico PLUS Chemiluminescence Substrate reagents in a 1:1 ratio and incubated for 5 minutes. For weak signals SuperSignal™ West Femto Maximum Sensitivity Substrate reagents were added to the Pico substrate in a 1:1 ratio, diluted 1:6 in Pico PLUS substrate. All steps were performed on a shaker. Chemiluminescence was visualized with the Vilber Fusion FX7 Edge and quantified using ImageJ.

Since the amount of material is often limited, multiple proteins were quantified on the same membrane. Therefore, previous signals were removed using two different buffers. Membranes were incubated with a common stripping buffer containing glycine for 10 minutes before rinsing in dest. H₂O and washing with TBS-T three times for 5 minutes each, and incubated in blocking buffer for 10 minutes, or para-toluenesulfonic acid (PTSA) two times 5 minutes each followed by rinsing with TBS-T twice and washing with TBS-T twice for 5 minutes each. Subsequently, a new primary antibody was added to the membrane as described above. The common glycine stripping buffer with a pH 2.2 dissociates protein interactions such as those of primary and secondary antibody. PTSA however, inactivates the HRP from the secondary antibody [97], enabling the specific detection of the subsequent reprobe.

2.2.5 Molecular biological methods

2.2.5.1 RNA isolation

RNA was isolated from cell pellets, obtained from approximately 80000 human podocytes. For this, the pellet was dissolved in 900 µl RNA-Solv reagent and incubated

Material and Methods

5 minutes at room temperature. Afterwards, 200 μ l chloroform were added, vigorously shaken and incubated for 10 minutes on ice, followed by 15 minutes of centrifugation at 10000 x g, at 4°C. The upper, aqueous phase, containing the RNA was transferred to a fresh tube and 500 μ l ice cold isopropanol were added to precipitate the RNA. The samples were shaken for 1 minute and incubated for 30 minutes on ice, followed by centrifugation at 10000 x g for 10 minutes at 4°C. After removing the supernatant, the RNA containing pellets were washed in 800 μ l of 70% ethanol and centrifuged for 15 minutes at 12000 x g at 4°C, twice. To isolate RNA from mouse glomeruli, a glomeruli pellet was dissolved in 250 μ l RNA-Solv reagent and lysed in the TissueLyzer with a Wolfram-Carbide Ball at 30 Hz for 1 minute. The solution was then incubated 5 minutes at room temperature and afterwards 50 μ l chloroform were added and vigorously shaken. After incubation on ice for 10 minutes, the samples were centrifuged for 15 minutes at 10000 x g, and 4°C. As for the cell pellet RNA isolation, the upper, aqueous phase was transferred to a fresh tube and 150 μ l ice cold isopropanol were added. The tubes were shaken for 1 minute and incubated for 30 minutes on ice, followed by centrifugation at 10000 x g for 10 minutes at 4°C. The supernatant was removed, and the pellet was washed twice in 250 μ l of 70% ethanol and centrifuged for 15 minutes at 12000 x g at 4°C. The RNA pellets were dried in the speed Vac and afterwards dissolved in RNase-free water. Concentration was determined photometrically (described in 2.2.5.3), and RNA was stored at -80°C until further analysis.

2.2.5.2 DNA digest and cDNA synthesis

Master mix I (per sample)

10.5 μ l	H ₂ O
1 μ l	Random Hexamer Primer (100 ng/ μ l)
1 μ l	dNTPs (10 mM)

Master mix II (per sample)

4 μ l	RT buffer,
0.5 μ l	RNase Out,
1 μ l	Reverse Transcriptase

Prior to cDNA synthesis the RNA was treated with DNase digest, to remove DNA contamination. For this, the rDNase Set was used and rapid DNase was added in a 1:10 dilution to the rDNase buffer to obtain the DNase solution. In total 200 ng of RNA were used for transcription into cDNA. The RNA was diluted in DNase solution to a concentration of 100 ng/ μ l and incubated for 10 minutes at 37°C. For cDNA synthesis

Material and Methods

2 µl of digested RNA were first incubated with Master mix I for 5 minutes at 65°C. Afterwards, Master mix II was added to the RNA solution and cDNA was synthesized for 10 minutes 25°C, 1 hour 42°C, 10 minutes 70°C and finally held at 4°C. The cDNA was stored at -20°C until further analysis.

2.2.5.3 Photometric quantification of nucleic acids

For quantification of the RNA amount, 1 µl of RNA solution was measured at the NanoPhotometer® at an absorption wavelength of 260 nm. Samples were measured against RNase free water as a blank.

2.2.5.4 Establishment of primer

PCR master mix

14,3 µl	H ₂ O
2 µl	10 x Dream Taq Green Buffer
0.4 µl	dNTP's (10 mM)
1 µl	sense primer (fw) (5 µM)
1 µl	antisense primer (rev) (5 µM)
0.3 µl	Taq DNA Polymerase

Primers were generated using Primer-BLAST (NIH NCBI) and ordered via Invitrogen. The primers were tested using 1 µl of cDNA, obtained from corresponding messenger (m)RNA, which was added to 19 µl of PCR master mix. Subsequently polymerase chain reaction (PCR) was performed following the same steps as the real-time quantitative PCR (qPCR) (Table 10). After PCR reaction, samples were evaluated for expected base pair size on a 3% agarose gel. The gel was run at 200 V for approximately one hour. Primers that showed expected base pair size and the least unspecific base pair bands were verified in real-time qPCR for proper melt curves and afterwards used for qPCR analysis (described in 2.2.5.5).

2.2.5.5 Real-Time qPCR

qPCR master mix

5 µl	SYBR™ Green
2 µl	sense primer (fw) (5 µM)
2 µl	antisense primer (rev) (5 µM)

The cDNA from corresponding mRNA was used for real-time qPCR using the QuantStudio 5. For this, 1 µl of cDNA per reaction was added to 9 µl of qPCR master mix, containing the DNA binding dye SYBR™ Green and respective primer (Table 9).

Material and Methods

The 18S ribosomal subunit was used as a housekeeper. For the 18S qPCR cDNA was diluted 1:500 in RNase free water. For quality control samples without reverse transcriptase and with H₂O instead of cDNA were analyzed as well.

Relative changes of target genes were quantified in comparison to the 18S housekeeper as the reference gene, using the $\Delta\Delta C_t$ method [98].

Table 9: qPCR Primer

Primer		Sequence (5' → 3')	Tm [°C]	size (bp)
human and mouse 18S	18S-Fw	CAC GGC CGG TAC AGT GAA AC		70
	18S-Rev	AGA GGA GCG AGC GAC CAAA		
human collagen IV $\alpha 1$	hu_COL4A1_Fw	GGG GAG CCT GGT GAG TTT TA	59,3	163
	hu_COL4A1_Rev	TCA ATC CTA CAG AAC CCG GC	59,46	
human collagen IV $\alpha 3$	hu_COL4A4_Fw	TCA CAC CTC ACG ATT TTG ATG AA	60,2	108
	hu_COL4A4_Rev	TGG CAT CTA TCC ATT GCT GTC TA	60,9	
human laminin $\alpha 5$	hu_Lama5_Fw	AGA GGA GGG CAG GTC GG	60,01	129
	hu_Lama5_Rev	TTC AGC ACA AAG GGC TCT CC	60,25	
mouse UCH-L1 (PGP9.5)	ms_PGP9.5_Fw	AGC TGG AAT TTG AGG ATG GA	58	111
	ms_PGP9.5_Rev	GGC CTC GTT CTT CTC GAAA	58	
mouse collagen IV $\alpha 1$	ms_Col4a1_Fw	ACA TCC GGC CCT TCA TTA GC	60	76
	ms_Col4a1_Rev	ATG GTC TGA CTG TGT ACC GC	60	

mouse collagen IV $\alpha 3$	ms_Col4a3_Fw	TTA TGG GGG ATG TTG GAC CC	59,07	300
	ms_Col4a3_Rev	CAC CTC TGA CAC CGG GAA G	59,71	
mouse laminin $\alpha 5$	ms_Lama5_Fw	GCG GAG ATC CCA ATC AGA CA	60	95
	ms_Lama5_Rev	ATC GAT GGC GTT GCT CAC A	60	

Table 10: Real-time qPCR program

	Temperature (°C)	Time (min)	Cycles
Hold Stage	50.0	02:00	1
	95.0	10:00	
PCR Stage	95.0	00:15	40
	60.0	01:00	
Melt Curve Stage	95.0	00:15	1
	60.0	01:00	
	95.0	00:01	

2.2.5.6 Photometric quantification of protein solution

Protein concentration of isolated proteins, e.g. purified antibodies was determined using the NanoPhotometer®. For this, 1 μ l of the protein solution was measured at 280 nm. Samples were measured against the corresponding buffer as a blank.

2.2.5.7 Protein quantification

To quantify the proteins concentration from cell or tissue lysates, the colorimetric biuret test ROTI®Quant was used. This assay is based on the reduction of copper ions in the alkaline milieu leading to a color change proportional to the protein amount in the sample, which was measured after 30 min of incubation at 37°C at an absorption of 492 nm in the Multiskan FC reader. The protein solution was diluted in dest. H₂O prior to the addition of the working solution, which contained ROTI®Quant reagent 1 and reagent 2 in a ratio of 16:1. Protein amount was quantified according to a standard

curve ranging from 0.6 to 10 µg protein, which was generated using an albumin standard.

2.2.6 Histology and Immunofluorescence

Blocking buffer

5% horse serum
 0.05% Tx-100
 in PBS

Prior to immunofluorescent staining, samples were fixed in 4% paraformaldehyde (PFA). Fixation cross-links proteins, leading to a preservation of the sample by inhibiting proteolytic enzymes, microorganisms and by maintaining stability of the sample [99]. Due to their two-dimensional structure, cell culture podocytes are more accessible to liquids and were fixed for 5 minutes at room temperature, while kidney pieces were fixed overnight at 4°C to ensure sufficient PFA penetration.

Microscopic examinations were performed in paraffin sections. The tissues were embedded in paraffin automatically in the spin tissue processor by the following dehydration procedure (Table 11), to allow the paraffin to penetrate the tissue.

Table 11: Dehydration and paraffin embedding protocol

Substance	Duration
50% EtOH	>2h
60% EtOH	2h 30min
70% EtOH	1h
96% EtOH	1h
96% EtOH	1h
100% EtOH	1h
100% EtOH	1h
100% EtOH	1h 30min
Xylol	1h
Xylol	1h
Xylol	1h 30min
Paraffin	1h
Paraffin	1h 30min

Material and Methods

Paraffin embedded kidney pieces were cut in 1-3 μm sections using a Leica M2255 Microtome and after stretching on a warm water bath, taken up onto super plus glass slides. The slides were baked overnight at 40°C, to allow water under the paraffin sections to evaporate and to mount the kidney sections on the slide. Prior to staining, the paraffin was removed from the sections by incubation in decreasing alcohol concentrations. Incubation steps were made as followed, 3 x xylol, 3 x 100% ethanol, 2 x 96% ethanol, 2 x 70% ethanol and 2 x ddH₂O. Paraffin sections were further processed for antigen retrieval, to enable epitope recognition by antibodies for immunofluorescent staining. For this, antigen retrieval was performed by two different methods. 1) Heat-induced epitope retrieval with incubation in sodium citrate (10 mM) buffer pH 6.1 in conjunction with boiling for 40 minutes at 98°C, followed by a washing step with water after cooling. 2) Protease-induced antigen retrieval using protease XXIV (Sigma, 5 $\mu\text{g/ml}$), where enzymes cleave protein cross-links [100]. For this, sections were digested for 15 minutes at 37°C, followed by a total of three wash steps each 5 minutes with PBS.

Prior to immunofluorescent staining with primary antibody, samples were incubated in blocking buffer for 30 minutes at room temperature, to prevent unspecific antibody binding. Primary antibodies, diluted (as stated in table 4) in blocking buffer were applied on samples overnight at 4°C, followed by washing with PBS for a total of three times 5 minutes each. The fluorochrome coupled secondary antibody diluted in blocking buffer (Table 4), was applied for 30 minutes at room temperature and afterwards samples were washed again for a total of three times 5 minutes each in PBS. The samples were then mounted with Fluoromount-G and visualized using the LSM800 Airyscan 1 (Zeiss) and LSM900 Airyscan 2 (Zeiss) and Zen Blue Software (Zeiss).

2.2.6.1 Podocyte exact morphology measurement (PEMP)

Podocyte foot process (FP) effacement is one of the hallmarks of podocyte injury, which can be examined by podocyte exact morphology measurement (PEMP). This technique is based on super-resolution microscopy of nephrin stained kidney sections and an automated quantification of the nephrin staining pattern. Nephrin is a podocyte slit diaphragm protein, which thus connects the interdigitating podocyte FPs [101]. Measurement of the nephrin signal calculated per capillary area of glomeruli describes the filtration slit density (FSD), which inversely correlates with the podocyte FP width [101].

Material and Methods

To analyze FSD values of mouse glomeruli, paraffin kidney sections were mounted on high precision poly-L-lysine coated cover slips and stained for nephrin (described in 2.2.6). The stained sections were then mounted with ProLongGold and visualized at the Visitron SD-TIRF spinning disk microscope. Pictures were taken as z-stacks with 0.2 μm slice distance from the whole glomerulus with the 100 x objective and SORA-Disk and processed via Richardson-Lucy deconvolution. Z-stacks were projected (maximum intensity projection) as a 2D image using ImageJ. For FSD measurement the area of the capillary (visualized by nephrin) was encircled, and the filtration length was determined with the PEMP macro for ImageJ [102]. The FSD was calculated from the total filtration slit diaphragm length per capillary area. 3 to 8 capillary areas of 6 glomeruli per animal were analyzed.

2.2.7 Statistical analysis

Statistical analyses were performed using GraphPad Prism 10. Results were expressed as median with individual values for single time points or mean \pm SEM for time course analyses and significance was set at $*p < 0.05$. Values of four different treatment groups were compared using the Kruskal-Wallis test with Dunn's multiple comparisons test. For comparison of two different treatment groups Mann Whitney U-test was performed. The means in time course experiments were compared using the Mixed-effects analysis with Tuckey's multiple comparisons test. Replicates used were biological replicates using different samples from distinct experiments.

3 Results

3.1 UCH-L1 antigen expression in membranous nephropathy

Membranous nephropathy as one of the major causes of nephrotic syndrome is a complex, heterogenous autoimmune disease, with antibody formation against an emerging number of target antigens. *De novo* expression of the Ubiquitin C-terminal Hydrolase L1 (UCH-L1), a potential target antigen is known to occur in injured podocytes upon kidney disease, especially in MN [42]. To identify specific localization patterns of UCH-L1, human kidney biopsies of a PLA₂R1⁺-MN and a non-MN nephrotic minimal change disease (MCD) patient were utilized. UCH-L1 *de novo* expression appeared to be more abundant in podocytes of the MN patient, especially localized to the membrane of the podocyte cell body and podocyte foot processes (FPs) (Fig. 1, white arrows). UCH-L1 expression in the MCD patient, however, showed a different pattern without a clear localization of UCH-L1 to the podocyte FP membrane (Fig. 1).

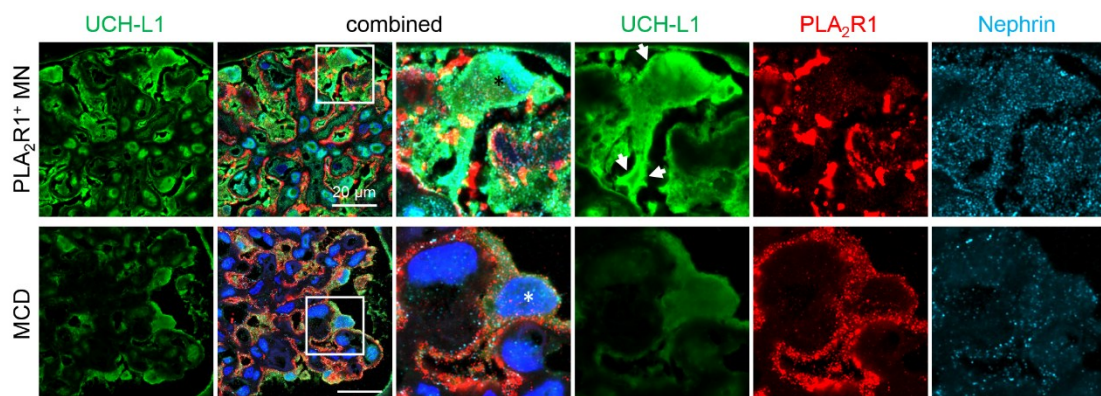


Figure 1: UCH-L1 localizes to the podocyte membrane and FP in MN patients. Confocal images of UCH-L1 (green) staining in kidney biopsies from a PLA₂R1⁺-MN and a minimal change disease (MCD) patient, PLA₂R1 (red), nephrin (light blue), and DNA (Hoechst, blue). Asterisks highlight podocyte nuclei; white arrows point towards UCH-L1 membrane pattern expression.

Mice however lack endogenous expression of the major MN antigen PLA₂R1 [57, 58]. As THSD7A was discovered as a novel target antigen in MN, the heterologous (passive) model of THSD7A-associated MN was developed, targeting THSD7A directly [59]. To ascertain the UCH-L1 expression in podocytes in this model of THSD7A-associated MN, BALB/c mice were injected with specific rabbit anti(α)-THSD7A antibodies (abs), while control mice were treated with unspecific rabbit antibodies. The disease develops over the course of 14 days and mice were sacrificed on day 14.

Results

UCH-L1 expression and localization were confirmed via high-resolution immunofluorescent imaging (Fig. 2 A). UCH-L1 localizes specifically to the cytoplasm of the podocytes as well as to FPs (Fig. 2 B, white arrows). Further, a high accumulation of mouse antibodies (mIlgG) can be observed along the GBM in α -THSD7A-abs treated mice (Fig. 2 B). In this model, mouse anti-rabbit IgG antibodies could be shown to develop as an autologous reaction, about 1 week after injection of rabbit α -THSD7A-abs [59]. This shows that mice of the THSD7A-associated MN model develop similar *de novo* expression of UCH-L1 in the podocytes as MN patients, making them a suitable model for further investigations on anti-UCH-L1 antibody pathogenicity and antigen alterations.

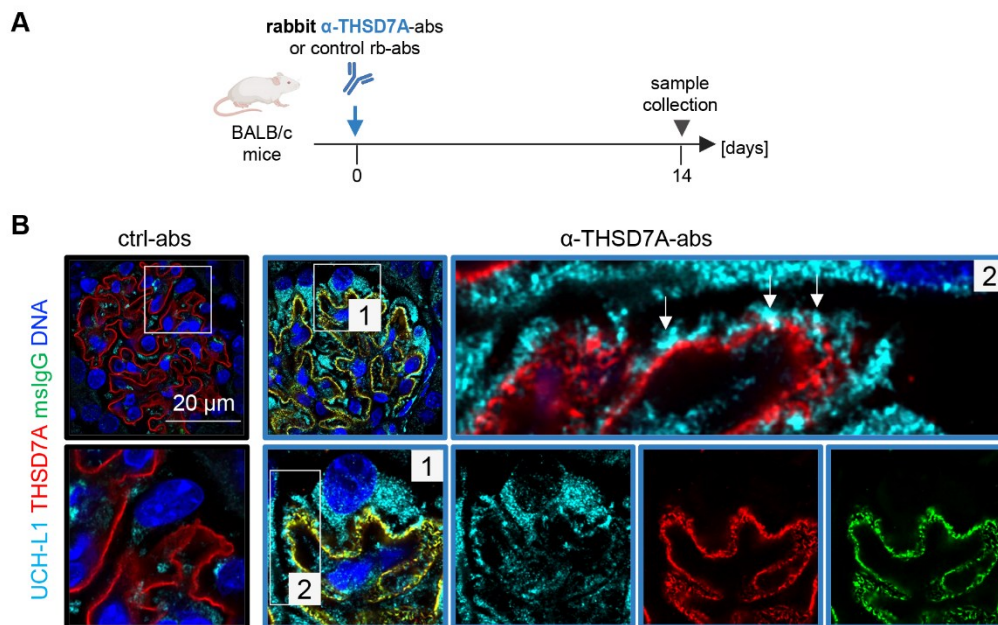


Figure 2: UCH-L1 in the passive mouse model of THSD7A-associated MN. (A) Scheme depicting the treatment of male BALB/c mice with specific anti(α)-THSD7A-antibodies (abs) or control (ctrl)-rabbit (rb)-abs. (B) Confocal images of kidney sections show UCH-L1 (light blue) localization in the glomerulus of THSD7A-abs or control ctrl-rb-abs treated mice, THSD7A (red), mouse (ms)-IgG (green) and DNA (Hoechst, blue). Arrows point towards podocyte foot process localization of UCH-L1.

3.2 Anti-UCH-L1 antibody second hit aggravates membranous nephropathy

Previous work from our group identified anti-UCH-L1 autoantibodies to be present in patients with primary MN as an additional antibody, next to their initial disease-causing anti-THSD7A or anti-PLA₂R1 autoantibodies. These anti-UCH-L1 autoantibodies predominantly recognize the non-functional, oxidative-modified form of UCH-L1 [43]. As oxidative stress is generated during MN disease progression, we hypothesize that

Results

anti-UCH-L1 autoantibodies are generated as a secondary immune reaction. Therefore, experiments were performed with rabbit α -THSD7A antibodies for MN induction followed by exposure of mice, in the setting of established MN, to anti-UCH-L1 antibodies as a second hit further referred to as “THSD7A-MN+2nd hit”, to determine whether these autoantibodies aggravate MN progression. Preliminary data show that UCH-L1 *de novo* expression is detectable starting at day 3 after α -THSD7A-abs induction (unpublished data from our lab). Further, mice exhibit a mild proteinuria at day 6 [59], which allows for a more specific discrimination of aggravation of proteinuria. The anti-UCH-L1-abs 2nd hit was therefore performed six days after MN disease induction with anti-THSD7A-abs.

3.2.1 Characterization of anti-UCH-L1 antibodies

Prior to *in vivo* application, anti-UCH-L1 antibodies had to be produced in sufficient quantities and validated for their reactivity towards the different UCH-L1 forms (intact and non-functional UCH-L1). Specific anti-UCH-L1 antibodies were obtained from the U104 hybridoma clone (rat) further referred to as “U104 anti(α)-UCH-L1-abs”, while unspecific purified anti-rat antibodies (ctrl-rat-abs) were commercially available. Cell lysates from HEK293 T cells were used, which were either transfected with myc-flag-tagged human or murine wildtype (WT)- or I93M-UCH-L1 or non-transfected (n.t.) as negative control. To control and confirm specific UCH-L1 detection, murine UCH-L1^{WT}, and UCH-L1^{KO} brain lysates were added. Purified U104 α -UCH-L1-abs and ctrl-rat-abs were used as primary antibodies for western blot detections. The purified U104 α -UCH-L1 antibody recognized both murine and human UCH-L1 under reducing as well as non-reducing conditions (Fig. 3 A). Calculations relative to the total protein load (Stain-FreeTM) showed a slightly higher affinity for the non-functional I93M form (Fig. 3 C). Unspecific ctrl-rat-abs showed not immunoreactivity to UCH-L1, making them suitable as control antibodies (Fig. 3 B).

Results

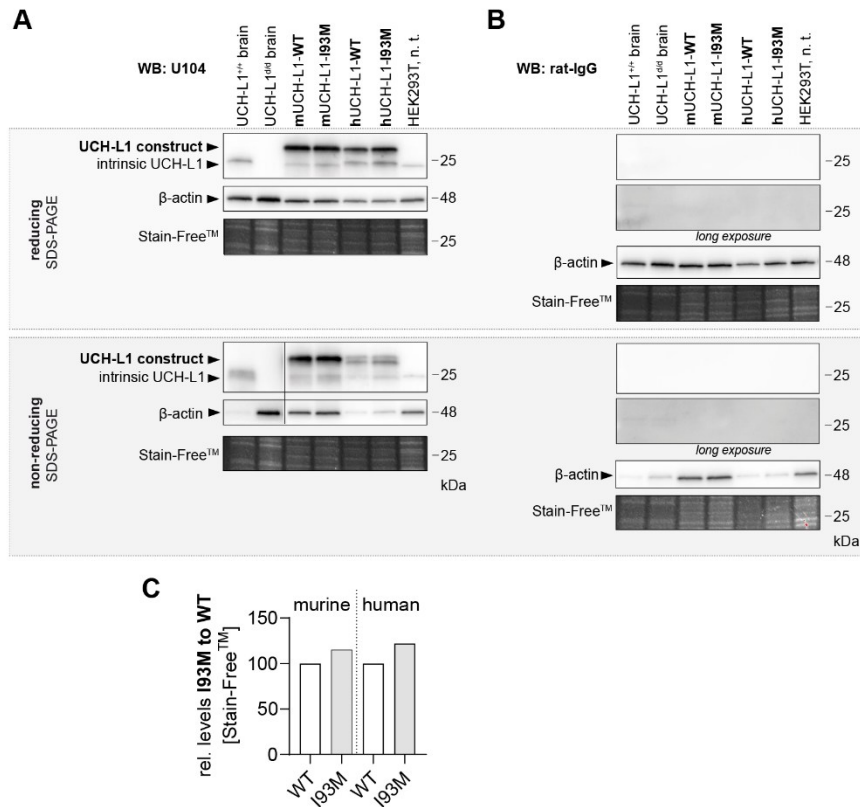


Figure 3: Characterization of the U104 anti-UCH-L1 antibody. Western blots of reducing and non-reducing SDS-PAGEs for (A) specific anti-UCH-L1 antibodies of the U104 hybridoma clone, or (B) unspecific rat-IgG, β-actin and Stain-Free™ were used to control for equal loading. (C) Graph shows densitometric quantification of the detection specificity towards the I93M-UCH-L1 compared to WT-UCH-L1.

3.2.2 Verification of UCH-L1 antibody localization in the kidney of the THSD7A-MN+2nd hit mouse model

Glomerular *de novo* expressed UCH-L1 specifically locates to podocytes in MN [42]. Apart from that, the in MN well described autoantibodies directed against foot process proteins (PLA₂R1 and THSD7A) are deposited along the glomerular filtration barrier (GFB) [28]. Consequently, the applied 2nd hit U104 α-UCH-L1-abs are predicted to accumulate in the glomeruli as well, especially bound to podocytes if the target antigen is accessible. To ascertain whether this accumulation occurs, a first THSD7A-MN+2nd hit experiment was performed with a total number of 2 animals per group.

To verify, if anti-UCH-L1 antibodies bound to glomerular structures, especially to podocytes, U104 α-UCH-L1 antibodies and their corresponding control (ctrl) anti-rat antibodies were biotinylated using EZ-Link Sulfo-NHS-LC-Biotin. This ensures a specific detection via streptavidin, since cross-species reactivity may hinder reliable

Results

distinction of rat and intrinsic mouse antibodies. Acidic elution of antibodies from kidney cryosections allows for specific validation of the antibodies via western blot analyses, using them as primary antibodies for protein detection. The applied biotinylated antibodies (biotinylated U104 α -UCH-L1-abs and biotinylated anti-rat-abs) can be detected via streptavidin-HRP. Non-biotinylated eluted antibodies however can be detected via appropriate secondary antibodies, for example anti-rabbit-HRP for the rabbit α -THSD7A-abs.

Non-reducing SDS-PAGE and western blot analyses were used to validate successful biotinylation as well as integrity of antibodies after the biotinylation process. Antibodies loaded on the gel showed specific bands at approximately 150 kDa in Stain-Free™ visualization. Western blot against biotin showed specific biotinylation of the antibodies (Fig. 4 A), making those antibodies suitable for mouse experiments. THSD7A-MN was induced in male BALB/c mice by application of rabbit α -THSD7A-abs or unspecific control rabbit abs. Six days after disease induction biotinylated U104 α -UCH-L1-abs or biotinylated unspecific anti-rat-abs were applied for additional five days. Mice were sacrificed and samples were taken on day 11 (Fig. 4 B). First, the presence of biotinylated antibodies in the kidney was verified through western blot detection with previously described acidic eluted antibodies, using them as primary antibodies. UCH-L1^{WT} and UCH-L1^{KO} mouse brain lysates were used to assure specific reactivity towards UCH-L1. As a proof of principle, eluted antibodies were further tested on THSD7A OE human cell culture podocyte lysates for specific recognition of THSD7A by the applied rabbit α -THSD7A-abs. Afterwards immunoblot membranes were re probed with commercial antibodies for UCH-L1 and THSD7A to verify the presence of the specific proteins. As evident from Fig 4 C, biotinylated anti-UCH-L1-abs were only present in THSD7A-MN+2nd hit mice. The western blots showed specific bands at the expected molecular weight for UCH-L1 (25 kDa) when visualized by streptavidin-HRP (Fig. 4 C, red asterisks). Although showing a weaker signal, anti-UCH-L1-abs were likewise present in control (ctrl)-rabbit (rb)-abs + U104 α -UCH-L1-abs 2nd hit control mice (Fig. 4 C, red asterisks). Eluted antibodies from control mice (ctrl-rb-abs and ctrl-rat-abs) showed no specific reactivity towards the antigens (Fig. 4 C). Subsequently, immunofluorescent staining of kidney sections demonstrated a specific pattern of biotinylated anti-UCH-L1 antibodies, when stained with streptavidin-AF488 for biotin. Antibodies were localized along the GBM (Fig. 4 D, white arrows, red bordered) and in podocytes, especially at the FP membrane in THSD7A-MN+2nd hit

Results

mice (Fig. 4 D, white arrowheads, red bordered). Unspecific biotinylated anti-rat-abs however, showed only weak background signal (Fig. 4 D).

Taken together these results revealed a specific deposition of biotinylated U104 α -UCH-L1-abs in the glomeruli podocytes and moreover along the GBM in THSD7A-MN+2nd hit mice. This shows that this experimental setup is suitable for investigations on the pathogenicity of anti-UCH-L1 antibodies in the *in vivo* THSD7A-MN mouse model.

Results

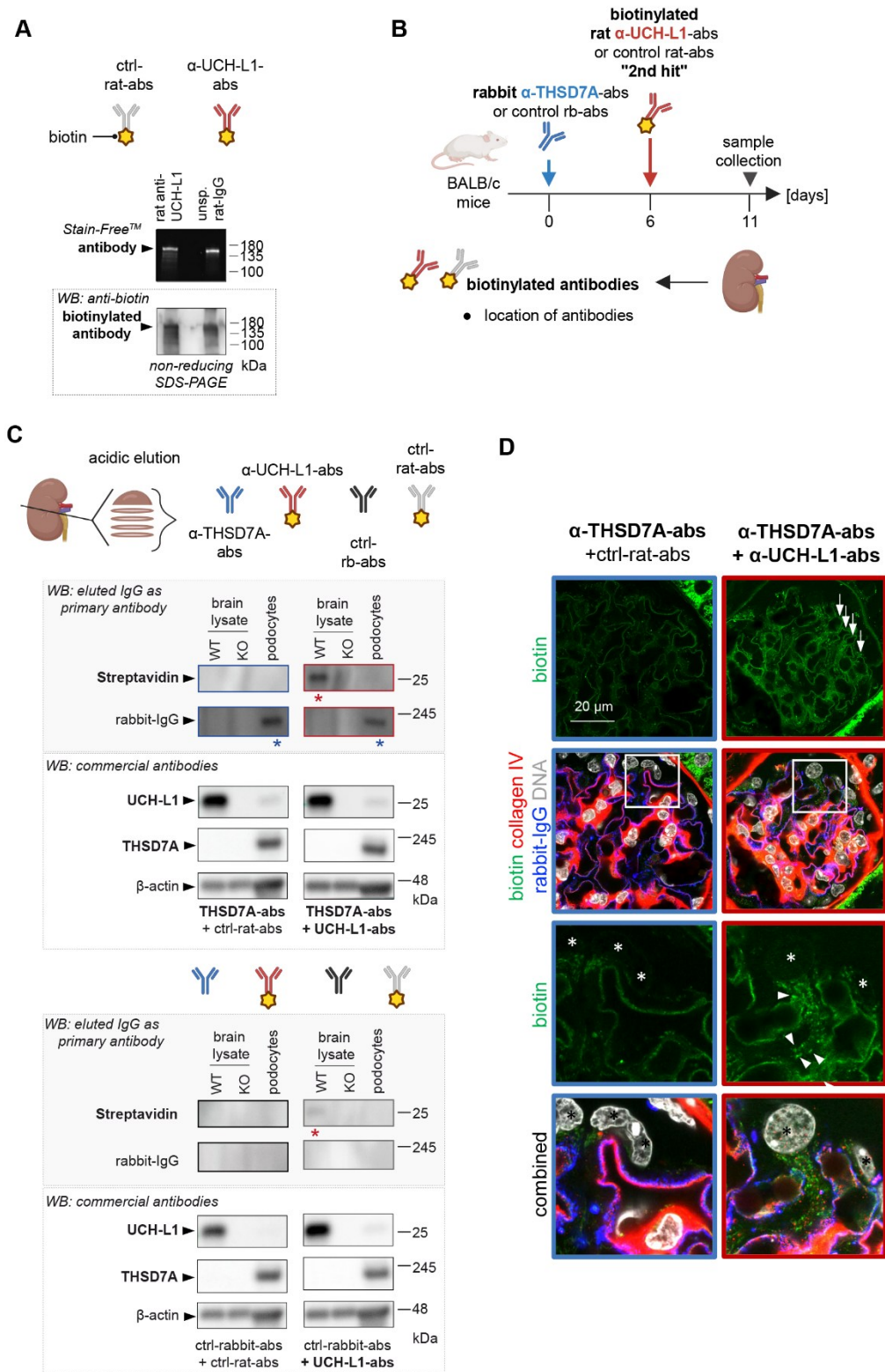


Figure 4: Second hit anti-UCH-L1 antibodies are found in the kidney. (A) Non-reducing SDS-PAGE and western blot analyses of biotinylated U104 anti(α)-UCH-L1 and control (ctrl) rat antibodies (abs). **(B)** Treatment scheme for α -THSD7A-abs MN disease induction with respective ctrl- rabbit (rb)-abs and 2nd hit with biotinylated U104 α -UCH-L1-abs or biotinylated ctrl-rat-abs in male BALB/c mice. **(C)** Western blots with acidic eluted antibodies from kidney cryosections as primary detecting antibodies, tested on UCH-L1^{WT} and UCH-L1^{KO} mouse brain lysates as well as human THSD7A overexpressing (OE) cell culture podocyte lysates. Red asterisks point to UCH-L1 detection by eluted biotinylated U104

Results

α -UCH-L1-abs, blue asterisks point to THSD7A detection by rabbit α -THSD7A-abs. **(D)** Immunofluorescent staining for biotin (streptavidin-AF488, green) showing a signal at the GBM (collagen IV, red) (white arrows) and at podocytes (white arrowheads) in THSD7A-MN+2nd hit (α -THSD7A-abs + α -UCH-L1-abs) mice, rabbit-IgG (blue), DNA (Hoechst, grey). Asterisks highlight podocyte nuclei.

3.2.3 Membranous nephropathy is aggravated in THSD7A-MN with anti-UCH-L1 second hit in mice

To determine the impact of anti-UCH-L1-abs on MN disease, clinical parameters were assessed. *In vivo* studies were carried out in the previous described cohort in addition to a larger cohort, with a total of 21 mice that received α -THSD7A-abs to induce MN, and 17 mice that received unspecific control (ctrl)-rabbit (rb)-abs. The 2nd hit was performed six days after THSD7A-MN disease induction with a total of 13 mice which received specific U104 α -UCH-L1-abs (THSD7A-MN+2nd hit) and another 9 mice unspecific ctrl-rat-abs. For the assessment of disease development and progression, urine was collected prior to disease induction (day -1) and on days 5, 7, 9 and 11 after initial disease induction, for the measurement of albuminuria (Fig. 5 A).

At first, general disease severity was assessed according to the clinical disease score. The comparison of α -THSD7A-abs treated mice (THSD7A-MN) (including U104 α -UCH-L1 and ctrl-rat-abs treated 2nd hit mice) and control-abs (unspecific rabbit-abs) treated mice showed a relatively mild induction of disease. THSD7A-MN mice exhibited a mean disease score of 1.9, with mice reaching up to 4 points while others only reached 1-2 points. Two mice, however presented with 0 points, and showed no alteration in any parameters. Control mice were not sick, with a mean disease score of 0.4. The comparison between the different 2nd hit groups, depicted a significant elevation of the disease score in THSD7A-MN+2nd hit mice. The mean disease score showed 2.2 points and was noticeably higher than in THSD7A-MN + ctrl-rat-abs mice with a mean of 1.5 points. There was no difference between the ctrl-rb-abs treated mice with unspecific rat-abs and specific U104 α -UCH-L1-abs 2nd hit (Fig. 5 B).

A detailed portrait of the clinical parameters showed significantly elevated levels of the albumin to creatinine ratio in THSD7A-MN+2nd hit animals in contrast to only α -THSD7A-abs treated mice, relative to control mice (unspecific ctrl-rb-abs + ctrl-rat-abs) (Fig. 5 C). The albumin loss through the urine was furthermore depicted in the mildly decreased serum albumin (sAlbumin) levels of the THSD7A-MN+2nd hit mice (Fig. 5 D). In contrast, serum lipid (sLipids) levels are not altered, although hyperlipidemia is a common clinical manifestation of MN [1].

Results

The intactness of the glomerular filtration barrier, which consists of glomerular endothelial cells, the GBM and podocytes with their foot processes (FPs) spanning the capillaries, determines protein loss to the urine. The podocyte FPs are connected to FPs of neighboring podocytes via slit diaphragm spanning proteins such as nephrin. Podocyte FP effacement, one of the hallmarks of MN [28] leads to a disruption of the filtration slit. To analyze filtration slit density, podocyte exact morphology measurement (PEMP) was used. With this method, the nephrin-positive slit diaphragm (SD) is measured automatically and then calculated per glomerular area to obtain the filtration slit density (FSD) [102]. Lower FSD values are caused by less nephrin signal per area, which is a sign for foot process effacement, with broader FPs, disrupting the tight nephrin meanders. PEMP analyses of the two 2nd hit cohorts demonstrated a significant lower FSD of THSD7A-MN mice with a median of $4.1 \mu\text{m}^{-1}$ compared to control-mice (unspecific ctrl-rb-abs and ctrl-rat-abs, median $4.7 \mu\text{m}^{-1}$) (Fig. 5 E). Furthermore, THSD7A-MN+2nd hit mice had a significantly lower FSD with a median of $3.8 \mu\text{m}^{-1}$, than α -THSD7A-abs only treated mice (Fig. 5 E). A reduction of the FSD, due to decreased nephrin per glomerular capillary area could in theory be accompanied by reduced total nephrin protein in isolated glomeruli. However, no significant changes of total nephrin values in the different treatment groups could be observed by western blot analysis, relative to control mice (unspecific ctrl-rb-abs + ctrl-rat-abs) (Fig. 5 F). Because a total amount of 200 glomeruli was loaded, no correlations to any housekeeper were performed. Stain-FreeTM visualization, however, showed general protein abundances. In addition, western blot analyses were performed for different elution-fractions of isolated glomeruli. The first elution with standard T-PERTM buffer eluted predominantly soluble, cytoplasmic proteins from the isolated glomeruli. The subsequent isolation with urea buffer eluted remaining insoluble, membrane-bound proteins. Nephrin protein could be detected in both, soluble and insoluble fraction, however no difference between the treatment groups could be observed (Fig. 5 F). Nevertheless, evaluation of the distribution of nephrin in the different elution fractions showed a distinct presence within the insoluble fraction (Fig. 5 F).

Taken together these results exhibited an influence of anti-UCH-L1 antibodies on MN disease severity. Mice showed an aggravation of disease when additionally challenged with anti-UCH-L1 antibodies, compared to mice that only received anti-THSD7A antibodies.

Results

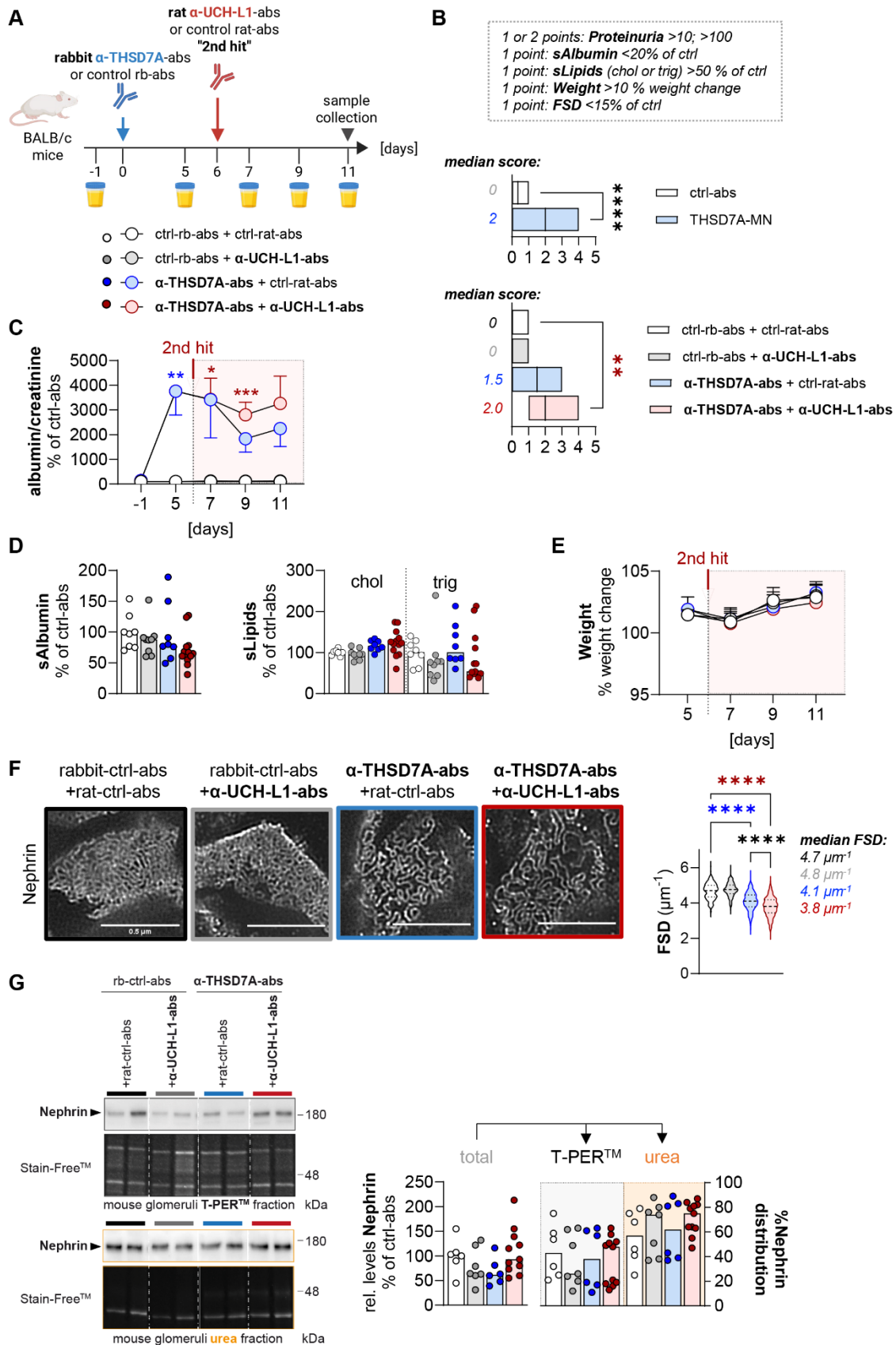


Figure 5: Anti-UCH-L1-abs 2nd hit worsened disease development in THSD7A-MN mice. (A) Scheme depicting the experimental setup of α -THSD7A-antibodies (abs) MN disease induction with respective control (ctrl)-rabbit (rb)- abs and U104 α -UCH-L1-abs 2nd hit with respective ctrl-rat-abs in

Results

male BALB/c mice, as well as urine collection at different time points. **(B)** Clinical score, based on points for different clinical parameters for ctrl-abs (unspecific ctrl-rb-abs treated) vs THSD7A-MN (α -THSD7A-abs treated) mice. $n \geq 17$, min to max with line at median, upper graph; Mann Whitney U-test. And for 2nd hit mice relative to ctrl-abs (unspecific ctrl-rb-abs and ctrl-rat-abs). $n \geq 8$ mice, min to max with line at median, lower graph; Kruskal-Wallis test with Dunn's multiple comparisons test. **(C)** Albumin to creatinine ratio in the urine relative to ctrl-abs (unspecific ctrl-rb-abs and ctrl-rat-abs) treated mice. $n \geq 8$ mice, mean \pm SEM; Mixed-effects analysis with Tuckey's multiple comparisons test. **(D)** Serum (s) albumin and lipids (cholesterol [chol] and triglycerides [trig]) measurements relative to ctrl-abs (unspecific ctrl-rb-abs and ctrl-rat-abs) of $n \geq 8$ mice, median with individual values; Kruskal-Wallis test with Dunn's multiple comparisons test. **(E)** Weight change per mouse % of weight before disease induction (day -1). $n \geq 8$ mice, mean \pm SEM; Mixed-effects analysis with Tuckey's multiple comparisons test. **(F)** Filtration slit density (FSD) measured via podocyte exact morphology measurement (PEMP) of nephrin signal per area. Measurements of 6 glomeruli from $n \geq 8$ mice violin plot with line at median and quartiles; Kruskal-Wallis test with Dunn's multiple comparisons test. **(G)** Western blot analysis of nephrin levels in glomerular T-PERTM and urea lysates. Densitometric analyses of total nephrin relative to ctrl-abs (unspecific ctrl-rb-abs and ctrl-rat-abs) and relative distribution within different lysate fractions of total protein (% distribution), without correlation to housekeeper, Stain-FreeTM shows general protein content. $n \geq 6$ mice, median with individual values; Kruskal-Wallis test with Dunn's multiple comparisons test. * $p < 0.05$, ** $p < 0.01$, *** $p < 0.001$, **** $p < 0.0001$

3.2.4 Antibody burden is increased in THSD7A-MN+2nd hit

Disease aggravation by secondary anti-UCH-L1 antibodies can be caused by multiple mechanisms which potentially together lead to a pathogenic effect. As such antigen-unspecific mechanisms can contribute to pathogenicity by influencing podocyte injury and antigen-specific mechanisms through directly interfering with the UCH-L1 antigen. A first antigen-unspecific mechanism could be caused by an enhanced antibody burden. After application of α -THSD7A-abs to mice, those antibodies bind to the THSD7A antigen, leading to THSD7A/rabbit (rb)-IgG immune deposits at the GBM. Challenged mice furthermore produce intrinsic autoantibodies against the foreign applied rabbit antibodies, which are as well found to accumulate at the GBM. An additional deposition of applied anti-UCH-L1-abs bound to UCH-L1, or aggravation of mouse autoantibody formation could in line further enhance immune deposit formation.

To evaluate this, western blot analyses of mouse-IgG were performed in THSD7A-MN+2nd hit experiments (Fig. 6 A), in the soluble and insoluble lysate fraction of isolated glomeruli. Due to species cross-reactivity a distinction between anti-mouse antibodies and anti-rat antibodies was not reliable possible. As can be seen from Fig. 6 B total mouse/rat-IgG levels showed a significantly increased amount, most prominent in THSD7A-MN+2nd hit mice, when calculated relative to control mice (unspecific ctrl-rb-abs + ctrl-rat-abs). Analyses of mouse/rat-IgG distribution within the soluble or insoluble fraction, exhibited a predominant appearance in the insoluble fraction, when calculated relative to total mouse/rat-IgG amounts. Western blot signals were not correlated to a housekeeper, as for the soluble fraction a defined amount of 200

Results

glomeruli was loaded. Furthermore, the insoluble fraction represented enriched immune complexes, and is assumed to contain only proteins of those, making a correlation to a housekeeper rather difficult.

Furthermore, total rabbit-IgG levels were significantly increased in THSD7A-MN mice but were not significantly different between the U104 α -UCH-L1 2nd hit and non-2nd hit group, when calculated relative to control mice (unspecific ctrl-rb-abs + ctrl-rat-abs). Distributions within the different protein fractions showed a clear abundance of rabbit-IgG in the insoluble fraction in MN mice. THSD7A protein levels show no significant alterations in total amounts when compared to control mice, but distribution analyses show a reduction of THSD7A protein in the soluble fraction.

This leads to the conclusion that higher antibody burden is present as enhanced immune complex formation in THSD7A-MN+2nd hit mice, either through the addition of specific anti-UCH-L1 antibodies or enhanced intrinsic mouse autoantibody production.

Results

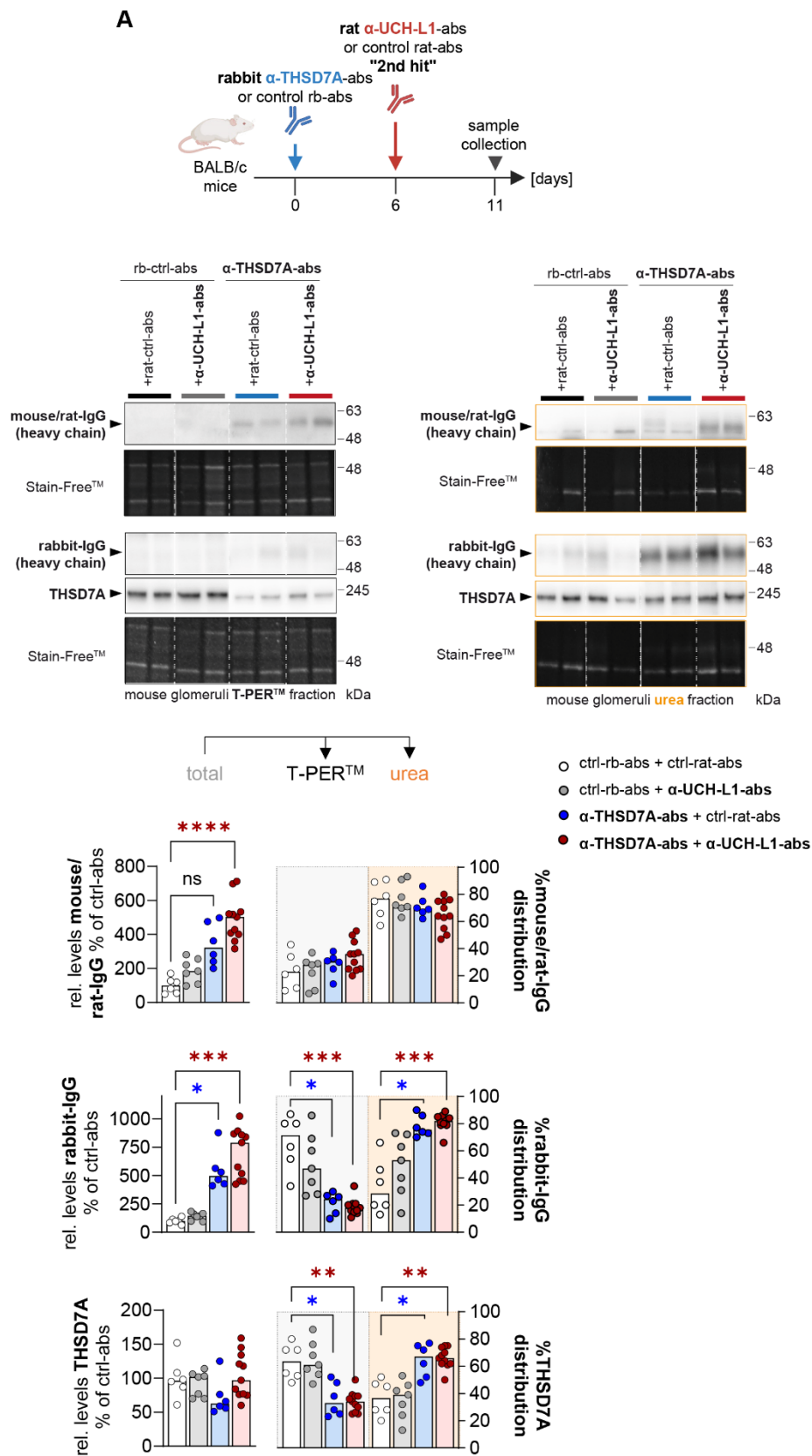


Figure 6: Antibody burden of mouse/rat-IgG is increased in THSD7A-MN+2nd hit mice. (A) Treatment scheme for α -THSD7A-antibodies (abs) MN disease induction with respective control (ctrl) rabbit (rb)-abs and U104 α -UCH-L1-abs 2nd hit with respective ctrl-rat-abs in male BALB/c mice. **(B)**

Results

Western blot analyses of mouse/rat-IgG (mouse autoantibodies and U104 rat α -UCH-L-abs), rabbit-IgG (α -THSD7A-abs) and THSD7A antigen in glomeruli T-PER™ as well as urea lysates. Densitometric analyses of total mouse/rat-IgG, rabbit-IgG and THSD7A relative to ctrl-abs (unspecific ctrl-rb-abs and ctrl-rat-abs) and relative distribution within different lysate fractions of total protein (% distribution), without correlation to housekeeper, Stain-Free™ shows general protein content. $n \geq 6$ mice, median with individual values; Kruskal-Wallis test with Dunn's multiple comparisons test. * $p < 0.05$, ** $p < 0.01$, *** $p < 0.001$, **** $p < 0.0001$

3.3.5 Collagen IV production is increased in THSD7A-MN+2nd hit

The glomerular basement membrane (GBM) as a central part of the glomerular filtration barrier, plays a crucial role in the size selectivity of macromolecules [19]. Therefore, intactness of the GBM is important for the prevention of proteinuria. One of the hallmarks of MN is a thickening of the GBM [27], possibly pointing to a dysregulation of GBM synthesis.

To investigate a potential influence of the U104 α -UCH-L1-abs 2nd hit on the GBM synthesis as another antigen-unspecific mechanism, GBM components were analyzed in glomeruli of the THSD7A-MN+2nd hit model (Fig. 7 A). Immunofluorescence staining of kidney sections revealed aggregates of collagen IV that co-stained with α -THSD7A rabbit-IgG, which were only present in THSD7A-MN+2nd hit mice (Fig. 7 B, white arrows). Further qPCR analysis showed a significant upregulation of the collagen IV $\alpha 1$ chain (Col4a1) in THSD7A-MN+2nd hit mice when compared to control mice (unspecific ctrl-rb-abs + ctrl-rat-abs). All other GBM components investigated, namely collagen IV $\alpha 3$ chain (Col4a3) and laminin $\alpha 5$ (Lama5), were not altered (Fig. 7 C). Additionally, an upregulation of collagen IV on protein level could be observed in the THSD7A-MN+2nd hit mice compared to control mice (unspecific ctrl-rb-abs + ctrl-rat-abs). This upregulation was most prominent in the soluble protein fraction (Fig. 7 D). A single collagen IV α -chain has an approximate MW of 171 kDa, which consists of the 26 kDa N-terminal 7S domain, the 120 kDa collagenous domain and the 25 kDa C-terminal NC1 domain [103]. Therefore, all bands present at approximately 80-310 kDa molecular weight (MW) were analyzed. Further, denaturation of the protein during SDS-PAGE sample preparation might lead to processing of the α -chains, resulting in the appearance at different MW.

This leads to the assumption that collagen IV synthesis is altered when specific anti-UCH-L1 antibodies are present in the context of MN. mRNA analyses confirm this as the expression of the collagen IV $\alpha 1$ chain is induced. This points to a clear dysregulation, as in mature glomeruli collagen IV is assembled by $\alpha 3$, $\alpha 4$ and $\alpha 5$

Results

chains, while $\alpha 1$ and $\alpha 2$ chains are only present during glomeruli/kidney development [19, 20].

Results

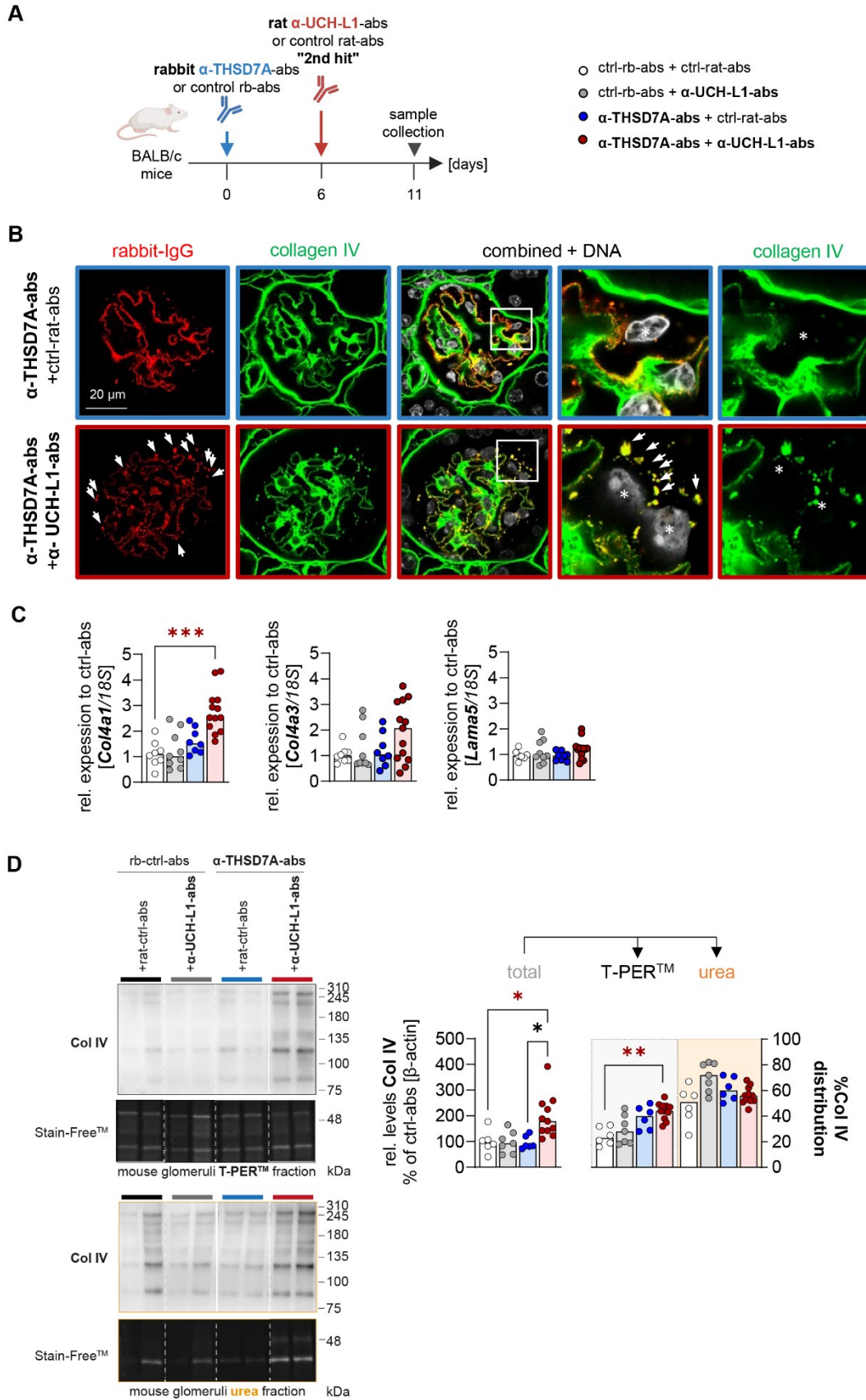


Figure 7: Collagen IV synthesis is altered in THSD7A-MN+2nd hit mice. (A) Scheme depicting the experimental setup of α -THSD7A-antibodies (abs) MN disease induction with respective control (ctrl) rabbit (rb)-abs and U104 α -UCH-L1-abs 2nd hit with respective ctrl-rat-abs in male BALB/c mice. **(B)**

Results

Immunofluorescent staining of collagen IV (green) shows aggregates which co-localize with rabbit-IgG (red) (white arrows) in THSD7A-MN+2nd hit (red bordered). DNA (grey), asterisks show podocyte nuclei. **(C)** Quantitative (q)PCR analysis of glomerular mRNA levels of Col4a1, Col4a3 and Lama5 relative to ribosomal 18S housekeeper, calculated in relation to ctrl-abs (unspecific ctrl-rb-abs and ctrl-rat-abs) n≥6 mice, median with individual values; Kruskal-Wallis test with Dunn's multiple comparisons test. **(D)** Western blot analysis of collagen IV (Col IV) for glomeruli T-PER™ as well as urea lysates. Graphs showing densitometric analyses of total Col IV in glomeruli relative to ctrl-abs (unspecific ctrl-rb-abs and ctrl-rat-abs) and relative distribution within different lysate fractions of total protein (% distribution), without correlation to housekeeper, Stain-Free™ shows general protein content. n≥6 mice, median with individual values; Kruskal-Wallis test with Dunn's multiple comparisons test. *p < 0.05, **p < 0.01, ***p < 0.001

3.2.6 Anti-UCH-L1 second hit leads to an altered pattern and increased *de novo* expression of UCH-L1

Next to antigen-unspecific effects of anti-UCH-L1 antibodies, antigen-specific effects directly targeting UCH-L1 function are a potential mechanism leading to disease aggravation. To evaluate the potential influence of anti-UCH-L1 antibodies, cell culture and mouse experiments were performed.

Cell culture experiments were performed with THSD7A overexpressing (OE) podocytes, which were first challenged with rabbit α-THSD7A antibodies (abs) or unspecific control (ctrl)-rabbit (rb)-abs for 3 hours prior to application of specific rat U104 α-UCH-L1-abs or unspecific ctrl-rat-abs for additional 3 hours as the 2nd hit (Fig. 8 A). At first, immunofluorescent staining for UCH-L1 antigen (performed with the U104 anti-UCH-L1 antibody) was performed to investigate potential alterations in UCH-L1 antigen expression and simultaneously detecting applied U104 anti-UCH-L1-abs, upon U104 anti-UCH-L1-abs treatment. Fig. 8 B revealed a “patch-shaped” pattern of UCH-L1 in THSD7A-abs+2nd hit treated cells, which localized to the membrane of the podocyte. Those “patches” were absent in only THSD7A-abs treated cells (Fig. 8 B, white arrows). Further, UCH-L1 as well as rabbit-IgG were found in line-like structures outside of the cell in THSD7A-abs+2nd hit treated cells (Fig. 8 B, white arrowheads). Those were very likely proteins, which stuck to the chamber slide surface and were either “left behind” by the podocyte or represented thin actin-rich protrusions, found in THSD7A-expressing podocytes [93]. Subsequently, general protein levels as well as the ubiquitin-binding “activity” of UCH-L1 protein were determined. Relative levels of total UCH-L1 protein were clearly upregulated in THSD7A-abs only as well as THSD7A-abs+2nd hit treated cells (Fig. 8 C). Activity-based protein profiling (ABPP) using the ABP *Cy5-Ub-VME* was used to identify the “activity” status of UCH-L1 represented by the ability of UCH-L1 to bind the ubiquitin (ub) of the ABP (Fig 8 D). As can be seen from Fig. 8 D, the majority of UCH-L1 protein was able to bind ubiquitin of

Results

the ABP, suggesting it was enzymatically active. Moreover, amounts of active UCH-L1 were significantly elevated in THSD7A-abs+2nd hit treatment when compared to ctrl-abs (unspecific ctrl-rb-abs + ctrl-rat-abs) (Fig. 8 D). In this setting the UCH-L1 protein was detected using a mouse anti-UCH-L1 antibody (Abcam, clone 13C4) and an anti-mouse TrueBlot® secondary antibody, which predominantly recognizes the non-reduced form of mouse-IgG (Rockland). This system was used to avoid detection of the IgG light chain (25 kDa) of the applied treatment antibodies (rabbit-IgG and rat-IgG) at the same MW as the UCH-L1 protein at 25 kDa.

Taken together, these results indicate that anti-UCH-L1-abs treatment leads to alterations in UCH-L1 protein abundance and distribution but does not influence its ability to bind ubiquitin.

Results

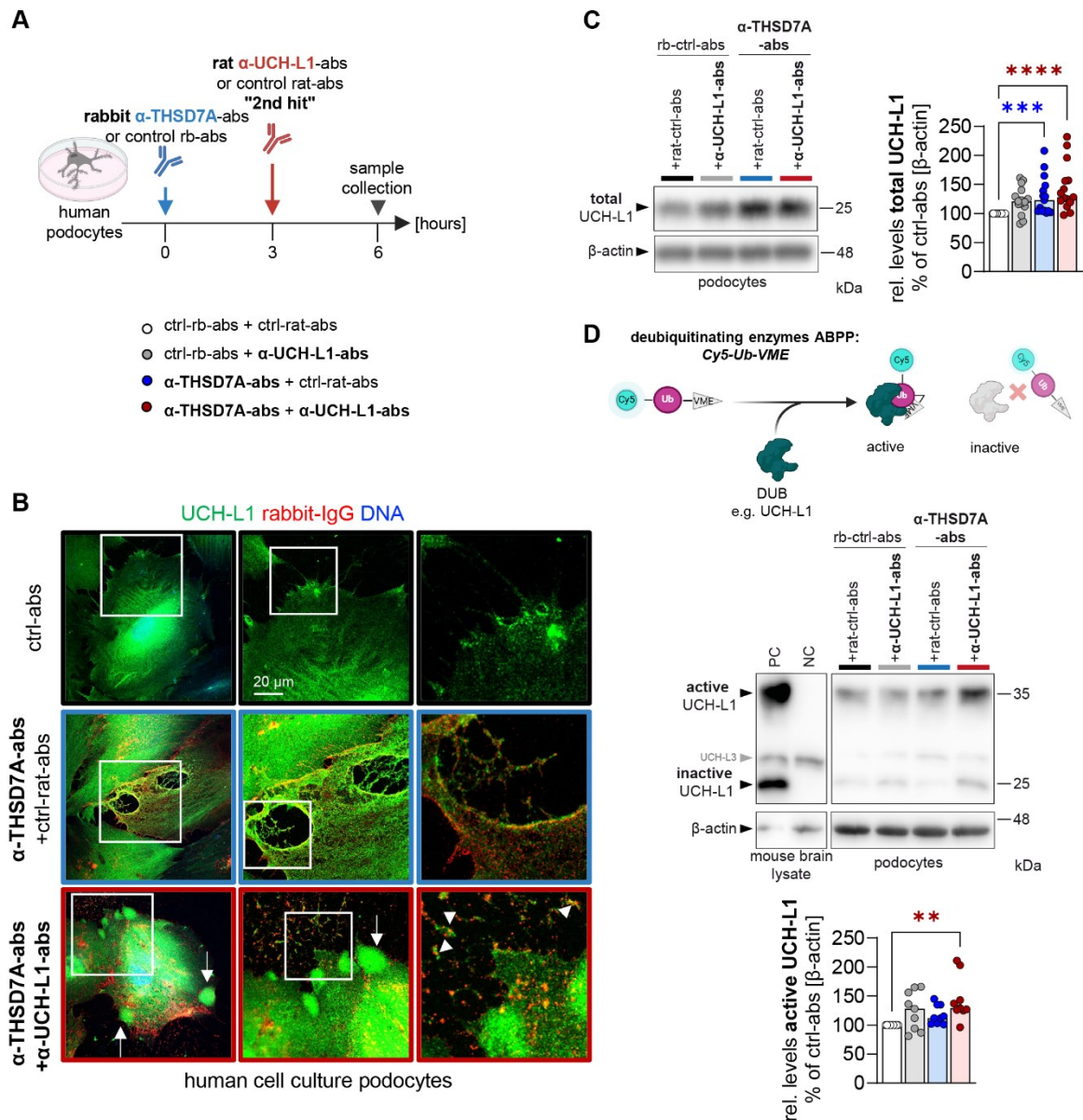


Figure 8: UCH-L1 expression pattern is altered in human cell culture podocytes. (A) Scheme depicting the experimental setup of α -THSD7A antibodies (abs) or respective control (ctrl)-rabbit (rb)-abs treatment and rat U104 α -UCH-L1-abs or ctrl-rat-abs 2nd hit treatment in human THSD7A overexpressing (OE) cell culture podocytes. **(B)** Confocal images of human podocytes show “patch-like” structures of UCH-L1 (green) (white arrows) in THSD7A-abs+2nd hit treated cells. Staining for rabbit-IgG (red) shows THSD7A-abs and DNA (blue). Arrowheads point towards rabbit-IgG and UCH-L1 structures presumably outside of the cell. **(C)** Western blot analyses of total UCH-L1 protein relative to ctrl-abs (unspecific ctrl-rb-abs and ctrl-rat-abs) correlated to the housekeeper β -actin, for $n \geq 7$ per treatment group is shown. PC = positive control, UCH-L1^{WT} mouse brain lysate; NC = negative control, UCH-L1^{KO} mouse brain lysate. Statistical analysis (C-D): median with individual values; Kruskal-Wallis test with Dunn’s multiple comparisons test. ** $p < 0.01$, *** $p < 0.001$, **** $p < 0.0001$

Results

Alongside the cell culture experiments, mouse 2nd hit experiments were analyzed regarding UCH-L1 transcript expression, protein amount as well as activity (Fig. 9 A).

Firstly, UCH-L1 mRNA levels showed a significant increase in THSD7A-MN+2nd hit glomeruli in comparison to glomeruli isolated from control mice (unspecific ctrl-rb-abs + ctrl-rat-abs). The other treatment groups, including THSD7A-abs treatment, showed no alterations of glomerular UCH-L1 transcript expression levels when compared to control mice (Fig. 9 B). Next, total glomerular UCH-L1 protein levels were determined by western blot analysis, which showed a significantly increased amount in glomeruli of THSD7A-MN+2nd hit mice in comparison to control mice (Fig. 9 C). The glomerular UCH-L1 activity, measured by *Cy5-Ub-VME*, showed an increase of inactive (non-functional) UCH-L1 in THSD7A-MN+2nd hit glomeruli which, however, did not reach significance (Fig. 9 D). Here, only the T-PERTM lysate fraction could be analyzed, due to too high amounts of mouse/rat-IgG light chain in the urea lysate fraction which would be present at the same MW as the UCH-L1 protein at 25 kDa. To circumvent this problem in the T-PERTM lysate fraction, UCH-L1 protein was detected via biotinylated rat anti-UCH-L1 antibodies (U104), which is highly sufficient to detect UCH-L1 in BALB/c mouse glomeruli, followed by a goat anti-biotin antibody and an anti-goat detection antibody.

These analyses demonstrate that UCH-L1 *de novo* mRNA expression is increased when anti-UCH-L1 antibodies are applied as a 2nd hit, which however does not lead to increased UCH-L1 activity suggesting the enhanced presence of non-functional UCH-L1 in THSD7A-MN+2nd hit glomeruli.

Results

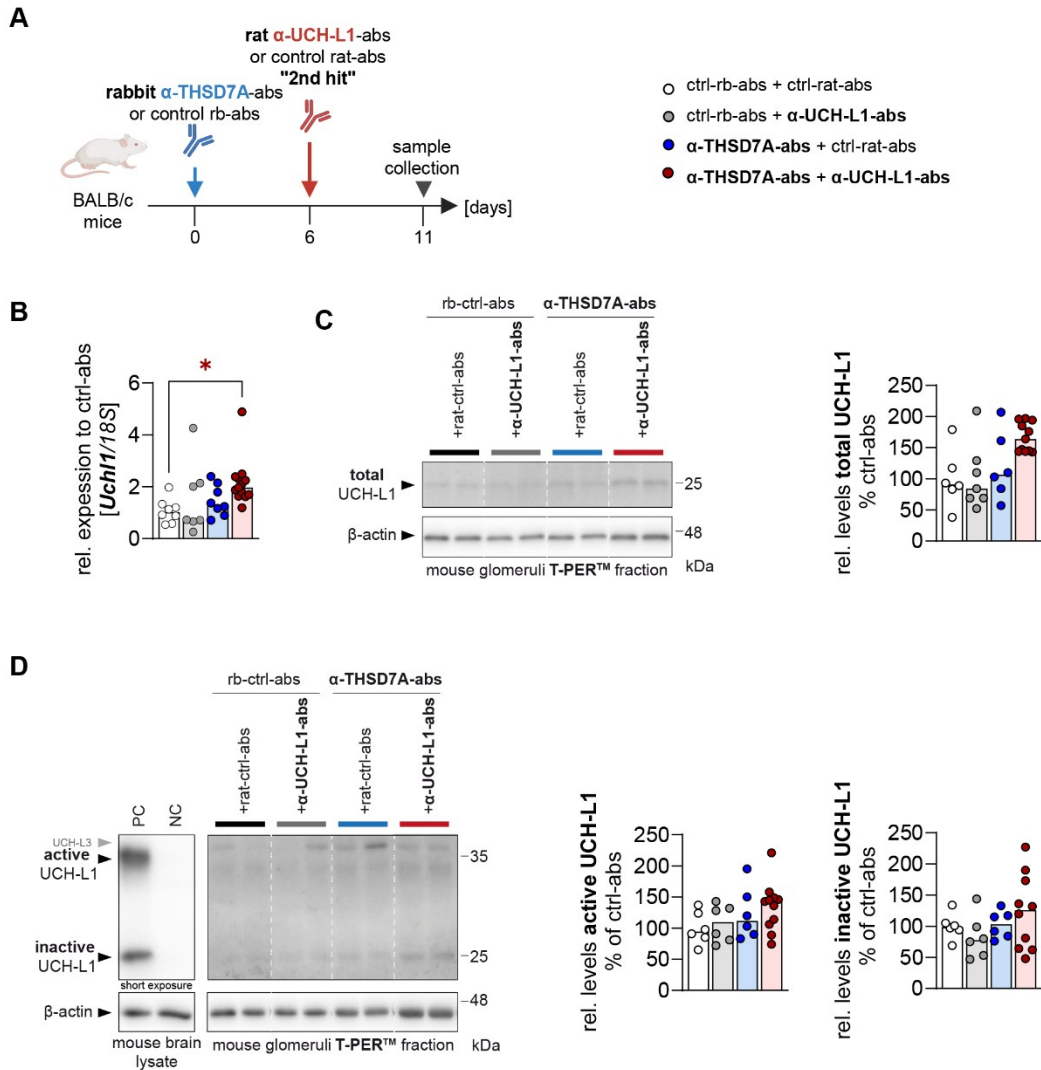


Figure 9: UCH-L1 antigen levels are elevated in THSD7A-MN+2nd hit. (A) Treatment scheme for α -THSD7A-antibodies (abs) MN disease induction with respective control (ctrl) rabbit (rb)-abs and U104 α -UCH-L1-abs 2nd hit with respective ctrl-rat-abs in male BALB/c mice. **(B)** Quantitative (q) PCR analysis of glomerular mRNA levels of *Uchl1* relative to ribosomal 18S housekeeper, calculated relative to ctrl-abs (unspecific ctrl-rb-abs and ctrl-rat-abs). **(C)** Western blot analyses of T-PER™ lysates of glomeruli. Graph depicts densitometric analyses of total UCH-L1 protein calculated relative to ctrl-abs (unspecific ctrl-rb-abs and ctrl-rat-abs) without correlation to housekeeper β -actin. **(D)** ABPP with the DUB ABP *Cy5-Ub-VME* of glomeruli T-PER™ lysates. Graphs depict densitometric analyses of intact "active" (35 kDa) or non-functional "inactive" (25 kDa) UCH-L1 protein relative to ctrl-abs (unspecific ctrl-rb-abs and ctrl-rat-abs). PC = positive control, UCH-L1^{WT} mouse brain lysate; NC = negative control, UCH-L1^{KO} mouse brain lysate. Statistical analysis (B-D): glomeruli of $n \geq 6$ mice were analyzed, median with individual values; Kruskal-Wallis test with Dunn's multiple comparisons test. * $p < 0.05$

3.3 Extracellular vesicles as an exit route for MN antigens

Extracellular vesicles (EVs) could contribute to the clearance of antibody bound antigen such as THSD7A from the glomerular filtration barrier or of non-functional intracellular proteins such as UCH-L1, as they were initially described as "waste carriers" [86]. Furthermore, EVs are known to interplay with the immune system directly by acting as antigen presenters or by activating inflammatory pathways [88]. Therefore,

Results

they can potentially contribute to the formation of autoantibodies especially for secondary intracellular antigens like UCH-L1. In this section EV release dynamics as well as the presence of non-functional antigens were assessed in the setting of THSD7A-MN and THSD7A-MN+2nd hit. Detailed investigations were conducted in cell culture podocytes since this system enables faster and easier access as well as higher amounts of EVs. However, mouse and MN patient urinary EVs were analyzed regarding MN antibody presence and UCH-L1 presence respectively.

3.3.1 EV release is increased in MN

EV release dynamics of MN challenge in cell culture podocytes and mice were analyzed, as it could be shown that stress conditions such as hypoxia, inflammation and oxidative stress increase EV release [90].

Cell culture experiments were performed in a α -THSD7A-abs time course experiment. Therefore, human THSD7A overexpressing (OE) podocytes were challenged for different time points with specific rabbit α -THSD7A antibodies (abs) or as a control with unspecific control (ctrl)-rabbit (rb)-abs, to mimic aspects of THSD7A-associated MN in a cell culture setting. Cells and their corresponding EVs were harvested 1, 6, 24 and 48 hours after treatment to investigate the time-dependent dynamics of antigen and EV release (Fig. 10 A). Total EV amounts released from a defined number of cells (80,000 for ImageStream and 240,000 for western blot analyses) were analyzed after enrichment from cell culture media by ultracentrifugation. Western blot analysis for the general EV markers Flotillin-1, TSG101, 14-3-3 and Annexin A1 revealed elevated amounts of all analyzed EV markers, which were significant only for Annexin A1 of specific (α -THSD7A-abs) as well as unspecific (ctrl-rb-abs) antibody treatment in comparison to untreated (UT) controls (Fig. 10 B). EV levels were shown dynamic changes especially after 1 and 6 hours of treatment. Because of that, the 6-hour timepoint was selected for detailed analyses of released EV amounts via ImageStream and size via nanoparticle tracking analysis (NTA). EVs were stained with MemBrite® Fix Stain (*Mb594*), a fluorescent dye reacting with cell surface proteins, validated to stain EVs and rabbit-IgG (rblgG) to stain for rabbit α -THSD7A-abs which were bound to their target antigen. Significantly increased amounts of rabbit-IgG positive EVs were released by α -THSD7A-abs treated podocytes compared to UT or unspecific ctrl-rb-abs treated podocytes (Fig. 10 C). Further, analysis of the EV size via NTA

Results

measurement showed an increased size of EVs derived from antibody treated cells (Fig. 10 D).

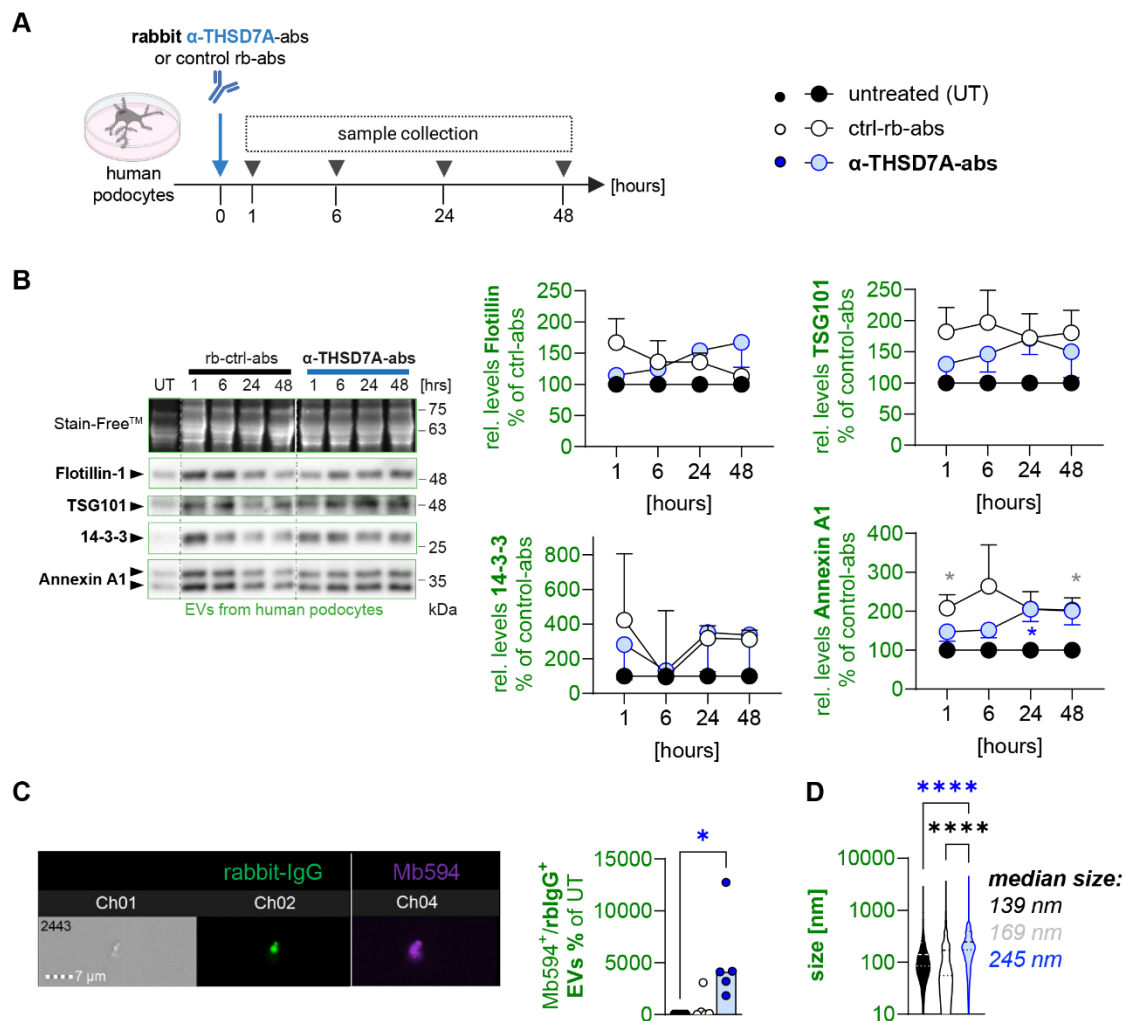


Figure 10: Characterization of human cell culture podocyte-derived extracellular vesicles. (A) Treatment scheme of human THSD7A OE cell culture podocytes. 8×10^4 cells were seeded per well in a 6-well plate and treated with either specific rabbit α -THSD7A-antibodies (abs) or unspecific control (ctrl) rabbit (rb)-abs for 1, 6, 24 or 48 hours. Control cells were not treated with any antibody (untreated [UT]). **(B)** Western blot analysis for the EV marker Flotillin-1, TSG101, 14-3-3 and Annexin A1. Stain-Free™ shows overall protein abundance. Graphs show densitometric quantification relative to UT without correlation to StainFree™, of $n \geq 4$ per time point and group, mean \pm SEM; Mixed-effects analysis with Tuckey's multiple comparisons test. **(C)** ImageStream analysis of EVs from 6-hour treated cells stained for rabbit-IgG (green) and MemBrite Fix 594/615 (*Mb594*, purple). Graph shows values for *Mb594* and rabbit (rb)-IgG double positive EVs from $n=5$ independent experiments calculated relative to UT, median with individual values; Kruskal-Wallis test with Dunn's multiple comparisons test. **(D)** Nanoparticle tracking analysis (NTA) of EVs from 6-hour treated cells of 5 measurements from $n=1$ experiment calculated relative to UT, Kruskal-Wallis test with Dunn's multiple comparisons test. * $p < 0.05$, **** $p < 0.0001$

Subsequently, the THSD7A-MN+2nd hit mouse cohorts as detailed previously (Fig. 11 A) were analyzed for their urinary EV release dynamics. As for the cultured podocytes amounts of specific rb α -THSD7A-abs containing EVs were determined via ImageStream analysis of *Mb594* and rabbit-IgG. The analysis showed an increased

Results

release in THSD7A-MN mice. Measurements of urine collected prior to α -THSD7A-abs treatment (day -1) showed no staining for rabbit-IgG, pointing to a specific staining of rabbit α -THSD7A-abs, bound to their target antigen (Fig. 11 B). Over the course of disease, the amount of rabbit-IgG positive EVs increased, and reached significance on day 11 (Fig. 11 B). However, detailed analyses of the different 2nd hit treatment groups showed no significant differences. Unspecific ctrl-rb-abs + U104 α -UCH-L1-abs treated mice exhibited lower levels of rabbit-IgG positive EVs, when compared to rabbit-IgG control animals with rat-IgG 2nd hit. However, values of rabbit-IgG positive events were below 10% of total EVs in both groups, and therefore relatively low, which makes a definite statement difficult. Rabbit-IgG positive EV amounts were slightly but not significantly increased in THSD7A-MN+2nd hit mice compared to only α -THSD7A-abs treated animals (Fig. 11 C).

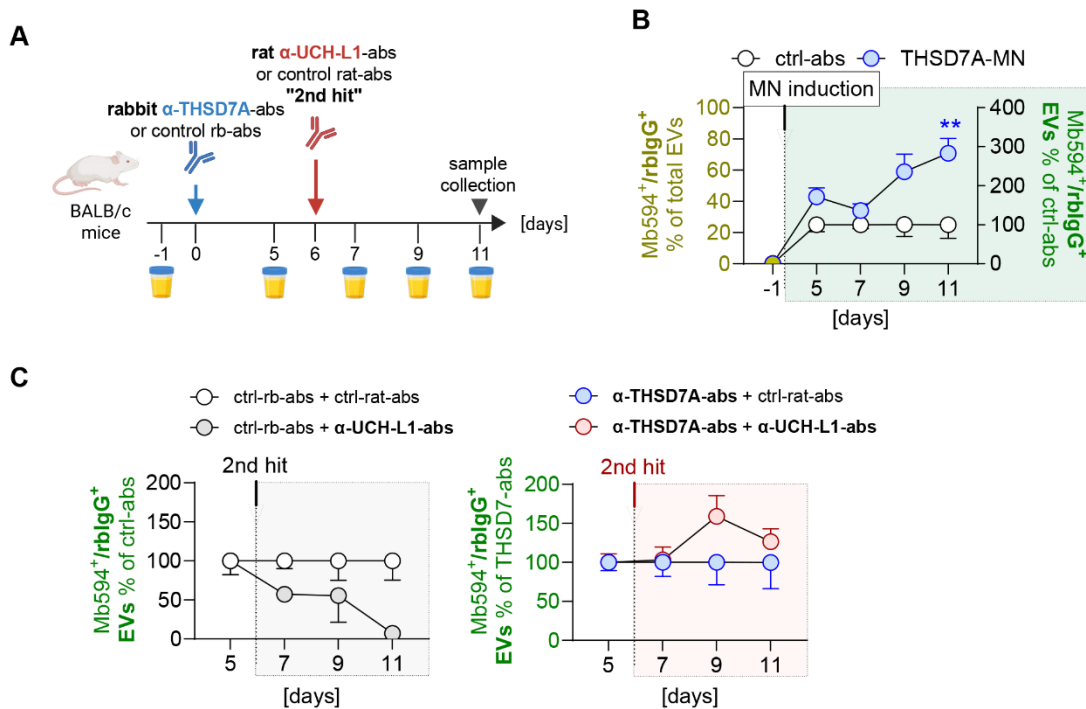


Figure 11: EV release is increased in MN conditions. (A) Treatment scheme of the experimental setup of α -THSD7A-antibodies (abs) MN disease induction with respective control (ctrl) rabbit (rb)-abs and U104 α -UCH-L1-abs 2nd hit with respective ctrl-rat-abs in male BALB/c mice, as well as urine collection at different time points for urinary EV analysis. **(B)** ImageStream analysis of *Mb594* and rabbit (rb)-IgG double positive EVs enriched from the urine of THSD7A-MN relative to control (unspecific ctrl-rb-abs and ctrl-rat-abs), $n \geq 13$ mice. **(C)** Detailed analysis of different 2nd hit groups ctrl-rb-abs with U104 α -UCH-L1-abs 2nd hit relative to ctrl-abs (unspecific ctrl-rb-abs and ctrl-rat-abs) and THSD7A-MN + 2nd hit relative to only α -THSD7A-abs treated mice, $n \geq 9$ mice. Statistical analysis (B-C) mean \pm SEM; Mixed-effects analysis with Tuckey's multiple comparisons test. ** $p < 0.01$

Results

Taken together these results demonstrate, that the release of α -THSD7A-abs containing EVs is triggered upon THSD7A-MN challenge. The anti-UCH-L1-abs 2nd hit, however, only slightly further increases this release.

3.3.2 UCH-L1 is released in EVs as a non-functional form

As a first step to determine whether EVs are an exit route for non-functional UCH-L1, podocyte-specific EVs obtained from urine of different patients, including two MN patients (PLA₂R1-associated and Nell1-associated) as well as a non-MN nephrotic patient with focal segmental glomerulosclerosis (FSGS) were analyzed via ABPP with the ABP *Cy5-Ub-VME* and western blot analysis for the presence of UCH-L1 protein and its enzymatic activity.

Podocyte-specific EVs were isolated from enriched urinary EVs via an immunoprecipitation with antibodies against the podocyte-specific proteins Glepp1 and CD35 (Fig. 12 A). To ensure the comparability of the antigen amount within the EV fraction of the different patients, a total of 1×10^{10} EV particles (determined by ImageStream measurement) were used for each EV subgroup. Furthermore, EVs were analyzed for the general EV markers TSG101, Annexin A1, and Flotillin-1. As shown in Fig. 12 B, UCH-L1 could only be detected in podocyte-specific EVs from MN patients (red asterisks), while in the FSGS patient UCH-L1 could only be observed in the total EVs and the non-podocyte-specific “rest” EVs (black asterisk). Apart from that, UCH-L1 protein released within in EVs, was not able to bind ubiquitin, thus is non-functional (Fig. 12 B).

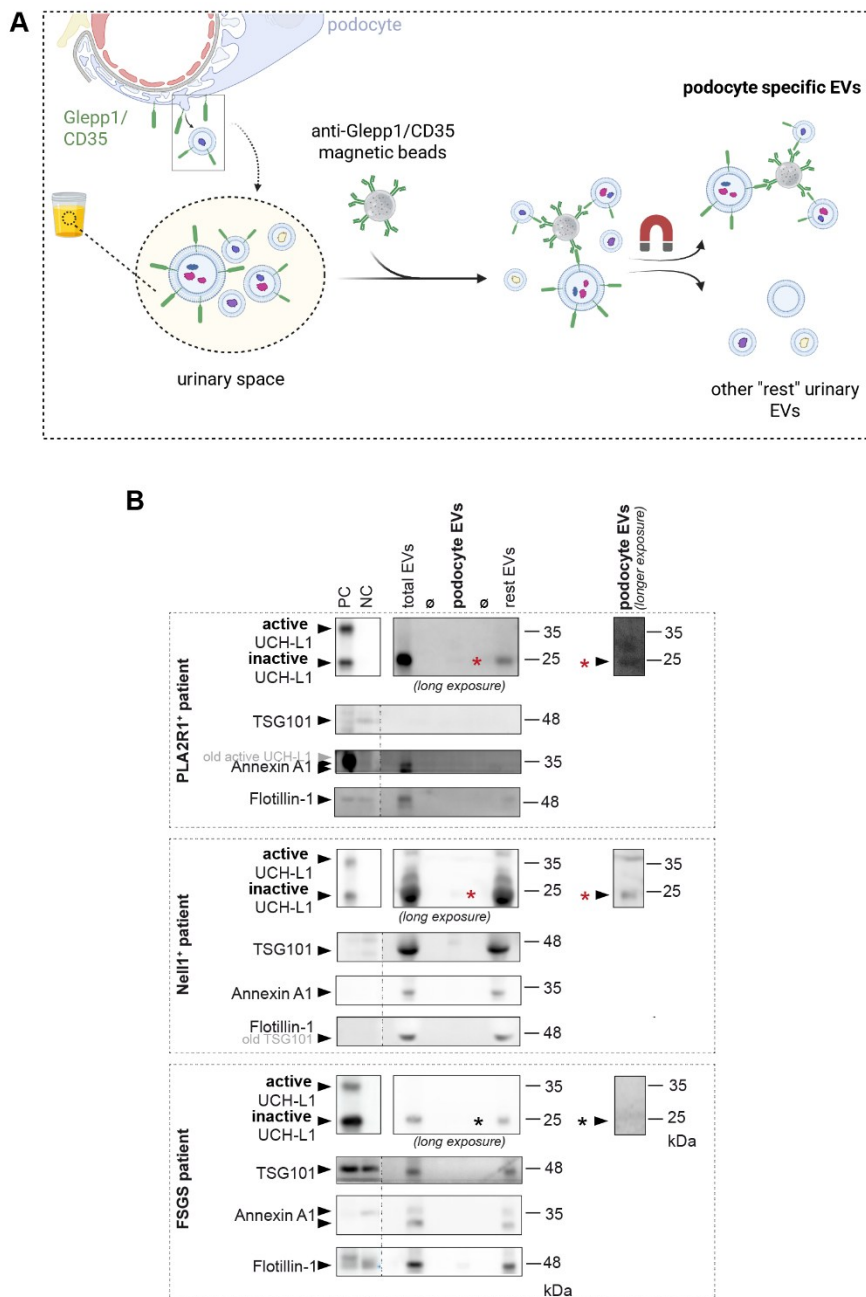


Figure 12: Non-functional UCH-L1 is found in urinary EVs in MN patients. (A) Scheme depicting the workflow of podocyte-specific EVs isolation from patient urine via immunoprecipitation with Glepp1/CD35 coupled magnetic beads. **(B)** In PLA₂R1⁺- and Nell1⁺-MN patients UCH-L1, which is not able to bind the ABP, can be detected in podocyte-specific EVs (red asterisks), while in the FSGS patient podocyte specific EVs, no UCH-L1 can be found (black asterisks). A total amount of 1 × 10¹⁰ EV particles was loaded for total EVs, podocyte EVs as well as rest EVs. PC = positive control, UCH-L1^{WT} mouse brain lysate; NC = negative control, UCH-L1^{KO} mouse brain lysate.

Dynamics of UCH-L1 protein release within EVs and the biochemical properties of EV-released UCH-L1 were in detail investigated in cell culture 2nd hit experiments. As detailed previously, THSD7A OE human podocytes were challenged with α-THSD7A-abs or unspecific control (ctrl)-rabbit (rb)-abs, followed by U104 α-UCH-L1-abs or ctrl-

Results

rat-abs 2nd (Fig. 13 A) and total EV amounts released from a defined number of cells were analyzed after enrichment from cell culture media.

As detailed in Fig. 13 B, ImageStream analysis showed an increased release of rabbit-IgG positive EVs from α -THSD7A-abs challenged cells. Interestingly, no difference between α -THSD7A-abs and U104 α -UCH-L1-abs 2nd hit treated cells could be observed (Fig. 13 B). Furthermore, western blot analysis of the EV markers Flotillin-1, 14-3-3 and Annexin A1 revealed no differences in the abundance of these EV markers in the enriched total EV particles between the treatment groups (Fig. 13 C). Next to EV dynamics, UCH-L1 antigen presence was evaluated with respect to abundance and biochemical properties. Western blot analyses showed no alterations in total UCH-L1 amount in the EVs (Fig. 13 D). However, UCH-L1 protein released within EVs was not detectable by western blotting under non-reducing SDS-PAGE analyses by any of the available anti-UCH-L1 antibodies. Western blot analysis for the corresponding podocytes of the same membrane however, showed detectable amounts of UCH-L1 protein under reducing as well as non-reducing conditions (Fig. 13 D). In addition, ABPP with the *Cy5-Ub-VME* ABP showed that UCH-L1 in EVs was not able to bind ubiquitin, demonstrated by the presence of mainly “inactive”, non-functional UCH-L1 at 25 kDa, which was not bound to the *Cy5-Ub-VME* ABP (Fig. 13 E). As detailed previously for the podocytes, UCH-L1 levels were detected via biotinylated U104 anti-UCH-L1 antibodies.

Together these data indicate that EVs represent a glomerular exit route for non-functional UCH-L1. However, release dynamics are not affected by α -THSD7A-abs or α -THSD7A-abs+2nd hit treatment.

Results

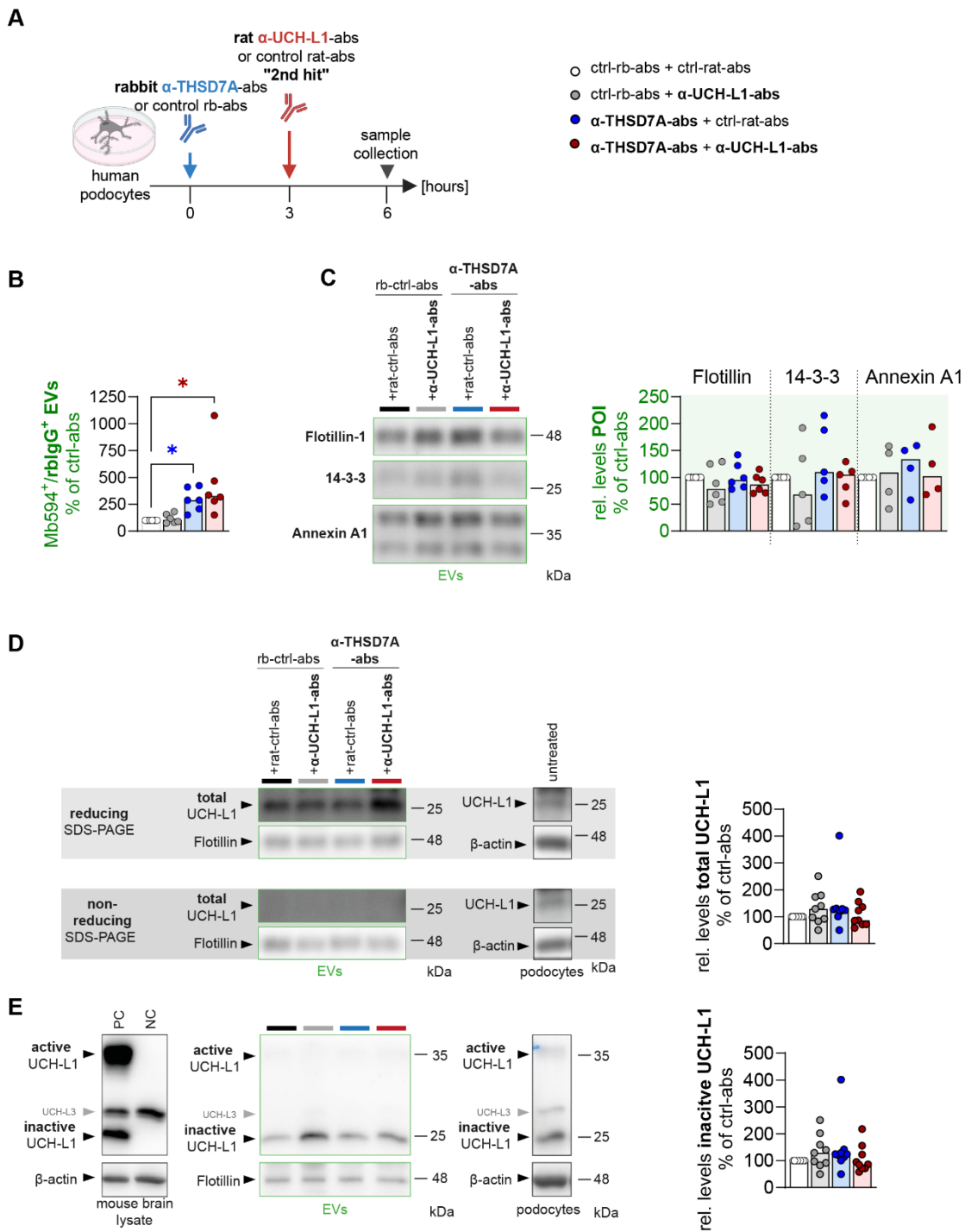


Figure 13: UCH-L1 antigen is altered in EVs. (A) Treatment scheme of α -THSD7A antibodies (abs) or respective control (ctrl)-rabbit (rb)-abs treatment and rat U104 α -UCH-L1-abs or ctrl-rat-abs 2nd hit treatment in human THSD7A overexpressing (OE) cell culture podocytes. (B) Graph showing ImageStream analyses for Mb594 and rabbit-IgG of $n=6$ per treatment group, calculated relative to ctrl-abs (unspecific ctrl-rb-abs and ctrl-rat-abs). (C) Western blot analyses of EVs for the EV marker Flotillin-1, 14-3-3 and Annexin A1. Graphs showing densitometric analyses of $n \geq 4$ per treatment group, calculated relative to ctrl-abs (unspecific ctrl-rb-abs and ctrl-rat-abs). (D) Western blot analyses of reducing and non-reducing SDS-PAGEs showing total UCH-L1 protein in EVs. Graph shows densitometric analyses for $n=5$ per treatment group, calculated relative to ctrl-abs (unspecific ctrl-rb-abs and ctrl-rat-abs). (E) ABPP analyses, using the DUB ABP *Cy5-Ub-VME* show intact (35 kDa) vs non-functional (25 kDa) UCH-L1 in EVs. Densitometric analysis of intact "active" (35 kDa) or non-functional

Results

“inactive” (25 kDa) UCH-L1 for $n \geq 7$ per treatment group is shown, calculated relative to ctrl-abs (unspecific ctrl-rb-abs and ctrl-rat-abs). PC = positive control, UCH-L1^{WT} mouse brain lysate; NC = negative control, UCH-L1^{KO} mouse brain lysate. Statistical analysis (B-E): median with individual values; Kruskal-Wallis test with Dunn’s multiple comparisons test. * $p < 0.05$

3.3.3 THSD7A is released as a proteolytically cleaved protein within cell culture podocyte derived EVs

To investigate in detail whether podocyte-specific EVs carry altered amounts or modified forms of the established antigens such as THSD7A, time course cell culture experiments were conducted as detailed above (Fig. 14 A).

Release dynamics of THSD7A as the primary antigen were evaluated using western blot analyses of the podocytes and their corresponding released EVs. As can be seen in Fig. 14 B, the majority of THSD7A antigen was released in EVs within the first 6 hours after α -THSD7A-abs treatment in comparison to cells treated with control antibodies. Interestingly, a shift in the size of THSD7A protein towards a 230 kDa form could be observed in the released EVs derived from α -THSD7A-abs treated cells (Fig. 14 B, blue arrowhead). To further investigate, if this could represent a proteolytically cleaved (shed) extracellular domain (ECD) of THSD7A, in which the observed size shift could be attributed to the loss of the C-terminal intracellular domain (ICD), western blot analysis with an anti-myc antibody as well as with a self-made specific antibody directed against the C-terminal domain were performed. As can be observed in Fig. 14 C, the anti-myc-tag western blot showed no specific signal in the EVs, while a reprobe with an anti-THSD7A antibody directed against the ECD of the protein exhibited clear bands for THSD7A. Mock cells, which expressed an empty backbone vector were used as a negative control. Secondly, western blot analyses with the C-terminal α -THSD7A antibody showed only a slight band at the expected 245 kDa MW of THSD7A and was missing the smaller approximately 230 kDa fragment. Moreover, a band at about 17 kDa could be observed which was absent in mock cells, confirming that this was the ICD of THSD7A. However, there was no difference in abundance of the 17 kDa ICD THSD7A fragment in the EVs derived from the different treatment groups (Fig. 14 C).

Taken together, these observations indicate that EVs are an exit route for a cleaved form of the THSD7A protein.

Results

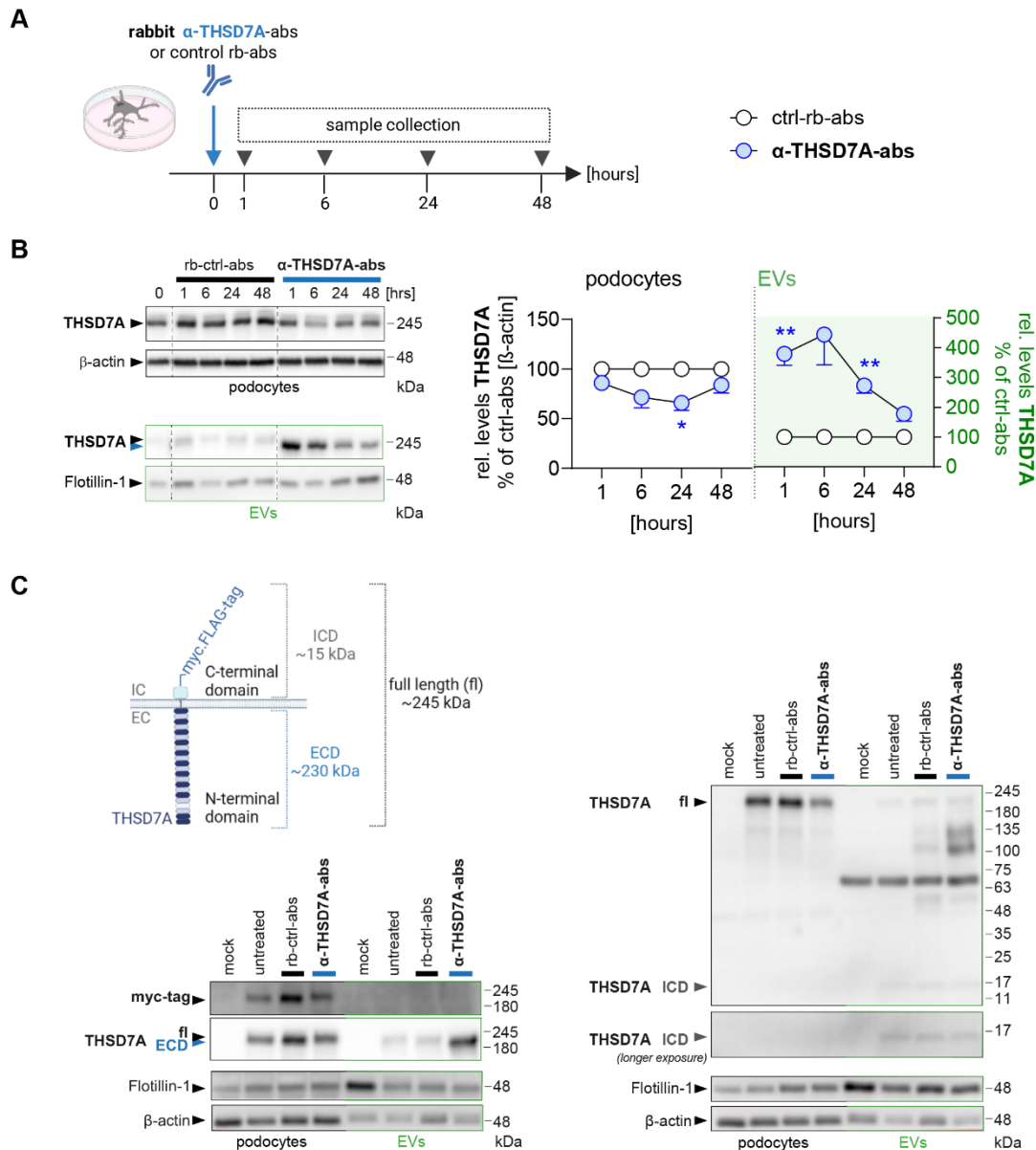


Figure 14: THSD7A is predominantly present as a cleaved fragment in EVs in MN conditions. (A) Treatment scheme of human THSD7A OE cell culture podocytes. 8×10^4 cells were seeded per well in a 6-well plate and treated with either specific rabbit anti-THSD7A-antibodies (abs) or unspecific control rabbit-antibodies (rb-abs) for 1, 6, 24 or 48 hours. Control cells were not treated with any antibody (untreated [UT]). **(B)** General THSD7A-levels were evaluated by western blot analyses of time course experiments in THSD7A OE human podocytes and EVs. Note: the smaller 230 kDa THSD7A fragment in EVs (blue arrowhead). Graphs show densitometric quantification of both THSD7A fragments, correlated to the housekeeper β -actin for podocytes and without correlation for EVs, of $n=5$ per time point and group, mean \pm SEM; Mixed-effects analysis with Tuckey's multiple comparisons test $*p < 0.05$, $**p < 0.01$ **(C)** Detailed analysis of the smaller 230 kDa extracellular domain (ECD) of THSD7A in EVs with western blot analysis against the myc-tag and an anti-THSD7A antibody directed against the intracellular domain (ICD). β -actin was used as loading control for podocytes, and Flotillin-1 as a general EV marker, to show general EV abundance. IC = intracellular, ICD = intracellular domain, EC = extracellular, ECD = extracellular domain, fl = full length.

4 Discussion

4.1 UCH-L1 expression in membranous nephropathy

To exhibit pathogenic effects, (auto)antibodies need to be able to interfere with the antigen. For the primary antigens PLA₂R1 and THSD7A, which possess an extracellular domain, an interference of antibody and antigen could be already proven, which leads to the formation of immune deposits [30]. The by injured podocytes *de novo* expressed Ubiquitin C-terminal Hydrolase L1 (UCH-L1), however, is an intracellular protein [42], which makes its accessibility to (auto)antibodies conceptionally more difficult. Nevertheless, intracellular proteins could be accessible to antibodies by two different mechanisms. First through their localization at the inner leaflet of the cell membrane, which “flips” over during plasma membrane alterations in stress situations, or by the uptake of antibodies i.e. through endocytosis by the cell.

The investigations performed in this project identify a potential UCH-L1 localization at the podocyte cell membrane. By immunohistological staining of a PLA₂R1-associated MN patient kidney biopsy, a specific localization of UCH-L1 at the podocyte foot process (FP) membrane was observed. Similar to the patient observation, the passive THSD7A-MN mouse model exhibited specific UCH-L1 *de novo* expression which likewise located to the podocyte FP membrane close to the THSD7A antigen. These morphologic analyses suggest that UCH-L1 antigen could in theory be accessible to antibodies at the plasma membrane of injured podocytes.

However, because of the limitation of confocal microscopy images, which are two-dimensional images of a three-dimensional system, no precise assumption can be made according to an actual association of UCH-L1 with the membrane. However, posttranslational modification of proteins by farnesylation, which is a lipid modification, causes an increased molecular hydrophobicity of the protein, allowing the farnesylated protein to interact with the cell membrane [104]. UCH-L1 is found to be farnesylated and in this setting to associate with the cell membrane [73]. Therefore, a potential farnesylation of UCH-L1 could be investigated. Another potential mechanism by which anti-UCH-L1 antibodies could access the intracellular protein is by the uptake of the antibodies by the cell. This could be accomplished by pinocytosis more precisely macropinocytosis, an endocytosis mechanism. Macropinocytosis is described in podocytes, where it is thought to be involved in the clearance of plasma proteins which cross the glomerular basement membrane (GBM) [105]. Reactive oxygen species

Discussion

(ROS), a common feature of MN [31], are described to cause lysosomal membrane permeabilization, leading to a damage of lysosomes [89]. Antibodies, internalized by macropinocytosis could then escape the endo-lysosomal pathway through damaged lysosomes to the cytoplasm. Another mechanism by which antibodies are internalized by cells is through Fc receptors. Immunoglobulin G (IgG) is bound by Fc γ receptors through its Fc fragment which initiates phagocytosis. In human and mouse podocytes the only to date validated Fc receptor is the neonatal Fc receptor (FcRn) [106]. This receptor is mainly expressed intracellularly where it is described to contribute to transcytosis of the bound IgG to the urinary space or returning it back to the cell surface [107, 108]. However, it can be present at the cell surface [107] where it contributes to the uptake of IgG into the cell. Investigations of increased membrane localizations of the FcRn could further contribute to the understanding of its role in IgG internalization.

Together these findings provide a first hint for a localization of UCH-L1 towards the podocyte cell membrane, an important requirement for accessibility to anti-UCH-L1 antibodies and a therefore pathogenic role of those. Furthermore, they verify the UCH-L1 *de novo* expression next to its membrane localization in the THSD7A-MN mouse model used for this study, making it a suitable model for investigating a potential pathogenic role of anti-UCH-L1 antibodies. However, more detailed analyses on an actual membrane association of UCH-L1 or other mechanisms by which antibodies could interfere with the antigen could shed light on mechanisms involved in pathogenesis and further reveal potential sites of therapeutic interventions.

4.2 MN is worsened in the THSD7A-MN+2nd hit mouse model

Membranous nephropathy is initiated by circulating autoantibodies against “primary” antigens such as PLA₂R1 and THSD7A. Autoantibodies bind their target and form immune complexes which accumulate in the subepithelial space along the GBM which in the course of disease lead to a thickening of the GBM and foot process effacement [27, 28]. This further leads to a break-down of the GFB and thereby causing proteinuria, the loss of proteins to the urine [29]. In addition, hypoalbuminemia and hyperlipidemia are common clinical characteristics of nephrotic diseases such as MN [1]. The disease outcome, however, appears to be heterogeneous as 40% of MN patients undergo spontaneous remission [27, 28] and another 30% face end-stage renal disease (ESRD) with the need for dialysis or a kidney transplant [27, 28]. Factors influencing disease outcome are to date only partly understood [27]. High levels of circulating

Discussion

autoantibodies in patients' sera, intramolecular epitope spreading as well as intermolecular epitope spreading with autoantibodies directed against intracellular proteins, are linked to a high risk of ESRD [40, 52]. Previous studies of our group [43] and others [40] found autoantibodies directed against the intracellular protein UCH-L1 in MN patient sera. Moreover, these autoantibodies were found to predominantly recognize a non-functional form of UCH-L1 (I93M), which shows structural and biochemical similarity with the oxidative modified protein [43]. As oxidative stress occurs during MN disease development [31], which could alter *de novo* expressed UCH-L1 protein structure, we postulated that anti-UCH-L1 autoantibody formation occurs as a secondary immune response. Those secondary autoantibodies could aggravate the disease through either antigen-unspecific mechanism such as a higher antibody burden or antigen-specific mechanisms by interfering with UCH-L1 protein and thereby modifying protein function. Therefore, we used an established THSD7A-MN mouse model to perform a second hit (2nd hit) with anti-UCH-L1 antibodies (abs) (THSD7A-MN+2nd hit) to mimic this situation.

Verification analysis of the used U104 α -UCH-L1-abs demonstrated that those recognized both human and murine UCH-L1 with a slight preference for the non-functional I93M form. Evaluations in the mouse model revealed that applied U104 α -UCH-L1-abs accumulated along the GBM, the site of MN disease development 5 days after U104 α -UCH-L1-abs application. This verified the used model as suitable for detailed investigations of pathogenic effects of anti-UCH-L1 antibodies.

To be able to identify even mild changes towards worsening or even possible improvement of disease outcome, and to not risk a severity which might lead to termination of the experiment, a relatively "mild" disease development was intended. Therefore, quantity of anti-THSD7A antibodies and rabbit-IgG respectively were adjusted to 0.75 mg instead of the described 1.4 mg per mouse [59]. THSD7A-MN mice from two different cohorts exhibited a mean disease score of 1.9 out of 6 points maximum, confirming a mild disease development. Comparison of THSD7A-MN and THSD7A-MN+2nd hit revealed a slightly higher disease score for mice with U104 α -UCH-L1-abs 2nd hit. Detailed analyses of the clinical parameters showed a particularly higher proteinuria accompanied by a more severe foot process effacement in THSD7A-MN+2nd hit mice, pointing to a greater leakiness of the GFB originating from structural and morphological podocyte alterations.

Discussion

These investigations provide evidence for a pathogenic effect of anti-UCH-L1 antibodies which occur as a secondary immune response in MN, manifesting in a worsening of clinical parameters.

4.3 A higher antibody burden and altered GBM synthesis contribute to the worsening of MN in the anti-UCH-L1-abs 2nd hit

As mentioned earlier, primary autoantibodies cause disease by accumulating together with their antigen (PLA₂R1 or THSD7A) in immune complexes along the GFB, causing damage [30]. Anti-UCH-L1 secondary immune response antibodies could exhibit pathogenic effects through antigen-unspecific mechanisms by causing alteration and further damage on the GFB, without directly altering the function of UCH-L1 protein.

Investigations on the glomerular antibody load revealed an increased accumulation of mouse/rat-IgG in immune complexes. This could point either towards an accumulation of the applied U104 α -UCH-L1 antibodies (rat-IgG) or enhanced production of intrinsic unspecific mouse antibodies (mouse-IgG) as a reaction to the foreign applied antibodies from rabbits or rats. However, mouse and rat antibodies could not be distinguished in these settings, due to the cross-species reactivity of the mouse and rat IgG. Nevertheless, the verification analyses of the used biotinylated U104 α -UCH-L1-abs showed a clear accumulation along the GFB of the anti-UCH-L1-abs. Furthermore, Prunotto *et al.* who discovered the secondary anti-SOD2 and anti- α ENO antibodies in MN patients could demonstrate a localization of those antibodies in immune deposits along the GFB [40]. Together these findings indicate indeed an accumulation of anti-UCH-L1-abs in immune deposits along the GFB. The current understanding of MN disease development includes immune deposits to initiate complement activation, leading to an insertion of the membrane attack complex of the complement system to the plasma membrane, leading to sublytical podocyte stress and reactive oxygen species (ROS) production [30]. This process could be enhanced by the additional deposited anti-UCH-L1 antibodies. However, complement activation as well as ROS production have not been tested in this study.

Another finding of this study was an alteration in the synthesis of the GBM component collagen IV. In THSD7A-MN+2nd hit, but not THSD7A-MN only mice, the mRNA expression of the premature collagen IV α 1 isoform as well as general collagen IV protein levels were increased in the soluble fraction of isolated glomeruli. As collagen IV is synthesized inside the cell and assembled as the α -chain trimer, which then is

Discussion

trafficked outside of the cell [109], this points towards an actual upregulation of the collagen IV synthesis. Studies on MN patient biopsies and the rat MN model showed accumulations of laminin especially the $\beta 1$ subunit and collagen $\alpha 3\alpha 4\alpha 5$ within the thickened GBM [110, 111]. In late stages of MN disease development Kim *et al.* could identify the collagen IV $\alpha 1$ and $\alpha 2$ chains to be increased in the subendothelial space of the GBM [110]. The increased expression of the collagen IV $\alpha 1$ could either be due to the worsening of the disease in THSD7A-MN+2nd hit mice or to a direct effect of the anti-UCH-L1 antibodies on collagen synthesis in podocytes. As collagen IV mRNA levels of the $\alpha 3$ chain are not increased significantly, this may point towards a dedifferentiation of the podocytes. However, because of the analysis of total glomeruli no differentiation according to the origin of collagen IV $\alpha 1$ secretion can be made. To further evaluate this, experiments could be performed in isolated podocytes and endothelial cells using the timMEP technique. This technique enables cell-type specific analyses of the three glomerular cell types, namely podocytes, mesangial cells and endothelial cells [112]. Nevertheless, the premature collagen IV $\alpha 1\alpha 1\alpha 2$ is reported to be less resistant to proteolysis and less cross-linked compared to collagen IV $\alpha 3\alpha 4\alpha 5$, leading to a decreased stability of the GBM [113]. Furthermore, observations in Alport syndrome-associated mice, in which deletion of the Col4a3 gene led to a shift of collagen IV synthesis towards $\alpha 1\alpha 1\alpha 2$, found this form to locate adjacent to podocytes [114], which is not the case for collagen IV $\alpha 3\alpha 4\alpha 5$ in the healthy GBM, as it is located at the center of the GBM, surrounded by the laminin network [19, 114]. It is postulated that the location of collagen IV $\alpha 1\alpha 1\alpha 2$ towards the podocyte foot processes could further perturb podocyte-GBM interaction or impact organization of other components within the GBM [115]. Together these findings provide an explanation for the observed increased proteinuria in THSD7A-MN+2nd hit mice, due to a collagen IV dysregulation-induced GFB damage. However, a distinct localization of the increased collagen IV $\alpha 1$ towards podocytes in THSD7A-MN+2nd hit could not be performed yet. Another hypothesis was postulated by Butt *et al.*, as a compressed GBM is required for its proper function as a selective barrier. This GBM compression is regulated by the two forces affecting the GBM, namely the filtration pressure from the blood and the counteracting buttress force from podocyte foot processes. Podocyte injury with foot process effacement would therefore result in a reduced ability of the podocytes to counteract the filtration force, leading to a reduction of GBM fiber density and a subsequently increased permeability of the GBM to protein [116]. An increased

Discussion

podocyte foot process effacement, which was observed in the THSD7A-MN+2nd hit mice by a decreased filtration slit density (FSD), could hence result from the aforementioned collagen IV dysregulation and lead to a further thickened GBM which is less compressed and then lead to the observed increased proteinuria. In addition to that, future work could be conducted on the evaluation of the GBM thickness in THSD7A-MN+2nd hit mice.

Next to the increased synthesis, collagen IV was observed in aggregates co-localizing with rabbit-IgG in the urinary space in THSD7A-MN+2nd hit mice, which were absent in THSD7A-MN only mice. This could be a potential clearing mechanism of collagen from the subepithelial space, preventing further GFB damage. However, the antibody used for collagen IV detection is described to generally recognize collagen IV without any distinction between the different α -chains. Therefore, no assumptions can be made regarding the collagen subtype in those aggregates.

Together these data showed that anti-UCH-L1 antibodies exhibit pathogenicity through antigen-unspecific mechanisms, which involve a higher antibody burden at the GFB and a dysregulation of GBM synthesis. These mechanisms contribute to the breakdown of the GFB, leading to the previously described aggravation of the disease.

4.4 UCH-L1 *de novo* expression is altered by anti-UCH-L1-abs 2nd hit while activity (ubiquitin binding) is not impaired

As described earlier UCH-L1 was found to localize at the podocyte FP membrane. Investigations in THSD7A-abs+2nd hit treated cell culture podocytes showed a specific staining for UCH-L1 and the applied U104 α -UCH-L1-abs in “patch-like” structures. This further proves that *in vivo* applied α -UCH-L1-abs indeed can bind their mainly intracellular target antigen. Therefore α -UCH-L1 antibodies could exhibit antigen-specific mechanisms next to the previous mentioned antigen-unspecific mechanisms. UCH-L1 is well characterized to function in the stabilization of monoubiquitin levels [77], and is further reported to exhibit ubiquitin hydrolase as well as a highly debated ligase function [75]. Dysregulation of UCH-L1 expression and function are associated with neurodegenerative diseases [67, 80]. In detail, alterations in UCH-L1 protein structure such as mutations (e.g. I93M) or oxidative modifications lead to a toxic gain-of-function represented by altered protein interactions [79, 81], a partial loss of catalytic activity [78] and a decreased solubility of the protein [79]. In previous studies of our group, non-functional UCH-L1 (I93M) was shown to aberrantly interact with the

Discussion

proteasome, the central complex of the protein degrading ubiquitin-proteasome system (UPS), by blocking its activity [43]. In addition to the dysregulation of UCH-L1 in MN, a subset of patients was found to exhibit autoantibodies targeting UCH-L1, especially the non-functional form [40, 43]. However, it is not known in which manner anti-UCH-L1 autoantibodies affect UCH-L1 protein function.

As UCH-L1 is *de novo* expressed in injured podocytes in MN [32, 42], general UCH-L1 protein and mRNA expression levels were evaluated. THSD7A-abs+2nd hit treatment showed increased UCH-L1 levels in cell culture podocytes and mouse glomeruli. However, UCH-L1 levels were only slightly increased in THSD7A-abs only treatments. This could be due to the lower dose of the applied anti-THSD7A-abs for disease induction which might not be sufficient to induce strong *de novo* expression in mice.

Investigations on UCH-L1 enzymatic activity in human cell culture as well as mice experiments, via the ABP *Cy5-Ub-VME* revealed no influence of the anti-UCH-L1-abs on the ability of cytoplasmic UCH-L1 to bind ubiquitin. This could be due to disability of the antibodies to bind the catalytic site, which is usually restricted through an unstructured loop, until ubiquitin binding [67]. Furthermore, antibodies of the IgG subclass have a molecular weight of 150 kDa, which is rather “big” compared to the 25 kDa UCH-L1 protein. This could further point towards the inability of the antibodies to bind within the active site of UCH-L1. Therefore, anti-UCH-L1 could exhibit their antigen-specific pathogenic effects through the formation of the above-described UCH-L1/IgG aggregates rather than directly influencing its enzymatic activity. Next to its well described function in ubiquitin binding and mono-ubiquitin stabilization, it can hydrolyze ubiquitin from small C-terminal extensions [67]. Nevertheless, no assumptions can be made on a potential impact of anti-UCH-L1 antibodies on the UCH-L1 hydrolysis function. Therefore, other tests such as an Ub-AMC assay would be necessary to determine the hydrolase activity of UCH-L1 (functional and non-functional) in combination with anti-UCH-L1 antibodies.

Together these data support the hypothesis for a dysregulation of UCH-L1 localization and abundance in THSD7A-MN+2nd hit conditions. Specific anti-UCH-L1-abs impact the localization of UCH-L1 protein within the cell as well as the amount towards increased UCH-L1 levels. The enzymes ubiquitin binding ability, however, is not influenced by the antibodies.

4.5 Extracellular vesicles as a potential exit route for MN antigens

Extracellular vesicles (EVs) as membrane enclosed particles released by cells [85] play an important role in cell-cell interactions and signaling in homeostasis as well as disease [86, 87]. Kidney cells which face the urinary space, namely podocytes, cells of the proximal and distal tubule, and the collecting duct contribute to the secretion of urinary EVs [91]. Those urinary EVs are of great interest, as changes in amount and cargo appear during disease development [91]. Furthermore, EVs could act as exit routes for disease associated MN antigens. The main MN target antigen PLA₂R1 was found to be constitutively present in urinary EVs [117]. Similar to PLA₂R1, THSD7A and possibly UCH-L1 could leave podocytes through EVs as well. After secretion EVs can interact with other cells, and are found to directly interact with the immune system [88], thereby playing a role in the pathogenesis of diseases. As for the kidney, EVs were found to be taken up by tubular epithelial cells [90]. Through those routes antigens could be presented to the immune system and further lead to autoimmune reactions and trigger autoantibody production. However, those mechanisms are not yet fully understood in kidney diseases such as MN and need further investigations.

The present study revealed an increased amount of EVs carrying MN causing antibodies (α -THSD7A-abs) in EVs released from THSD7A-abs treated cell culture podocytes as well as THSD7A-MN mouse urinary EVs. This could be a general clearing mechanism of the podocytes to release antibody bound antigens, which accumulate in immune deposits along the GFB. Nevertheless, application of an α -UCH-L1-abs 2nd hit showed no significant influence on the amount of α -THSD7A-abs carrying EVs.

However, more relevant than the absolute EV amounts released may be their cargo, as they could carry damaged proteins including MN antigens. The in this study most relevant secondary antigen UCH-L1 was present within podocyte-derived EVs. Furthermore, the UCH-L1 protein within podocyte-derived EVs was not able to bind ubiquitin properly (via the ABP *Cy5-Ub-VME*) and was structurally altered in the way, that commercial antibodies could not recognize the protein. However, neither THSD7A-abs nor THSD7A-abs+2nd hit treatment exhibited an influence on the UCH-L1 amount released via EVs in cell culture experiments. THSD7A-abs associated UCH-L1 *de novo* expression could in theory result in an increased released (non-functional) UCH-L1 via EVs to prevent a potential cell damage by (non-functional) UCH-L1. Interestingly, anti-

Discussion

UCH-L1 autoantibodies found in MN patients predominantly recognize the non-functional form of UCH-L1, which is the prominent UCH-L1 form present in podocyte-derived EVs. Hence it is intriguing to hypothesize the released podocyte-derived EVs are taken up by other cells downstream of the nephron, namely proximal or distal tubular cells, for presentation of non-functional UCH-L1 as a neo-antigen to immune cells. Future experiments in which tubular cells are exposed to podocyte-derived EVs, could shed light on this hypothesis. Additionally, the released EVs themselves could activate immune cells. By this antigen presenting cells could be activated which in turn could lead to B cell activation and proliferation towards anti-UCH-L1 antibody-secreting plasma cells. This indicates that podocyte-derived EVs might represent the glomerular exit route for dysfunctional UCH-L1, required for the subsequent development of anti-UCH-L1 autoimmunity.

Next to UCH-L1, additional investigations on the primary MN antigen THSD7A revealed the presence of the cleaved extracellular domain (ECD) of the THSD7A protein in cell culture podocyte EVs. This could be proven by the expression system of a myc.FLAG-tagged THSD7A protein in human cell culture podocytes. Through the absence of the myc-tag in EVs, which is located at the C-terminal intracellular domain (ICD), the cleaved THSD7A represents the extracellular domain of the protein. Cleavage of THSD7A could be mediated through the A Disintegrin And Metalloproteinase 10 (ADAM10), which was recently shown by the Paul Saftig group (Kiel) and our group, to be involved in the shedding of THSD7A (Rosenbaum *et al.*, in revision). Together with the increased amounts of anti-THSD7A-abs carrying EVs, this could represent a clearing mechanism of the antibody-bound THSD7A antigen.

Taken together these data demonstrate that EVs play a role in the secretion of structurally altered antigens. Non-functional UCH-L1 is released via podocyte-derived EVs in cell culture and MN patients, which implicates that EVs may contribute to anti-UCH-L1 autoimmunity. Clearance of the primary MN antigen THSD7A involves predominantly release of the extracellular domain of THSD7A via EVs.

4.6 Conclusion

Taken together this study demonstrates a pathogenic role of anti-UCH-L1 antibodies which occur as a secondary immune reaction in MN with antigen-unspecific mechanisms as well as antigen-specific mechanism having an impact. As one antigen-unspecific mechanism an increased glomerular burden of mouse/rat antibodies

Discussion

contributes to a worsening of disease, which manifests as enhanced foot process effacement and proteinuria. Furthermore, GBM collagen IV synthesis is altered towards a premature form pointing to an enhanced podocyte injury. Besides that, antigen-specific mechanisms involve an altered distribution of UCH-L1 within the podocyte, leading to the assumption that UCH-L1 antigen is accessible to the antibodies. Regarding the accessibility of the intracellular protein UCH-L1 to the immune system, EVs as carriers of non-functional UCH-L1 might play an important role. This work highlights the impact of secondary antigens in MN and their contribution to MN disease development. It furthermore reveals the necessity for the search for other putative antigens to deepen the understanding of MN pathomechanisms.

5 Literature

1. Wendt, R., Sobhani, A., Diefenhardt, P., Trappe, M., and Völker, L.A., *An Updated Comprehensive Review on Diseases Associated with Nephrotic Syndromes*. Biomedicines, 2024. **12**(10).
2. Finco, D.R., *Kidney Function*, in *Clinical Biochemistry of Domestic Animals*. 1997, Elsevier, Inc. Philadelphia. p. 441-484.
3. Munger, K.A., Kost C.K., Brenner B.M., Maddox D.A., *The Renal Circulations and Glomerular Ultrafiltration*, in *Brenner and Rector's The Kidney*. 2016, Elsevier, Inc. Philadelphia. p. 83-111.
4. Lote, C.J., *Principles of Renal Physiology*. 2012: Springer.
5. Shankland, S.J., Mathieson, P. W., *The Podocyte*, in *Brenner and Rector's The Kidney*. 2016, Elsevier, Inc. Philadelphia. p. 112-121.
6. Meyer-Schwesinger, C., Huber, T. B., *Glomerular Cell Biology and Podocytopathies*, in *Brenner and Rector's The Kidney*. 2019, Elsevier, Inc. Philadelphia. p. 115-155.
7. Verlander, J.W., Clapp, W. L., *Anatomy of the Kidney*, in *Brenner and Rector's The Kidney*. 2020, Elsevier, Inc. Philadelphia. p. 38-79.
8. Abrahamson, D.R., *Structure and development of the glomerular capillary wall and basement membrane*. Am J Physiol, 1987. **253**(5 Pt 2): p. F783-94.
9. Holzman, L.B. and Garg, P., *Initial insight on the determinants of podocyte polarity*. J Am Soc Nephrol, 2009. **20**(4): p. 683-5.
10. Rodewald, R. and Karnovsky, M.J., *Porous substructure of the glomerular slit diaphragm in the rat and mouse*. J Cell Biol, 1974. **60**(2): p. 423-33.
11. Grahammer, F., Schell, C., and Huber, T.B., *The podocyte slit diaphragm--from a thin grey line to a complex signalling hub*. Nat Rev Nephrol, 2013. **9**(10): p. 587-98.
12. Grahammer, F., Wigge, C., Schell, C., Kretz, O., Patrakka, J., Schneider, S., Klose, M., Kind, J., Arnold, S.J., Habermann, A., Brauniger, R., Rinschen, M.M., Volker, L., Bregenzer, A., Rubbenstroth, D., Boerries, M., Kerjaschki, D., Miner, J.H., Walz, G., Benzing, T., Fornoni, A., Frangakis, A.S., and Huber, T.B., *A flexible, multilayered protein scaffold maintains the slit in between glomerular podocytes*. JCI Insight, 2016. **1**(9).
13. Boute, N., Gribouval, O., Roselli, S., Benessy, F., Lee, H., Fuchshuber, A., Dahan, K., Gubler, M.C., Niaudet, P., and Antignac, C., *NPHS2, encoding the glomerular protein podocin, is mutated in autosomal recessive steroid-resistant nephrotic syndrome*. Nat Genet, 2000. **24**(4): p. 349-54.
14. Welsh, G.I. and Saleem, M.A., *The podocyte cytoskeleton--key to a functioning glomerulus in health and disease*. Nat Rev Nephrol, 2011. **8**(1): p. 14-21.
15. Ichimura, K., Kurihara, H., and Sakai, T., *Actin filament organization of foot processes in rat podocytes*. J Histochem Cytochem, 2003. **51**(12): p. 1589-600.
16. Neal, C.R., *Podocytes ... What's Under Yours? (Podocytes and Foot Processes and How They Change in Nephropathy)*. Front Endocrinol (Lausanne), 2015. **6**: p. 9.
17. Faul, C., Asanuma, K., Yanagida-Asanuma, E., Kim, K., and Mundel, P., *Actin up: regulation of podocyte structure and function by components of the actin cytoskeleton*. Trends Cell Biol, 2007. **17**(9): p. 428-37.
18. Schell, C., Rogg, M., Suhm, M., Helmstadter, M., Sellung, D., Yasuda-Yamahara, M., Kretz, O., Kuttner, V., Suleiman, H., Kollipara, L., Zahedi, R.P.,

- Sickmann, A., Eimer, S., Shaw, A.S., Kramer-Zucker, A., Hirano-Kobayashi, M., Abe, T., Aizawa, S., Grahammer, F., Hartleben, B., Dengjel, J., and Huber, T.B., *The FERM protein EPB41L5 regulates actomyosin contractility and focal adhesion formation to maintain the kidney filtration barrier*. Proc Natl Acad Sci U S A, 2017. **114**(23): p. E4621-E4630.
19. Naylor, R.W., Morais, M., and Lennon, R., *Complexities of the glomerular basement membrane*. Nat Rev Nephrol, 2021. **17**(2): p. 112-127.
 20. Abrahamson, D.R., *Role of the podocyte (and glomerular endothelium) in building the GBM*. Semin Nephrol, 2012. **32**(4): p. 342-9.
 21. Miner, J.H., *Renal basement membrane components*. Kidney Int, 1999. **56**(6): p. 2016-24.
 22. Lennon, R., Randles, M.J., and Humphries, M.J., *The importance of podocyte adhesion for a healthy glomerulus*. Front Endocrinol (Lausanne), 2014. **5**: p. 160.
 23. Navar, L.G., Maddox, D. A., Munger, K. A., *The Renal Circulations and Glomerular Filtration*, in *Brenner and Rector's The Kidney*. 2020, Elsevier, Inc. Philadelphia. p. 80-114.
 24. Lerma, E.V., Sparks, M.A., and Topf, J., *Urinalysis*, in *Nephrology Secrets*. 2018, Elsevier, Inc. Philadelphia. p. 9-21.
 25. Borza, D.B., Zhang, J.J., Beck, L.H., Jr., Meyer-Schwesinger, C., and Luo, W., *Mouse models of membranous nephropathy: the road less travelled by*. Am J Clin Exp Immunol, 2013. **2**(2): p. 135-45.
 26. Glasscock, R.J., *The pathogenesis of membranous nephropathy: evolution and revolution*. Curr Opin Nephrol Hypertens, 2012. **21**(3): p. 235-42.
 27. Ronco, P. and Debiec, H., *Molecular Pathogenesis of Membranous Nephropathy*. Annu Rev Pathol, 2020. **15**: p. 287-313.
 28. Tomas, N.M., Huber, T.B., and Hoxha, E., *Perspectives in membranous nephropathy*. Cell Tissue Res, 2021. **385**(2): p. 405-422.
 29. Ronco, P., Beck, L., Debiec, H., Fervenza, F.C., Hou, F.F., Jha, V., Sethi, S., Tong, A., Vivarelli, M., and Wetzels, J., *Membranous nephropathy*. Nat Rev Dis Primers, 2021. **7**(1): p. 69.
 30. Hoxha, E., Reinhard, L., and Stahl, R.A.K., *Membranous nephropathy: new pathogenic mechanisms and their clinical implications*. Nat Rev Nephrol, 2022. **18**(7): p. 466-478.
 31. Neale, T.J., Ullrich, R., Ojha, P., Poczewski, H., Verhoeven, A.J., and Kerjaschki, D., *Reactive oxygen species and neutrophil respiratory burst cytochrome b558 are produced by kidney glomerular cells in passive Heymann nephritis*. Proc Natl Acad Sci U S A, 1993. **90**(8): p. 3645-9.
 32. Beeken, M., Lindenmeyer, M.T., Blattner, S.M., Radon, V., Oh, J., Meyer, T.N., Hildebrand, D., Schluter, H., Reinicke, A.T., Knop, J.H., Vivekanandan-Giri, A., Munster, S., Sachs, M., Wiech, T., Pennathur, S., Cohen, C.D., Kretzler, M., Stahl, R.A., and Meyer-Schwesinger, C., *Alterations in the ubiquitin proteasome system in persistent but not reversible proteinuric diseases*. J Am Soc Nephrol, 2014. **25**(11): p. 2511-25.
 33. Stahl, R., Hoxha, E., and Fechner, K., *PLA2R autoantibodies and recurrent membranous nephropathy after transplantation*. N Engl J Med, 2010. **363**(5): p. 496-8.
 34. Quintana, L.F., Blasco, M., Seras, M., Perez, N.S., Lopez-Hoyos, M., Villarroel, P., Rodrigo, E., Vinas, O., Ercilla, G., Diekmann, F., Gomez-Roman, J.J., Fernandez-Fresnedo, G., Oppenheimer, F., Arias, M., and Campistol, J.M., *Antiphospholipase A2 Receptor Antibody Levels Predict the Risk of*

- Posttransplantation Recurrence of Membranous Nephropathy*. Transplantation, 2015. **99**(8): p. 1709-14.
35. Debiec, H., Guignonis, V., Mougenot, B., Decobert, F., Haymann, J.P., Bensman, A., Deschenes, G., and Ronco, P.M., *Antenatal membranous glomerulonephritis due to anti-neutral endopeptidase antibodies*. N Engl J Med, 2002. **346**(26): p. 2053-60.
 36. Vivarelli, M., Emma, F., Pelle, T., Gerken, C., Pedicelli, S., Diomedi-Camassei, F., Klaus, G., Waldegger, S., Ronco, P., and Debiec, H., *Genetic homogeneity but IgG subclass-dependent clinical variability of alloimmune membranous nephropathy with anti-neutral endopeptidase antibodies*. Kidney Int, 2015. **87**(3): p. 602-9.
 37. Beck, L.H., Jr., Bonegio, R.G., Lambeau, G., Beck, D.M., Powell, D.W., Cummins, T.D., Klein, J.B., and Salant, D.J., *M-type phospholipase A2 receptor as target antigen in idiopathic membranous nephropathy*. N Engl J Med, 2009. **361**(1): p. 11-21.
 38. Tomas, N.M., Beck, L.H., Jr., Meyer-Schwesinger, C., Seitz-Polski, B., Ma, H., Zahner, G., Dolla, G., Hoxha, E., Helmchen, U., Dabert-Gay, A.S., Debayle, D., Merchant, M., Klein, J., Salant, D.J., Stahl, R.A.K., and Lambeau, G., *Thrombospondin type-1 domain-containing 7A in idiopathic membranous nephropathy*. N Engl J Med, 2014. **371**(24): p. 2277-2287.
 39. Sethi, S., Beck, L.H., Jr., Glassock, R.J., Haas, M., De Vriese, A.S., Caza, T.N., Hoxha, E., Lambeau, G., Tomas, N.M., Madden, B., Debiec, H., D'Agati, V.D., Alexander, M.P., Amer, H., Appel, G.B., Barbour, S.J., Caravaca-Fontan, F., Cattran, D.C., Casal Moura, M., D'Avila, D.O., Eick, R.G., Garovic, V.D., Greene, E.L., Herrera Hernandez, L.P., Jennette, J.C., Lieske, J.C., Markowitz, G.S., Nath, K.A., Nasr, S.H., Nast, C.C., Pani, A., Praga, M., Remuzzi, G., Rennke, H.G., Ruggenenti, P., Roccatello, D., Soler, M.J., Specks, U., Stahl, R.A.K., Singh, R.D., Theis, J.D., Velosa, J.A., Wetzels, J.F.M., Winearls, C.G., Yandian, F., Zand, L., Ronco, P., and Fervenza, F.C., *Mayo Clinic consensus report on membranous nephropathy: proposal for a novel classification*. Kidney Int, 2023.
 40. Prunotto, M., Carnevali, M.L., Candiano, G., Murtas, C., Bruschi, M., Corradini, E., Trivelli, A., Magnasco, A., Petretto, A., Santucci, L., Mattei, S., Gatti, R., Scolari, F., Kador, P., Allegri, L., and Ghiggeri, G.M., *Autoimmunity in membranous nephropathy targets aldose reductase and SOD2*. J Am Soc Nephrol, 2010. **21**(3): p. 507-19.
 41. Bruschi, M., Carnevali, M.L., Murtas, C., Candiano, G., Petretto, A., Prunotto, M., Gatti, R., Argentiero, L., Magistroni, R., Garibotto, G., Scolari, F., Ravani, P., Gesualdo, L., Allegri, L., and Ghiggeri, G.M., *Direct characterization of target podocyte antigens and auto-antibodies in human membranous glomerulonephritis: Alfa-enolase and borderline antigens*. J Proteomics, 2011. **74**(10): p. 2008-17.
 42. Meyer-Schwesinger, C., Meyer, T.N., Munster, S., Klug, P., Saleem, M., Helmchen, U., and Stahl, R.A., *A new role for the neuronal ubiquitin C-terminal hydrolase-L1 (UCH-L1) in podocyte process formation and podocyte injury in human glomerulopathies*. J Pathol, 2009. **217**(3): p. 452-64.
 43. Reichelt, J., Sachs, W., Frombling, S., Fehlert, J., Studencka-Turski, M., Betz, A., Loreth, D., Blume, L., Witt, S., Pohl, S., Brand, J., Czesla, M., Knop, J., Florea, B.I., Zielinski, S., Sachs, M., Hoxha, E., Hermans-Borgmeyer, I., Zahner, G., Wiech, T., Kruger, E., and Meyer-Schwesinger, C., *Non-functional ubiquitin C-terminal hydrolase L1 drives podocyte injury through impairing*

- proteasomes in autoimmune glomerulonephritis*. Nat Commun, 2023. **14**(1): p. 2114.
44. Sethi, S. and Madden, B., *Mapping antigens of membranous nephropathy: almost there*. Kidney Int, 2023. **103**(3): p. 469-472.
 45. Sethi, S., Madden, B.J., Debiec, H., Charlesworth, M.C., Gross, L., Ravindran, A., Hummel, A.M., Specks, U., Fervenza, F.C., and Ronco, P., *Exostosin 1/Exostosin 2-Associated Membranous Nephropathy*. J Am Soc Nephrol, 2019. **30**(6): p. 1123-1136.
 46. Sethi, S., Debiec, H., Madden, B., Charlesworth, M.C., Morelle, J., Gross, L., Ravindran, A., Buob, D., Jadoul, M., Fervenza, F.C., and Ronco, P., *Neural epidermal growth factor-like 1 protein (NELL-1) associated membranous nephropathy*. Kidney Int, 2020. **97**(1): p. 163-174.
 47. Sethi, S., Debiec, H., Madden, B., Vivarelli, M., Charlesworth, M.C., Ravindran, A., Gross, L., Ulinski, T., Buob, D., Tran, C.L., Emma, F., Diomedici-Camassei, F., Fervenza, F.C., and Ronco, P., *Semaphorin 3B-associated membranous nephropathy is a distinct type of disease predominantly present in pediatric patients*. Kidney Int, 2020. **98**(5): p. 1253-1264.
 48. Caza, T.N., Hassen, S.I., Kuperman, M., Sharma, S.G., Dvanajscak, Z., Arthur, J., Edmondson, R., Storey, A., Herzog, C., Kenan, D.J., and Larsen, C.P., *Neural cell adhesion molecule 1 is a novel autoantigen in membranous lupus nephritis*. Kidney Int, 2021. **100**(1): p. 171-181.
 49. Caza, T.N., Storey, A.J., Hassen, S.I., Herzog, C., Edmondson, R.D., Arthur, J.M., Kenan, D.J., and Larsen, C.P., *Discovery of seven novel putative antigens in membranous nephropathy and membranous lupus nephritis identified by mass spectrometry*. Kidney Int, 2023. **103**(3): p. 593-606.
 50. Tomas, N.M., Hoxha, E., Reinicke, A.T., Fester, L., Helmchen, U., Gerth, J., Bachmann, F., Budde, K., Koch-Nolte, F., Zahner, G., Rune, G., Lambeau, G., Meyer-Schwesinger, C., and Stahl, R.A., *Autoantibodies against thrombospondin type 1 domain-containing 7A induce membranous nephropathy*. J Clin Invest, 2016. **126**(7): p. 2519-32.
 51. Kanigicherla, D., Gummadova, J., McKenzie, E.A., Roberts, S.A., Harris, S., Nikam, M., Poulton, K., McWilliam, L., Short, C.D., Venning, M., and Brenchley, P.E., *Anti-PLA2R antibodies measured by ELISA predict long-term outcome in a prevalent population of patients with idiopathic membranous nephropathy*. Kidney Int, 2013. **83**(5): p. 940-8.
 52. Seitz-Polski, B., Dolla, G., Payre, C., Girard, C.A., Polidori, J., Zorzi, K., Birgy-Barelli, E., Jullien, P., Courivaud, C., Krummel, T., Benzaken, S., Bernard, G., Burtey, S., Mariat, C., Esnault, V.L., and Lambeau, G., *Epitope Spreading of Autoantibody Response to PLA2R Associates with Poor Prognosis in Membranous Nephropathy*. J Am Soc Nephrol, 2016. **27**(5): p. 1517-33.
 53. Ghiggeri, G.M., Seitz-Polski, B., Justino, J., Zaghrini, C., Payre, C., Brglez, V., Dolla, G., Sinico, A., Scolari, F., Vaglio, A., Prunotto, M., Candiano, G., Radice, A., Bruschi, M., Lambeau, G., and Italian Study Group for Membranous, N., *Multi-Autoantibody Signature and Clinical Outcome in Membranous Nephropathy*. Clin J Am Soc Nephrol, 2020. **15**(12): p. 1762-1776.
 54. Kurts, C. and Meyer-Schwesinger, C., *Protecting the kidney against autoimmunity and inflammation*. Nat Rev Nephrol, 2019. **15**(2): p. 66-68.
 55. Meyer-Schwesinger, C., *The ubiquitin-proteasome system in kidney physiology and disease*. Nat Rev Nephrol, 2019. **15**(7): p. 393-411.

Literature

56. Kerjaschki, D. and Neale, T.J., *Molecular mechanisms of glomerular injury in rat experimental membranous nephropathy (Heymann nephritis)*. J Am Soc Nephrol, 1996. **7**(12): p. 2518-26.
57. Godel, M., Grahammer, F., and Huber, T.B., *Thrombospondin type-1 domain-containing 7A in idiopathic membranous nephropathy*. N Engl J Med, 2015. **372**(11): p. 1073.
58. Meyer-Schwesinger, C., Lambeau, G., and Stahl, R.A., *Thrombospondin type-1 domain-containing 7A in idiopathic membranous nephropathy*. N Engl J Med, 2015. **372**(11): p. 1074-5.
59. Tomas, N.M., Meyer-Schwesinger, C., von Spiegel, H., Kotb, A.M., Zahner, G., Hoxha, E., Helmchen, U., Endlich, N., Koch-Nolte, F., and Stahl, R.A.K., *A Heterologous Model of Thrombospondin Type 1 Domain-Containing 7A-Associated Membranous Nephropathy*. J Am Soc Nephrol, 2017. **28**(11): p. 3262-3277.
60. Seifert, L., Zahner, G., Meyer-Schwesinger, C., Hickstein, N., Dehde, S., Wulf, S., Kollner, S.M.S., Lucas, R., Kylies, D., Froembling, S., Zielinski, S., Kretz, O., Borodovsky, A., Biniaminov, S., Wang, Y., Cheng, H., Koch-Nolte, F., Zipfel, P.F., Hopfer, H., Puelles, V.G., Panzer, U., Huber, T.B., Wiech, T., and Tomas, N.M., *The classical pathway triggers pathogenic complement activation in membranous nephropathy*. Nat Commun, 2023. **14**(1): p. 473.
61. Meyer-Schwesinger, C., Tomas, N.M., Dehde, S., Seifert, L., Hermans-Borgmeyer, I., Wiech, T., Koch-Nolte, F., Huber, T.B., and Zahner, G., *A novel mouse model of phospholipase A2 receptor 1-associated membranous nephropathy mimics podocyte injury in patients*. Kidney Int, 2020. **97**(5): p. 913-919.
62. Pohl, C. and Dikic, I., *Cellular quality control by the ubiquitin-proteasome system and autophagy*. Science, 2019. **366**(6467): p. 818-822.
63. Dikic, I., *Proteasomal and Autophagic Degradation Systems*. Annu Rev Biochem, 2017. **86**: p. 193-224.
64. Heintz, L. and Meyer-Schwesinger, C., *The Intertwining of Autophagy and the Ubiquitin Proteasome System in Podocyte (Patho)Physiology*. Cell Physiol Biochem, 2021. **55**(S4): p. 68-95.
65. Baixauli, F., Lopez-Otin, C., and Mittelbrunn, M., *Exosomes and autophagy: coordinated mechanisms for the maintenance of cellular fitness*. Front Immunol, 2014. **5**: p. 403.
66. Sachs, W., Blume, L., Loreth, D., Schebsdat, L., Hatje, F., Koehler, S., Wedekind, U., Sachs, M., Zielinski, S., Brand, J., Conze, C., Florea, B.I., Heppner, F., Kruger, E., Rinschen, M.M., Kretz, O., Thunauer, R., and Meyer-Schwesinger, C., *The proteasome modulates endocytosis specifically in glomerular cells to promote kidney filtration*. Nat Commun, 2024. **15**(1): p. 1897.
67. Bishop, P., Rocca, D., and Henley, J.M., *Ubiquitin C-terminal hydrolase L1 (UCH-L1): structure, distribution and roles in brain function and dysfunction*. Biochem J, 2016. **473**(16): p. 2453-62.
68. Collins, G.A. and Goldberg, A.L., *The Logic of the 26S Proteasome*. Cell, 2017. **169**(5): p. 792-806.
69. Mevissen, T.E.T. and Komander, D., *Mechanisms of Deubiquitinase Specificity and Regulation*. Annu Rev Biochem, 2017. **86**: p. 159-192.
70. Snyder, N.A. and Silva, G.M., *Deubiquitinating enzymes (DUBs): Regulation, homeostasis, and oxidative stress response*. J Biol Chem, 2021. **297**(3): p. 101077.

Literature

71. Das, C., Hoang, Q.Q., Kreinbring, C.A., Luchansky, S.J., Meray, R.K., Ray, S.S., Lansbury, P.T., Ringe, D., and Petsko, G.A., *Structural basis for conformational plasticity of the Parkinson's disease-associated ubiquitin hydrolase UCH-L1*. Proc Natl Acad Sci U S A, 2006. **103**(12): p. 4675-80.
72. Radon, V., Czesla, M., Reichelt, J., Fehlert, J., Hammel, A., Rosendahl, A., Knop, J.H., Wiech, T., Wenzel, U.O., Sachs, M., Reinicke, A.T., Stahl, R.A.K., and Meyer-Schwesinger, C., *Ubiquitin C-Terminal Hydrolase L1 is required for regulated protein degradation through the ubiquitin proteasome system in kidney*. Kidney Int, 2018. **93**(1): p. 110-127.
73. Liu, Z., Meray, R.K., Grammatopoulos, T.N., Fredenburg, R.A., Cookson, M.R., Liu, Y., Logan, T., and Lansbury, P.T., Jr., *Membrane-associated farnesylated UCH-L1 promotes alpha-synuclein neurotoxicity and is a therapeutic target for Parkinson's disease*. Proc Natl Acad Sci U S A, 2009. **106**(12): p. 4635-40.
74. Jamin, A., Berthelot, L., Couderc, A., Chemouny, J.M., Boedec, E., Dehoux, L., Abbad, L., Dossier, C., Daugas, E., Monteiro, R.C., and Deschenes, G., *Autoantibodies against podocytic UCHL1 are associated with idiopathic nephrotic syndrome relapses and induce proteinuria in mice*. J Autoimmun, 2018. **89**: p. 149-161.
75. Liu, Y., Fallon, L., Lashuel, H.A., Liu, Z., and Lansbury, P.T., Jr., *The UCH-L1 gene encodes two opposing enzymatic activities that affect alpha-synuclein degradation and Parkinson's disease susceptibility*. Cell, 2002. **111**(2): p. 209-18.
76. Sakurai, M., Ayukawa, K., Setsuie, R., Nishikawa, K., Hara, Y., Ohashi, H., Nishimoto, M., Abe, T., Kudo, Y., Sekiguchi, M., Sato, Y., Aoki, S., Noda, M., and Wada, K., *Ubiquitin C-terminal hydrolase L1 regulates the morphology of neural progenitor cells and modulates their differentiation*. J Cell Sci, 2006. **119**(Pt 1): p. 162-71.
77. Osaka, H., Wang, Y.L., Takada, K., Takizawa, S., Setsuie, R., Li, H., Sato, Y., Nishikawa, K., Sun, Y.J., Sakurai, M., Harada, T., Hara, Y., Kimura, I., Chiba, S., Namikawa, K., Kiyama, H., Noda, M., Aoki, S., and Wada, K., *Ubiquitin carboxy-terminal hydrolase L1 binds to and stabilizes monoubiquitin in neuron*. Hum Mol Genet, 2003. **12**(16): p. 1945-58.
78. Leroy, E., Boyer, R., Auburger, G., Leube, B., Ulm, G., Mezey, E., Harta, G., Brownstein, M.J., Jonnalagada, S., Chernova, T., Dehejia, A., Lavedan, C., Gasser, T., Steinbach, P.J., Wilkinson, K.D., and Polymeropoulos, M.H., *The ubiquitin pathway in Parkinson's disease*. Nature, 1998. **395**(6701): p. 451-2.
79. Kabuta, T., Setsuie, R., Mitsui, T., Kinugawa, A., Sakurai, M., Aoki, S., Uchida, K., and Wada, K., *Aberrant molecular properties shared by familial Parkinson's disease-associated mutant UCH-L1 and carbonyl-modified UCH-L1*. Hum Mol Genet, 2008. **17**(10): p. 1482-96.
80. Choi, J., Levey, A.I., Weintraub, S.T., Rees, H.D., Gearing, M., Chin, L.S., and Li, L., *Oxidative modifications and down-regulation of ubiquitin carboxyl-terminal hydrolase L1 associated with idiopathic Parkinson's and Alzheimer's diseases*. J Biol Chem, 2004. **279**(13): p. 13256-64.
81. Kabuta, T., Furuta, A., Aoki, S., Furuta, K., and Wada, K., *Aberrant interaction between Parkinson disease-associated mutant UCH-L1 and the lysosomal receptor for chaperone-mediated autophagy*. J Biol Chem, 2008. **283**(35): p. 23731-8.
82. Meyer-Schwesinger, C., Meyer, T.N., Sievert, H., Hoxha, E., Sachs, M., Klupp, E.M., Munster, S., Balabanov, S., Carrier, L., Helmchen, U., Thaiss, F., and Stahl, R.A., *Ubiquitin C-terminal hydrolase-1 activity induces polyubiquitin*

- accumulation in podocytes and increases proteinuria in rat membranous nephropathy*. Am J Pathol, 2011. **178**(5): p. 2044-57.
83. Lohmann, F., Sachs, M., Meyer, T.N., Sievert, H., Lindenmeyer, M.T., Wiech, T., Cohen, C.D., Balabanov, S., Stahl, R.A., and Meyer-Schwesinger, C., *UCH-L1 induces podocyte hypertrophy in membranous nephropathy by protein accumulation*. Biochim Biophys Acta, 2014. **1842**(7): p. 945-58.
 84. Sosna, J., Voigt, S., Mathieu, S., Kabelitz, D., Trad, A., Janssen, O., Meyer-Schwesinger, C., Schutze, S., and Adam, D., *The proteases HtrA2/Omi and UCH-L1 regulate TNF-induced necroptosis*. Cell Commun Signal, 2013. **11**: p. 76.
 85. Welsh, J.A., Goberdhan, D.C.I., O'Driscoll, L., Buzas, E.I., Blenkiron, C., Bussolati, B., Cai, H., Di Vizio, D., Driedonks, T.A.P., Erdbrugger, U., Falcon-Perez, J.M., Fu, Q.L., Hill, A.F., Lenassi, M., Lim, S.K., Mahoney, M.G., Mohanty, S., Moller, A., Nieuwland, R., Ochiya, T., Sahoo, S., Torrecilhas, A.C., Zheng, L., Zijlstra, A., Abuelreich, S., Bagabas, R., Bergese, P., Bridges, E.M., Brucale, M., Burger, D., Carney, R.P., Cocucci, E., Crescitelli, R., Hanser, E., Harris, A.L., Haughey, N.J., Hendrix, A., Ivanov, A.R., Jovanovic-Talisman, T., Kruh-Garcia, N.A., Ku'ulei-Lyn Faustino, V., Kyburz, D., Lasser, C., Lennon, K.M., Lotvall, J., Maddox, A.L., Martens-Uzunova, E.S., Mizenko, R.R., Newman, L.A., Ridolfi, A., Rohde, E., Rojalin, T., Rowland, A., Saftics, A., Sandau, U.S., Saugstad, J.A., Shekari, F., Swift, S., Ter-Ovanesyan, D., Tosar, J.P., Useckaite, Z., Valle, F., Varga, Z., van der Pol, E., van Herwijnen, M.J.C., Wauben, M.H.M., Wehman, A.M., Williams, S., Zendrini, A., Zimmerman, A.J., Consortium, M., Thery, C., and Witwer, K.W., *Minimal information for studies of extracellular vesicles (MISEV2023): From basic to advanced approaches*. J Extracell Vesicles, 2024. **13**(2): p. e12404.
 86. van Niel, G., D'Angelo, G., and Raposo, G., *Shedding light on the cell biology of extracellular vesicles*. Nat Rev Mol Cell Biol, 2018. **19**(4): p. 213-228.
 87. Yokoi, A. and Ochiya, T., *Exosomes and extracellular vesicles: Rethinking the essential values in cancer biology*. Semin Cancer Biol, 2021. **74**: p. 79-91.
 88. Buzas, E.I., *The roles of extracellular vesicles in the immune system*. Nat Rev Immunol, 2023. **23**(4): p. 236-250.
 89. Meyer-Schwesinger, C., *Lysosome function in glomerular health and disease*. Cell Tissue Res, 2021. **385**(2): p. 371-392.
 90. Li, X.Q., Lerman, L.O., and Meng, Y., *Potential role of extracellular vesicles in the pathophysiology of glomerular diseases*. Clin Sci (Lond), 2020. **134**(20): p. 2741-2754.
 91. Sun, I.O. and Lerman, L.O., *Urinary Extracellular Vesicles as Biomarkers of Kidney Disease: From Diagnostics to Therapeutics*. Diagnostics (Basel), 2020. **10**(5).
 92. Lu, J., Hu, Z.B., Chen, P.P., Lu, C.C., Zhang, J.X., Li, X.Q., Yuan, B.Y., Huang, S.J., and Ma, K.L., *Urinary levels of podocyte-derived microparticles are associated with the progression of chronic kidney disease*. Ann Transl Med, 2019. **7**(18): p. 445.
 93. Herwig, J., Skuza, S., Sachs, W., Sachs, M., Failla, A.V., Rune, G., Meyer, T.N., Fester, L., and Meyer-Schwesinger, C., *Thrombospondin Type 1 Domain-Containing 7A Localizes to the Slit Diaphragm and Stabilizes Membrane Dynamics of Fully Differentiated Podocytes*. J Am Soc Nephrol, 2019. **30**(5): p. 824-839.
 94. Saleem, M.A., O'Hare, M.J., Reiser, J., Coward, R.J., Inward, C.D., Farren, T., Xing, C.Y., Ni, L., Mathieson, P.W., and Mundel, P., *A conditionally*

- immortalized human podocyte cell line demonstrating nephrin and podocin expression.* J Am Soc Nephrol, 2002. **13**(3): p. 630-638.
95. Ahuja, D., Saenz-Robles, M.T., and Pipas, J.M., *SV40 large T antigen targets multiple cellular pathways to elicit cellular transformation.* Oncogene, 2005. **24**(52): p. 7729-45.
 96. Moore, J.F. and Sharer, J.D., *Methods for Quantitative Creatinine Determination.* Curr Protoc Hum Genet, 2017. **93**: p. A 30 1-A 30 7.
 97. Shen, Y.F., Liu, M.J., Long, Z., Shi, X., and Liu, M.L., *A simple, flexible, and high-efficiency western blot analysis for age-related human induced neurons.* Biotechnol J, 2023. **18**(10): p. e2300089.
 98. Pfaffl, M.W., *A new mathematical model for relative quantification in real-time RT-PCR.* Nucleic Acids Res, 2001. **29**(9): p. e45.
 99. Canene-Adams, K., *Preparation of formalin-fixed paraffin-embedded tissue for immunohistochemistry.* Methods Enzymol, 2013. **533**: p. 225-33.
 100. Im, K., Mareninov, S., Diaz, M.F.P., and Yong, W.H., *An Introduction to Performing Immunofluorescence Staining.* Methods Mol Biol, 2019. **1897**: p. 299-311.
 101. Artelt, N., Siegerist, F., Ritter, A.M., Grisk, O., Schluter, R., Endlich, K., and Endlich, N., *Comparative Analysis of Podocyte Foot Process Morphology in Three Species by 3D Super-Resolution Microscopy.* Front Med (Lausanne), 2018. **5**: p. 292.
 102. Siegerist, F., Ribback, S., Dombrowski, F., Amann, K., Zimmermann, U., Endlich, K., and Endlich, N., *Structured illumination microscopy and automatized image processing as a rapid diagnostic tool for podocyte effacement.* Sci Rep, 2017. **7**(1): p. 11473.
 103. LeBleu, V.S., Macdonald, B., and Kalluri, R., *Structure and function of basement membranes.* Exp Biol Med (Maywood), 2007. **232**(9): p. 1121-9.
 104. Novelli, G. and D'Apice, M.R., *Protein farnesylation and disease.* J Inherit Metab Dis, 2012. **35**(5): p. 917-26.
 105. Chung, J.J., Huber, T.B., Godel, M., Jarad, G., Hartleben, B., Kwoh, C., Keil, A., Karpitskiy, A., Hu, J., Huh, C.J., Cella, M., Gross, R.W., Miner, J.H., and Shaw, A.S., *Albumin-associated free fatty acids induce macropinocytosis in podocytes.* J Clin Invest, 2015. **125**(6): p. 2307-16.
 106. Typiak, M., Audzeyenka, I., and Dubaniewicz, A., *Presence and possible impact of Fcγ receptors on resident kidney cells in health and disease.* Immunol Cell Biol, 2022. **100**(8): p. 591-604.
 107. Dylewski, J.F., Haddad, G., and Blaine, J., *Exploiting the neonatal crystallizable fragment receptor to treat kidney disease.* Kidney Int, 2024. **105**(1): p. 54-64.
 108. Akilesh, S., Huber, T.B., Wu, H., Wang, G., Hartleben, B., Kopp, J.B., Miner, J.H., Roopenian, D.C., Unanue, E.R., and Shaw, A.S., *Podocytes use FcRn to clear IgG from the glomerular basement membrane.* Proc Natl Acad Sci U S A, 2008. **105**(3): p. 967-72.
 109. Chioran, A., Duncan, S., Catalano, A., Brown, T.J., and Ringuette, M.J., *Collagen IV trafficking: The inside-out and beyond story.* Dev Biol, 2017. **431**(2): p. 124-133.
 110. Kim, Y., Butkowski, R., Burke, B., Kleppel, M.M., Crosson, J., Katz, A., and Michael, A.F., *Differential expression of basement membrane collagen in membranous nephropathy.* Am J Pathol, 1991. **139**(6): p. 1381-8.
 111. Floege, J., Johnson, R.J., Gordon, K., Yoshimura, A., Campbell, C., Iruela-Arispe, L., Alpers, C.E., and Couser, W.G., *Altered glomerular extracellular*

Literature

- matrix synthesis in experimental membranous nephropathy*. *Kidney Int*, 1992. **42**(3): p. 573-85.
112. Hatje, F.A., Wedekind, U., Sachs, W., Loreth, D., Reichelt, J., Demir, F., Kosub, C., Heintz, L., Tomas, N.M., Huber, T.B., Skuza, S., Sachs, M., Zielinski, S., Rinschen, M.M., and Meyer-Schwesinger, C., *Tripartite Separation of Glomerular Cell Types and Proteomes from Reporter-Free Mice*. *J Am Soc Nephrol*, 2021. **32**(9): p. 2175-2193.
113. Miner, J.H., *The glomerular basement membrane*. *Exp Cell Res*, 2012. **318**(9): p. 973-8.
114. Suleiman, H., Zhang, L., Roth, R., Heuser, J.E., Miner, J.H., Shaw, A.S., and Dani, A., *Nanoscale protein architecture of the kidney glomerular basement membrane*. *Elife*, 2013. **2**: p. e01149.
115. Randles, M.J., Collinson, S., Starborg, T., Mironov, A., Krendel, M., Konigshausen, E., Sellin, L., Roberts, I.S., Kadler, K.E., Miner, J.H., and Lennon, R., *Three-dimensional electron microscopy reveals the evolution of glomerular barrier injury*. *Sci Rep*, 2016. **6**: p. 35068.
116. Butt, L., Unnersjo-Jess, D., Hohne, M., Edwards, A., Binz-Lotter, J., Reilly, D., Hahnfeldt, R., Ziegler, V., Fremter, K., Rinschen, M.M., Helmstadter, M., Ebert, L.K., Castrop, H., Hackl, M.J., Walz, G., Brinkkoetter, P.T., Liebau, M.C., Tory, K., Hoyer, P.F., Beck, B.B., Brismar, H., Blom, H., Schermer, B., and Benzing, T., *A molecular mechanism explaining albuminuria in kidney disease*. *Nat Metab*, 2020. **2**(5): p. 461-474.
117. Prunotto, M., Farina, A., Lane, L., Pernin, A., Schifferli, J., Hochstrasser, D.F., Lescuyer, P., and Moll, S., *Proteomic analysis of podocyte exosome-enriched fraction from normal human urine*. *J Proteomics*, 2013. **82**: p. 193-229.

6 Publications

Reichelt J, Sachs W, Frömbling S, Fehlert J, Studencka-Turski M, Betz A, Loreth D, Blume L, Witt S, Pohl S, Brand J, Czesla M, Knop J, Florea BI, Zielinski S, Sachs M, Hoxha E, Hermans-Borgmeyer I, Zahner G, Wiech T, Krüger E, Meyer-Schwesinger C. (2023). **Non-functional ubiquitin C-terminal hydrolase L1 drives podocyte injury through impairing proteasomes in autoimmune glomerulonephritis**, Nat Commun. 14(1):2114.

7 Acknowledgements

I would like to express my deepest gratitude to Prof. Catherine Meyer-Schwesinger for providing the delightful research topic, creating a great working environment and for the passionate and inspiring supervision. Special thanks should also go to Prof. Julia Kehr for taking on the responsibility of my second supervisor.

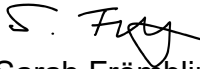
I would like to extend my sincere thanks to the Meyer-Schwesinger lab. Especially to our technicians Johannes Brand, Stephanie Zielinski and Marlies Sachs for their active support in the lab and for sharing their technical wisdom. I am also grateful for the support of the Postdocs Desirée Loreth, Wiebke Sachs and Julia Reichelt, who notably helped through their advanced scientific input.

Lastly, I would thank my mother. I could not have undertaken this journey without her everlasting support.

8 Eidesstattliche Versicherung

Hiermit versichere ich an Eides statt, die vorliegende Dissertationsschrift selbst verfasst und keine anderen als die angegebenen Hilfsmittel und Quellen benutzt zu haben. Sofern im Zuge der Erstellung der vorliegenden Dissertationsschrift generative Künstliche Intelligenz (gKI) basierte elektronische Hilfsmittel verwendet wurden, versichere ich, dass meine eigene Leistung im Vordergrund stand und dass eine vollständige Dokumentation aller verwendeten Hilfsmittel gemäß der Guten wissenschaftlichen Praxis vorliegt. Ich trage die Verantwortung für eventuell durch die gKI generierte fehlerhafte oder verzerrte Inhalte, fehlerhafte Referenzen, Verstöße gegen das Datenschutz- und Urheberrecht oder Plagiate.

Hamburg, den 17.03.2025


Sarah Frömbling

Ich versichere, dass dieses gebundene Exemplar der Dissertation und das in elektronischer Form eingereichte Dissertationsexemplar (über den Docata-Upload) und das bei der Fakultät (zuständiges Studienbüro bzw. Promotionsbüro Physik) zur Archivierung eingereichte gedruckte gebundene Exemplar der Dissertationsschrift identisch sind.

Hamburg, den 17.03.2025


Sarah Frömbling